University of Alberta
Department of Civil &
Environmental Engineering

Structural Engineering Report No. 239

BEHAVIOUR OF WELDED COLD-FORMED STEEL TENSION MEMBERS

by

Alvaro Lemenhe

and

J.J. Roger Cheng

July 2001

Structural Engineering Report No. 239

Behaviour of Welded Cold-Formed Steel Tension Members

by

Alvaro Lemenhe

and

J.J. Roger Cheng

Department of Civil and Environmental Engineering
University of Alberta
Edmonton, Alberta, Canada
T6G 2G7

July 2001

Abstract

Shear lag in a tension member is a condition of non-uniform stress distribution that occurs adjacent to the connection in the tension member in which all elements of the cross section are not directly connected. Past research on the subject of shear lag has focused mainly on bolted hot-rolled steel members. Some studies have been done for the cases of welded hot-rolled sections and bolted cold-formed members, but none in welded cold-formed members. The purpose of this study is to investigate the shear lag effect on welded cold-formed steel angles and channels in tension.

An experimental and numerical analysis program was undertaken to investigate the shear lag effect on welded angle and channel cold-formed tension members. A total of 12 specimens consisting of five channels and seven angles were fabricated and tested. The connection length and cross-sectional geometry were the two major parameters studied in this program. A finite element model was used to predict the response of the test specimens. Good correlation between the analytical and test results was observed. A comparison of test and analytical results obtained from this study with current design methods and existing test results was also made.

The strength capacity of welded cold-formed angles was found to be affected by the connection length and cross-sectional geometry. However, the effects of shear lag on the tensile strength of cold-formed sections were found to be much less than those on hot-rolled sections. It can be attributed to the thinness of the section, the cold-forming effect at the corner of the section, and the biaxial effect of the welded element. A lower bound net section efficiency factor of 0.95 for both welded cold-formed channel and angle sections is proposed based on the available test and analytical results.

ACKNOWLEDGEMENTS

This research project is funded by the Natural Science and Engineering Research Council of Canada to Dr. J.J.R. Cheng.

The technical assistance of Larry Burden and Richard Helfrich of I.F. Morrison Structural Engineering Laboratory is acknowledged. The thanks also extended to Mr. Clark Bicknell of the Welding Research Group in the Department of Chemical and Material Engineering for welding all the test specimens.

Special thanks are given to Dr. H.A. Khoo for his assistance during the analytical portion of this study and Anthony K.F. Ng for his assistance in conducting the experiments.

Table of Contents

List of Tables

List of Figures

List of Symbols

A	cross-sectional area of the tension coupon at rupture
A_0	initial cross-section area of the tension coupon
A_e, A_{ne}	effective net area
A_n	net sectional area
A_g	gross sectional area of the member
A'_{ne}	effective net area reduced for the shear lag
E_{ave}	average modulus of elasticity obtained from the tensions coupons at the flat portions.
F_y	yield strength of the material
F_u	ultimate strength of the material
K_4	shear lag factor
L	connection length.
P_{Test}	static ultimate strength of the test
P_{ult}	static ultimate capacity of the member
t	thickness of the member
T_r	factored tensile resistance of the member
U	net area efficiency, shear lag coefficient
U_{AISC}	net area efficiency based on AISC Specification
$U_{S16.1}$	net area efficiency based on CSA-S16.1-94 Standard
U_{UMR}	net area efficiency based on the equations proposed by University of Missouri-Rolla
w	plate element width

W_1, W_2	weld length of the test specimens
$\bar{x}$	connection eccentricity, distance from the face of the connection to the center of gravity of the member
$\Delta P/\Delta \varepsilon$	slope of the load-strain curve for corner tension coupons
ϕ	resistance factor

1. Introduction

1.1 General Overview

The use of steel tension members is found throughout building and bridge construction. Tension members may be cables, rods, angles, channels, wide-flange sections, or any sections that are built up from these individual shapes. The type of tension member used is largely a function of its end connection.

The common modes of failure that might occur when a member is loaded in tension are:

1) Member failure at gross area away from the connection;
2) Section failure at the connection;
3) Member bearing or tear-out failure at the connection (this mode of failure is mainly related to bolted connections);
4) Welds or bolts failure at the connection.

1.2 Statement of the Problem

The strength of a tension member is affected by its cross sectional properties and the way its ends are connected. For practical reasons, normally only part of the cross section is connected, one leg of an angle tension member, for example. Those conditions of attachment and the section geometry can cause a non-uniform stress distribution in the section at the connection, and hence decrease the ultimate strength of the member.

This loss of efficiency of the cross-section due to a non-uniform stress distribution adjacent to a connection is referred to as the shear lag effect. It is customary to evaluate the

efficiency of a cross section in terms of the ratio of the failure load to the theoretical rupture strength assuming a uniform stress distribution. The design provisions of the section efficiency of tension members in the current design standards (mode "2" failure as discussed in section 1.1), such as CSA S16.1-94 (1994) and AISC-LRFD (2000), are mainly based on the research results of hot-rolled bolted tension members (Chesson and Munse 1963). It was found that the way a tension member is connected at the ends (i.e. bolted or welded) has a significant effect on the failure load of the member (Davis and Boomsliter 1934, Esterling and Giroux 1993). Furthermore, cold-formed members are much more slender than hot-rolled sections. For this reason, some phenomena, which are of secondary concern for stockier members, are of decisive importance in cold-formed thin-walled members. Some of these phenomena include small torsional rigidity, local buckling and local crippling (Winter 1959). Tests have been carried out to investigate the shear lag effect in both cold-formed (Amy and Cheng 2000) and hot-rolled (Wu and Kulak 1993) bolted connections. It was found that cold-formed members behave differently from the hot-rolled members in tension. However, there is little information available about the behavior of welded cold-formed members in tension.

The shear lag effect on the section efficiency of welded cold-formed steel tension members is the objective of the investigation reported herein.

1.3 Objectives and Scope

The objectives of this study are to:

1. Conduct physical tests of welded single cold-formed angle and channel tension members in order to investigate the shear lag effects;

2. Compare the tests results with previous studies and current design provisions on the tensile strength of welded cold-formed steel tension members;
3. Develop finite element models to predict the load carrying capacity, stress distribution at the critical cross-section, and failure mode of welded cold-formed steel tension members;
4. Propose design criteria for welded cold-formed steel tension members;
5. Recommend areas of future study in this topic.

A total of 12 specimens (seven angles and five channels) were fabricated and tested. A finite element model was developed to predict the behaviour of welded cold-formed tension members. The results of the analytical model were compared to the results of the physical tests to validate the models. Previous studies and the current design specifications are then compared with the test results.

1.4 Outline of the Report

The report consists of seven chapters. Chapter 1 provides a general background and a brief description of the shear lag problem, objectives, and scope. Chapter 2 presents the literature review on the net section efficiency of both welded and bolted tension members along with the current design provisions. The experimental program, which describes the geometry of the specimens, instrumentation, test setup, and test procedures, is reported in Chapter 3. Chapter 4 gives the results of the test program. The finite element method used to predict the test results is presented in Chapter 5. Chapter 6 contains a comparison of the test results with previous studies and current design specifications. The summary and the conclusions are given in Chapter 7.

2. Literature Review

2.1 Previous Studies

2.1.1 Bolted Connections

Experimental studies have been performed to investigate the shear lag effect in steel tension members since the 1900s (McKibben 1906). Most of those investigations have focused primarily on hot-rolled steel members connected through bolts or rivets. Extensive literature reviews can be found in Yue and Kulak (1993) and Amy and Cheng (2000) for bolted hot-rolled steel members and bolted cold-formed steel members in tension, respectively. Shear lag provisions on bolted tension members included in the CSA S16.1-94 (1994) and AISC-LRFD (2000) are based mainly on the work performed by Chesson and Munse (1963) on hot-rolled steel members.

Chesson and Munse (1963) developed an empirical equation to calculate the net section efficiency of tension members. Although this research focused on riveted and bolted connections, its results were expanded to welded connections by others. Chesson and Munse conducted an experimental program on riveted and bolted connections to examine the behaviour of various cross sections of truss-type members. Their work showed that several factors contribute to the loss in efficiency of the net section, namely net section area, ductility of the material, geometry of the cross section, bearing strength of the member, and shear lag effect. An empirical equation to calculate the net section efficiency was proposed where the two most important factors were the net sectional area and the shear lag effect:

$$A_e = K_4 \cdot A_n \qquad [2.1]$$

where

K_4 = the shear lag factor;

A_n = the net sectional area.

The shear lag expression was given by:

$$K_4 = 1 - \frac{\bar{x}}{L} \qquad [2.2]$$

where

$\bar{x}$ = distance from the face of the connection to the center of gravity of the member;

L = connection length.

2.1.2 Welded Connections

In one of the earliest experimental investigations on the behavior of welded tension members, Davis and Boomsliter (1934) tested a series of specimens composed of one or more angles. The specimens tested included two welded single angles and one welded double angles (back-to-back). Balanced welds were used in this experiment and the size of angles in all cases was 76.2 x 76.2 x 7.94 mm (3 x 3 x 5/16 in). The stress distribution was found to be fairly uniform for the welded double angles and very unevenly distributed over the cross section for the single angle. Although the single angle tension members failed in the welds, the authors concluded that those members have a net section efficiency of 70 percent. The net section efficiency obtained for welded double angles specimens was 87 percent.

Gibson and Wake (1942) investigated the effectiveness of different arrangement of welds. They tested 54 tension members made of a single or double angles to obtain the

connection ultimate strength. A total of 15 different weld arrangements were investigated. The authors showed that both balanced and unbalanced connections lead to the same ultimate strength. They observed that, for a single angle, the eccentricity normal to the plane of the welds has a major effect on the strength of the members. The tests also indicated that there was a non-uniform stress distribution over the angle cross-section.

Easterling and Giroux (1993) conducted a series of tests to investigate the shear lag effect on welded tension members. The experimental program consisted of 27 welded tension members, welded back-to-back to gusset plates, loaded to failure. Four types of members were tested: channels, angles, plates, and tees. For the channels, angles, and tees, longitudinal, transverse, and a combination of both longitudinal and transverse fillet welds were used; while for the plates longitudinal and a combination of longitudinal and transverse welds were used. Longitudinal strains were recorded at the end of the welds to study the strain distribution at the critical section. Shear lag controlled the strength of the angles and plates specimens only, since all but one channel and two tees specimens failed in the cross section away from the weld. The experimental results for the plate and angle specimens indicated that the increased length of the longitudinal welds did not affect the net section efficiency. The net section efficiency was not increased either by the addition of a transverse weld. The experimental section efficiency was found to be greater than 90 percent for the plates and greater than 80 percent for the angles. Based on these test results, the shear lag expression given by Munse and Chesson (Equation 2.2) with an upper limit of 0.9 was found to be appropriate.

LaBoube and Yu (1995) conducted an experimental study with the intent of determining the effect of shear lag on bolted cold-formed steel tension members and

developing an appropriate design recommendation. The research work addressed primarily angles and channels. Particular emphasis was placed on connections designed to fail in bearing and in tensile strength of the connected parts. Based on the tests results, a design equation was developed for the ultimate strengths of bolted cold-formed angles and channels in tension. The equations consisted of a modification of the shear lag expression proposed by Chesson and Munse (Equation 2.2) and are stated as follows:

i) For angle members

$$U = 1 - 1.2\frac{\bar{x}}{L} \leq 0.9 \qquad \text{but} \geq 0.4 \qquad [2.3]$$

ii) For channel members

$$U = 1 - 0.357\frac{\bar{x}}{L} \leq 0.9 \qquad \text{but} \geq 0.5 \qquad [2.4]$$

Although this research focused only on bolted cold-formed tension members, to maintain a uniform approach, the design provisions derived (Equations 2.3 and 2.4) were also recommended for welded cold-formed members.

2.2 Current Design Specifications

2.2.1 CSA Standard S16.1-94 (1994)

CSA S16.1-94 (1994) requires that the factored resistance of a tension member be taken as the least of:

i) Yielding in the gross cross-sectional area

$$T_r = \phi F_y A_g \qquad [2.5]$$

ii) Fracture of the effective net area

$$Tr = 0.85\phi F_u A_{ne} \qquad [2.6]$$

iii) Fracture of the effective net area accounting for the shear lag effect

$$Tr = 0.85\phi F_u A'_{ne} \qquad [2.7]$$

where

F_y = yield strength of the material;

F_u = ultimate strength of the material;

A_g = gross area of the member;

A_{ne} = effective net area;

A'_{ne} = effective net area reduced for the shear lag;

ϕ = resistance factor taken as 0.90.

When a tension load is transmitted by welds, the reduced effective net area shall be computed as:

$$A'_{ne} = A_{ne1}+A_{ne2}+A_{ne3} \qquad [2.8]$$

where A_{ne1}, A_{ne2}, and A_{ne3} are defined as follows:

a) Elements connected by transverse welds, A_{ne1}:

$$A_{ne1} = wt \qquad [2.9]$$

where

w = plate element width;

t = thickness of the element.

b) Elements connected by longitudinal welds along two parallel edges, A_{ne2}:

when $L \geq 2w$, $A_{ne2} = 1.0$ wt [2.10a]

when $2w > L \geq 1.5w$, $A_{ne2} = 0.87$ wt [2.10b]

when $1.5w > L \geq w$, $A_{ne2} = 0.75$ wt [2.10c]

where

L = average length of welds on the two edges;

w = plate width (distance between welds).

c) Elements connected by a single line of weld, A_{ne3}:

$$A_{ne3} = (1 - \frac{\overline{x}}{L})wt \qquad [2.11]$$

where

$\overline{x}$ = connection eccentricity

L = length of the connection in the direction of the loading.

Equation 2.11 applies to sections with outstanding elements, therefore affecting mostly angles and channels.

2.2.2. AISC – LRFD Specification (2000)

According to this specification the factored design tensile strength shall be the lesser of the followings:

i) Yielding in the gross cross-sectional area

$$T_r = \phi F_y A_g \qquad [2.12]$$

ii) Fracture of the effective net area

$$Tr = \phi F_u A_e \qquad [2.13]$$

where

A_e = effective net area

ϕ = resistance factor.

The resistance factor is 0.90 for the yielding limit and is 0.75 for the fracture limit state.

AISC-LRFD (2000) states that when a tension load is transmitted by welds through some but not all of the cross-sectional elements of the member, the effective net area A_e shall be computed as:

$$A_e = UA \qquad [2.14]$$

where A and U (reduction coefficient) are as defined bellow:

a) Load transmitted only by longitudinal welds to other than a plate member or by longitudinal welds in combination with transverse welds

$$A = A_g = \text{gross cross-sectional area} \qquad [2.15a]$$

$$U = 1 - \frac{\bar{x}}{L} \leq 0.9 \qquad [2.15b]$$

where

$\bar{x}$ = connection eccentricity;

L = length of the connection in the direction of the loading.

b) Load transmitted only by transverse welds

$$A = \text{area of directly connected element} \qquad [2.16a]$$

$$U = 1.0 \qquad [2.16b]$$

c) Load transmitted to a plate by longitudinal welds along both sides of the plate

$$A = A_g = \text{gross cross-sectional area} \qquad [2.17a]$$

$$U = 1.0 \qquad \text{for } L \geq 2w \qquad [2.17b]$$

$$U = 0.87 \qquad \text{for } 2w > L \geq 1.5w \qquad [2.17c]$$

$$U = 0.75 \qquad \text{for } 1.5w > L \geq w \qquad [2.17d]$$

where

L = length of weld along one side of plate;

w = distance between longitudinal welds (plate width).

2.2.3 Specification for the Design of Cold-Formed Steel Structural Members

In North America the design of cold-formed steel members is based mainly on American Iron and Steel Institute (AISI) Specification (1996) and CSA Standard S136-94 (1994). Since past research on the subject of shear lag has focused primarily on hot-rolled bolted tension members, there is very little (or none) of data available on welded cold-formed tension members. Therefore, AISI Specification and CSA S136-94 have no provisions regarding to shear lag effect on welded tension members. In the current draft of North American Cold-Formed Steel Specification (2001), the equations (Equations 2.3 and 2.4) developed by LaBoube and Yu (1995) for bolted cold-formed tension members are proposed for the design of welded cold-formed tension members.

3. Experimental Program

3.1 General

The objective of the testing program was to investigate the behaviour of welded cold-formed steel angles and channels in tension. Specifically, the parameters considered in this experiment were:

1. Length of the connection;
2. Size of the cross-section.

Three different sizes (nominal size of 50, 75, and 100 mm) of angles and channels were tested. A total of 12 specimens were fabricated, which include seven angles and five channels. The specimens were instrumented with strain gauges to study the strain distribution at the critical section.

3.2 Tension Coupons

A series of tension coupon tests were performed in order to establish basic material properties of the specimens. All tension coupons were taken from the extremity of the 100 mm angle and channel. The locations of the coupons cut from the angle and channel sections are shown in Fig. 3.1. The tension coupons have a gauge length of 50 mm and a width of 12.5 mm. The dimensions of the coupons were prepared in accordance with the requirements of ASTM A370-00 (2000).

An extensometer with 50 mm gauge length was used to measure the strain in the coupons. One strain gauge was placed on each face of the coupons in order to verify the extensometer reading. The load and deformation during the test were provided by the MTS testing machine.

3.3 Specimen Description

All individual pieces shipped from manufacturer were 1500 mm long. The specimen length ranged from 700 mm to 980 mm depending on the weld length used in each specimen. Cross-section dimensions were measured and are reported in Table 3.1.

The experimental specimens consisted of single angles and single channels welded to gusset plates through longitudinal welds. Both balanced and unbalanced welds were used in the angle specimens. Description of the specimens along with the weld configuration is presented in Table 3.1 and shown in Fig. 3.2. The first parameter in the test designation in Table 3.1 denotes the member type, where A and C stand for angle and channel, respectively. The second parameter identifies the size of the specimen in inches and the digit to the right of the hyphen indicates the test number. For the cases of the angle specimens, "ba" (balanced) and "un" (unbalanced) after the size indicator, identifies the weld configuration.

Welding was performed by a qualified welder and weld quality was emphasized. E48018-1, 2.5 mm diameter electrodes were used for all specimens. Except at the toe of the angle specimens, where the weld size equals the member thickness, an average weld size of 6.0 mm was used. A duplicated test was made for specimen C2-1 since it failed in the weld. This duplicated test was labeled C2-2.

With the exception of specimens C3-2 and A3un-2, the welds were designed with a capacity 15% greater than the cross-sectional strength. The welds of specimens C3-2 and A3un-2 were designed to carry 80% of the cross-sectional strength.

Three sets of gusset plates were used throughout the entire experimental program. The gusset plate dimensions are shown in Fig. 3.3.

3.4 Test Setup and Instrumentation

The gusset plates were placed in tension grips with bolts as shown schematically in Fig. 3.4. To prevent any in-plane rotation of the gusset plate shins were inserted between the tension grips and the crosshead of the testing machine.

Measurements of loads, deformations, and strains were made, as the specimen was loaded. The instrumentation used is detailed in Fig. 3.5. Strain gauges were used to measure the strain distribution at the critical section of the specimens (Section A). For specimens A3un-1 and C3-1 strain gauges were also mounted at the mid-length (Section B). All strain gauges were oriented to measure the longitudinal strains only. The total elongation of each specimen was monitored by the stroke of the test machine. A dial gage was installed to in order to verify any slip between the gussets and the grips.

3.5 Test Procedure

After the member was welded to the gusset plates the specimen was installed in the tension grips. To avoid any slip between the gusset plates and the grips an impact wrench was used to tight them together. The specimen was subjected to a small initial load in order to align itself with the testing machine. Special attention was given to the alignment. With all instrumentation zeroed, the specimen was loaded under stroke control mode. Readings of load, deformation, and strain were taken at regular intervals. The specimen was loaded to failure or until a significant load drop was observed.

Table 3.1 Experimental Specimen Details

Test Designation	Member (mm x mm x mm)	Gross Area (mm^2)	Length (mm)	Weld Length (mm)	
				W1	W2
C2-1	50.4x28x2.63	257.6	900	75	75
C2-2	50.4x28x2.63	257.6	750	75	75
C3-1	76.6x28x2.63	326.5	940	95	95
C3-2	76.6x28x2.63	326.5	700	80	80
C4-1	101.3x28x2.63	391.5	980	115	115
A2ba-1	50.6x50.6x2.63	255.0	810	40	110
A2un-1	50.6x50.6x2.63	255.0	735	75	75
A3ba-1	75.6x75.6x2.63	386.6	850	60	165
A3un-1	75.6x75.6x2.63	386.6	980	125	125
A3un-2	75.6x75.6x2.63	386.6	700	80	80
A4ba-1	101.2x101.2x2.63	521.2	780	80	225
A4un-1	101.2x101.2x2.63	521.2	750	150	150

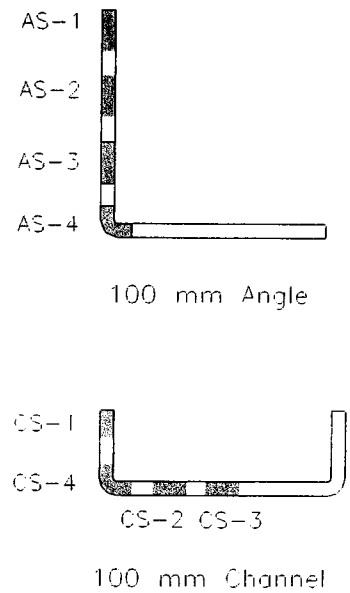

Figure 3.1 Tension Coupon Locations

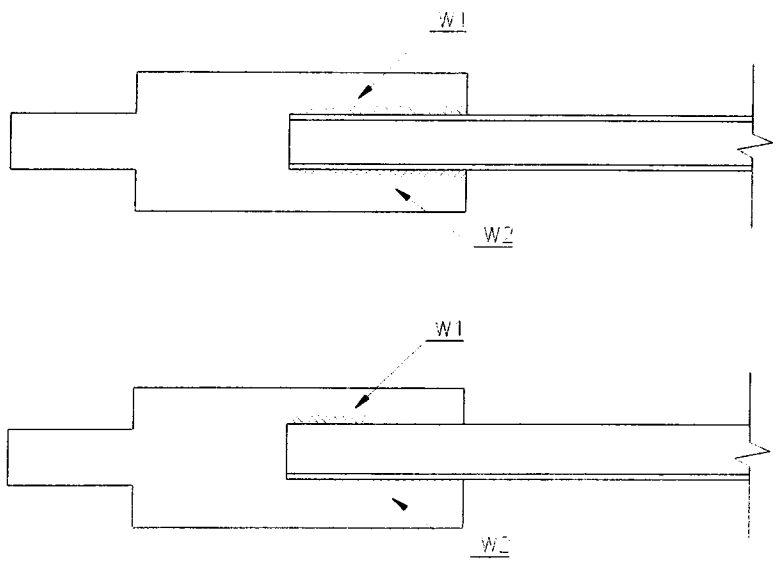

Figure 3.2 Weld Configuration

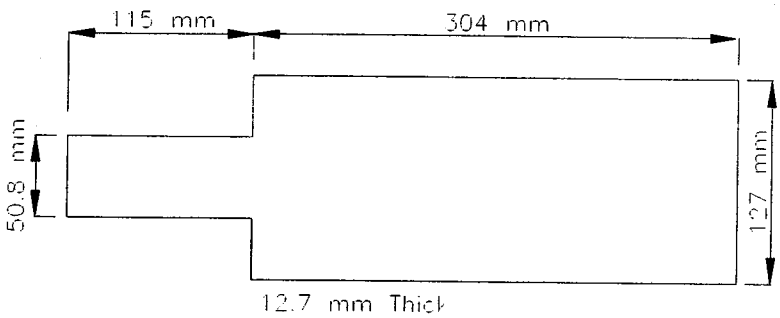

Figure 3.3 Gusset Plate Dimensions

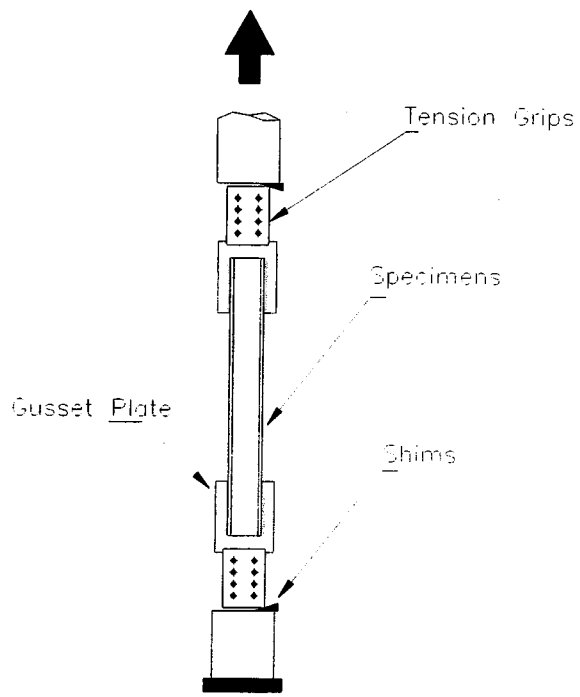

Figure 3.4 Test Setup

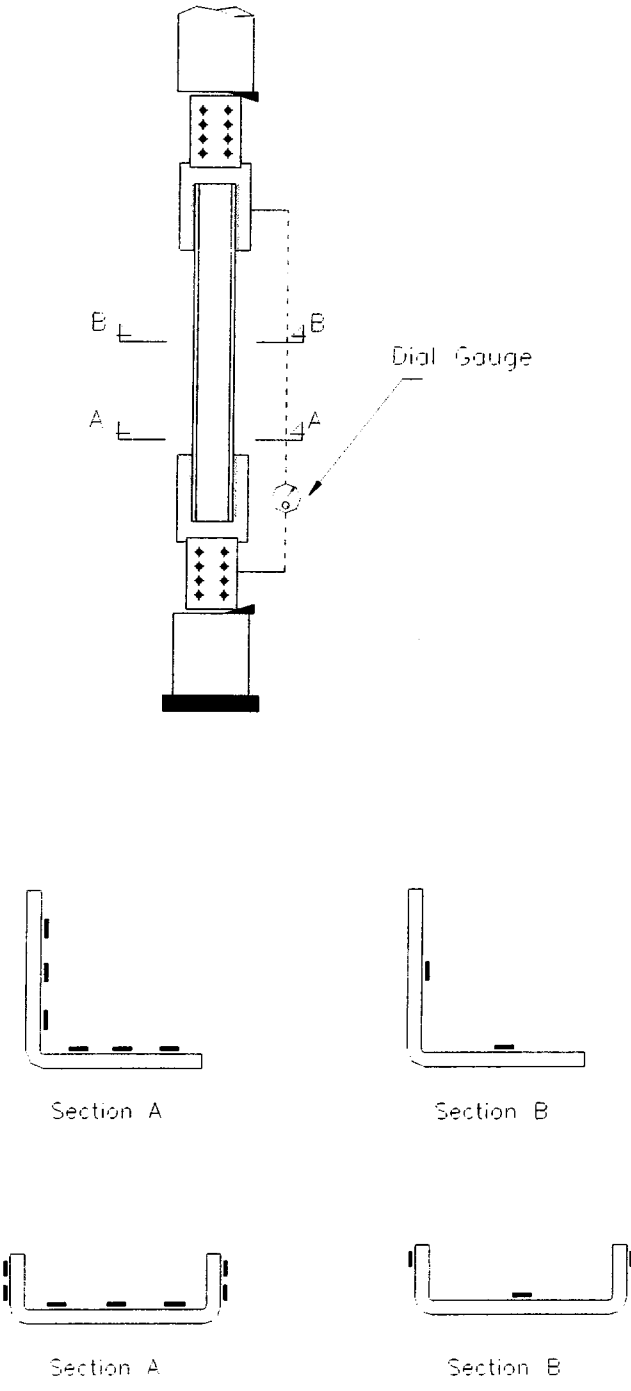

Figure 3.5 Instrumentation

4. Tests Results

4.1 General

This Chapter presents the results obtained in the experimental program described in Chapter 3. The results include the recorded strain distribution at the critical section and the load-deformation relationships for the full-scale tests. In addition, the material properties obtained from the tension coupon test are reported.

4.2 Tension Coupon Tests

Tension coupon specimens were tested to determine the specimens' actual material properties. Table 4.1 shows the measured material properties obtained from these tests. The average material properties for the flat coupons from the angle and channel sections are presented in Table 4.2. To calculate the material properties of the corner coupons it was assumed that both corner and flat coupons have the same modulus of elasticity. The initial cross-sectional area for the corner coupons, A_0, can then be calculated as follows:

$$A_0 = \frac{\Delta P}{\Delta \varepsilon} x \frac{1}{E_{ave}} \qquad [4.1]$$

where

$\Delta P/\Delta \varepsilon$ = slope of the load-strain curve for corner tension coupons.

E_{ave} = average modulus of elasticity obtained from the tensions coupons at the flat portions.

Plots of stress-strain curves resulting from the flat and corner coupons are shown in Figs. 4.1 and 4.2, respectively.

4.3 Full Scale Tests

4.3.1 General Observations

None of the channel specimens fractured at the critical section adjacent to the gusset plate. All channels but specimen C2-1 fractured away from the welds in the middle of the member, as presented in Fig. 4.3. Test C2-1 failed through the weld, as shown in Fig. 4.4. Inspection of the welds showed inadequate welding.

Only specimens A3un-2, A4ba-1, and A4un-1 failed at the connection. Initial yielding was concentrated near the web-flange intersection. Tearing in these angles began in the connected heel at the ends of the welds, as depicted in Fig. 4.5. All others angle specimens, failed at the gross-area away from the connection, as shown in Fig. 4.6.

The failure mode was similar for those channels and angles that failed at gross-area away from the connection. As load was applied, the first yield lines started at the critical section of the member around the corners. As the load increased, the yielded region extended out from the critical sections to the mid-length of the specimen. By the time the load reached its ultimate value, the member started to neck in at the mid-length and failure occurred.

During the loading process significant out-of-plane bending was observed, as shown in Fig. 4.7. Since the angles and channels are eccentric with the load application, they tended to align themselves with the tensile force. This behaviour caused a rotation of the connection that produced bending in a plane normal to the plane of the welds. The gusset plates are relatively flexible in this direction and offered little restraint to the rotation. Out-of-plane bending was more pronounced in the angles because their eccentricity was greater than that of the channels.

The static ultimate strength, mode of failure, and net-section efficiency are summarized in Table 4.3. The net-section efficiency was calculated based on the static ultimate load reached during the test and the measured static ultimate tensile strength of the tension coupon material.

$$\text{N.S.E} = \frac{P_{Test}}{F_u \times A_g} \qquad [4.2]$$

4.3.2 Load –Deformation Relationship

The load-deformation behaviour of the test specimens is reported in this section. The elongation of the specimen reported herein is the stroke recorded by the MTS machine, since, from the readings of dial gauge, there was no major slip between the gusset plates and grips. Load-deformation curves for all specimens are attached in Appendix A.

The load-deformation curve of all test specimens is characterized by a gradual yielding and by a high level of elongation, as shown in Fig. 4.8.

The difference in the behaviour of balanced and unbalanced welded connections of angle specimens is shown in Fig. 4.9. From the plot it is seen that both balanced and unbalanced connections lead to the same ultimate strength. The deformation of specimen A4un-1 was greater than that of specimen A4ba-1. This can be explained by the fact that specimen A4un-1 has a clear distance between the gusset plates greater than that of specimen A4ba-1.

The effect of different connection lengths for angles and channels can be seen in the load versus elongation curves of Fig. 4.10 and Fig. 4.11. Specimens A3un-1 and A3un-2 were 76.2 mm unbalanced welded angle with weld length of 125 and 80 mm, respectively. Figure 4.10 shows that both specimens reach almost the same ultimate strength. However,

specimen A3un-2 (with shorter weld length) failed at the critical section while specimen A3un-1 failed at the mid-length, and therefore specimen A3un-2 yielded a quite poor ductility. The weld lengths for specimen C3-1 and C3-2 were 95 and 80 mm long, respectively. Both specimens failed at the mid-length and reached the same ultimate strength and similar elongation.

From Figs. 4.9 and 4.10 it is apparent that the initial data points of the unbalanced welded angles are not linear. This behaviour is typical for all unbalanced welded angles tested, also shown in Appendix A. This phenomenon can be attributed to the initial accommodation of the in-plane eccentricity due to the unbalanced welds by the specimen. Since the specimen is unbalanced loaded it tends to align itself at the beginning of the loading. However, with increase of the loading this nonlinear behavior diminished.

4.3.3 Strain Distribution

Figure 4.12 shows the load versus strain curves at the critical section of specimen A3ba-1. As expected, the strain was larger in the corners at the end of the welds. Due to the eccentricity of load application the edge of the outstanding leg was in compression under loads up to about 60 percent of the ultimate load (beyond the yielding limit). As the load increased, the compressive strain shifted to tension and increased quickly.

The load versus strain curves for the mid-length section of specimen A3un-1 is shown in Fig. 4.13. At low loads the strain distribution was non-uniform, where the connected leg has a larger strain. Eventually, the strains of the whole section were about uniform as the load increased and the centroid of the angle coincided with the applied load.

The strain distributions across the critical section of specimen A3ba-1 for different levels of loads are shown in Fig. 4.14. At low load level, the strain distribution was relatively uniform; however as the load increased, the distribution became highly non-uniform, especially for the strain around the corner.

A comparison between the strain distributions at the critical section for the 76.2 mm angle with balanced and unbalanced welded connected is presented in Fig. 4.15. This graph was plotted for a load about 68 percent of the ultimate load (last strain gauge reading). At this load level the specimens have already yielded. At the heel location the unbalanced and balanced welded angles have about the same strain. The same situation happens at the toe, where there is little difference between the strain levels. As mentioned above, the stress concentration is quite high at the welded heel. This plot shows that the strains at the welded heel are twice as much as that at the toe. Although 76.2 mm specimens were taken as an example, this behaviour was typical for all angle specimens.

The channel critical section was instrumented with strain gauges from flange-to flange at the end of the welds. The load versus strain curves of specimen C3-1 at the critical section are illustrated in Fig. 4.16 and Fig. 4.17. A higher strain is seen at the corners than at the center of the web and top of the flanges. Fig. 4.18 shows the load versus strain at the mid-length of specimen C3-1. As would be expected the stress was quite uniform at the mid-length.

The experimental strain distributions across the critical section of specimen C3-1 for different levels of loads are shown in Fig. 4.19. As for the angles, at low load level, the strain distribution was relatively uniform; however as the load increased, the distribution became highly non-uniform, especially for the strain around the corners. Either slightly

unbalanced welding, or uneven gripping of the gusset plate contributed to the lack of symmetry in the strain contours.

Table 4.1 Measured Material Properties

Specimen	Modulus of Elasticity (MPa)	Static Yield Strength (MPa)	Dynamic Yield Strength (MPa)	Static Ultimate Strength (MPa)	Dynamic Ultimate Strength (MPa)
AS-1	201000	160	168	278	296
AS-2	206000	162	169	272	294
AS-3	200000	162	170	275	296
AS-4*	202000	315	319	319	340
CS-1	197000	169	178	273	294
CS-2	197000	169	180	276	296
CS-3	204000	169	182	276	297
CS-4*	199000	310	321	316	330

* corner coupon.

Table 4.2 Average Material Properties of Flat Coupons

Material	Modulus of Elasticity (MPa)	Static Yield Strength (MPa)	Dynamic Yield Strength (MPa)	Static Ultimate Strength (MPa)	Dynamic Ultimate Strength (MPa)
Angle	202000	161	169	275	295
Channel	199000	169	180	275	296

Table 4.3 Experimental Results

Test Specimen	Member (mm x mm x mm)	Gross Area (mm^2)	Ultimate Strength (MPa)	P_{test} (kN)	P_{ult} (kN)	Mode of Failure	Efficiency
C2-1	50.4x28x2.63	257.6	275	60.3	70.84	Weld failure	-
C2-2	50.4x28x2.63	257.6	275	74.1	70.84	Gross-area	1.046
C3-1	76.6x28x2.63	326.5	275	85	89.79	Gross-area	0.947
C3-2	76.6x28x2.63	326.5	275	85	89.79	Gross-area	0.947
C4-1	101.3x28x2.63	391.5	275	107.7	107.66	Gross-area	1.00
A2ba-1	50.6x50.6x2.63	255.0	275	71.8	70.13	Gross-area	1.024
A2un-1	50.6x50.6x2.63	255.0	275	73.42	70.13	Gross-area	1.047
A3ba-1	75.6x75.6x2.63	386.6	275	109.6	106.32	Gross-area	1.031
A3un-1	75.6x75.6x2.63	386.6	275	111	106.32	Gross-area	1.044
A3un-2	75.6x75.6x2.63	386.6	275	102	106.32	Net-section Fracture	0.959
A4ba-1	101.2x101.2x2.63	521.2	275	142.7	143.33	Net-section Fracture	0.996
A4un-1	101.2x101.2x2.63	521.2	275	142.7	143.33	Net-section Fracture	0.996

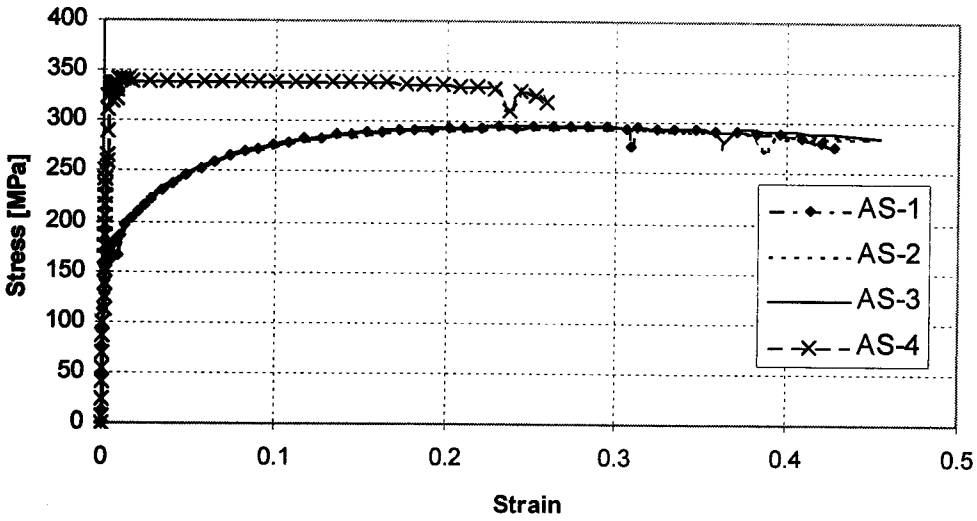

Figure 4.1 Stress-Strain Curve for Tension Coupons Cut from the Angle Section

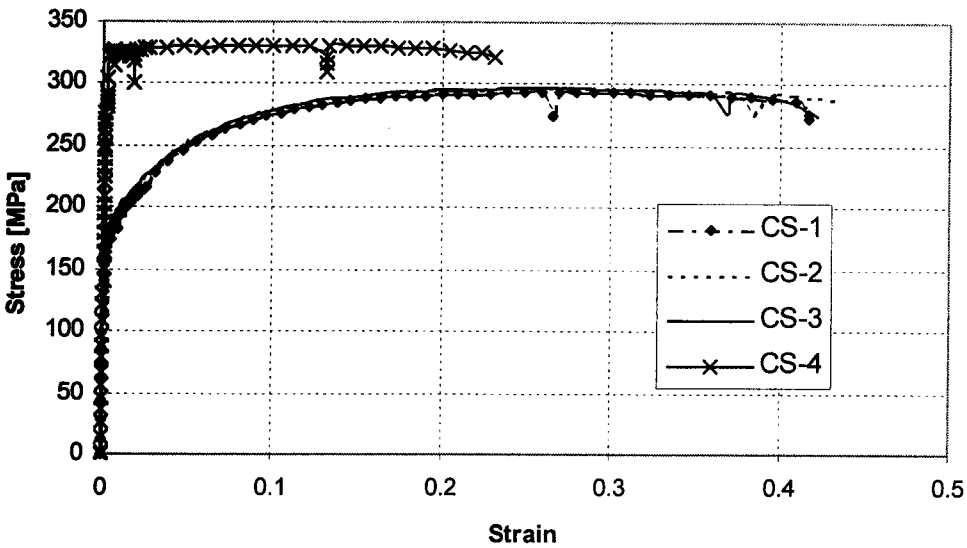

Figure 4.2 Stress-Strain curve for Tension Coupons cut from the Channel Section

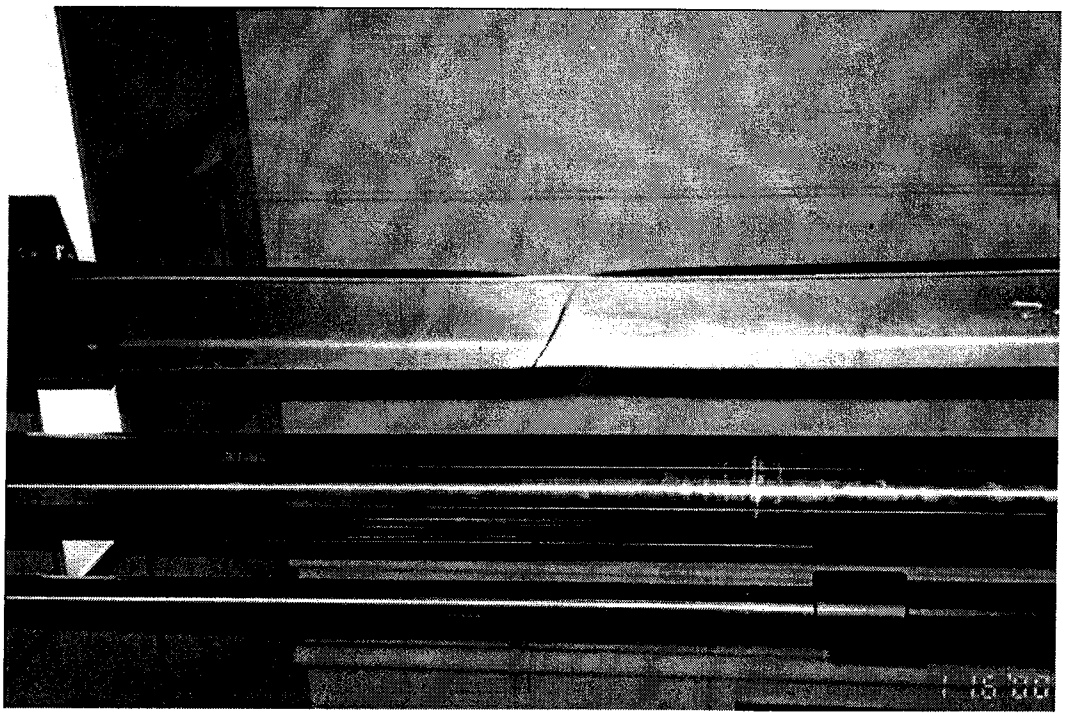

Figure 4.3 Typical Mode of Failure of the Channels (Specimen C3-2)

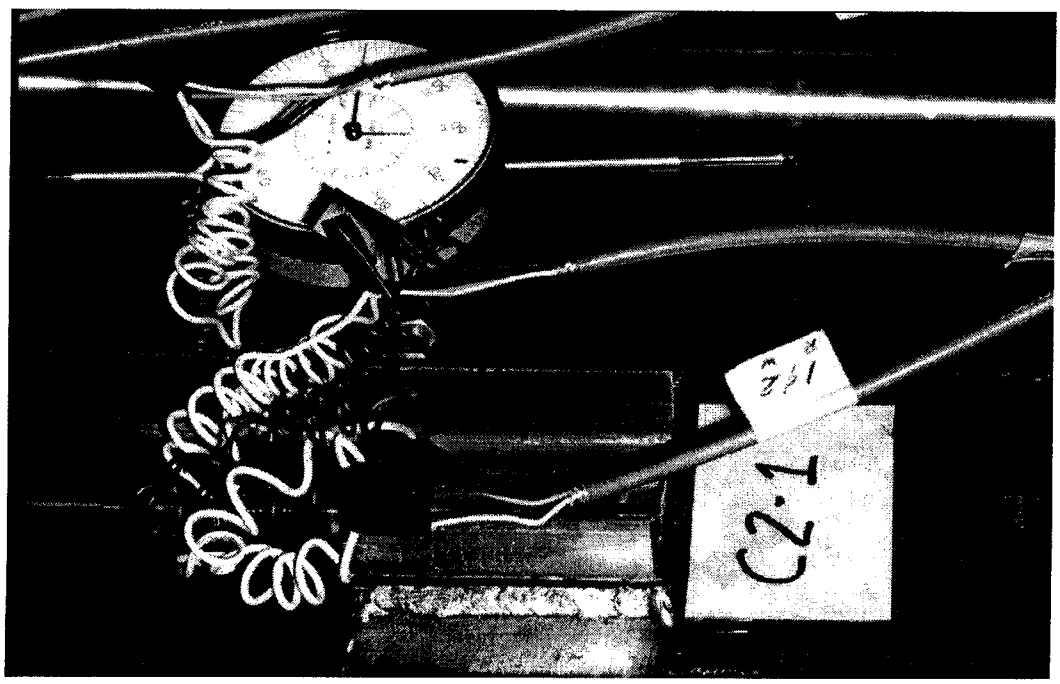

Figure 4.4 Mode of Failure of Specimen C2-1

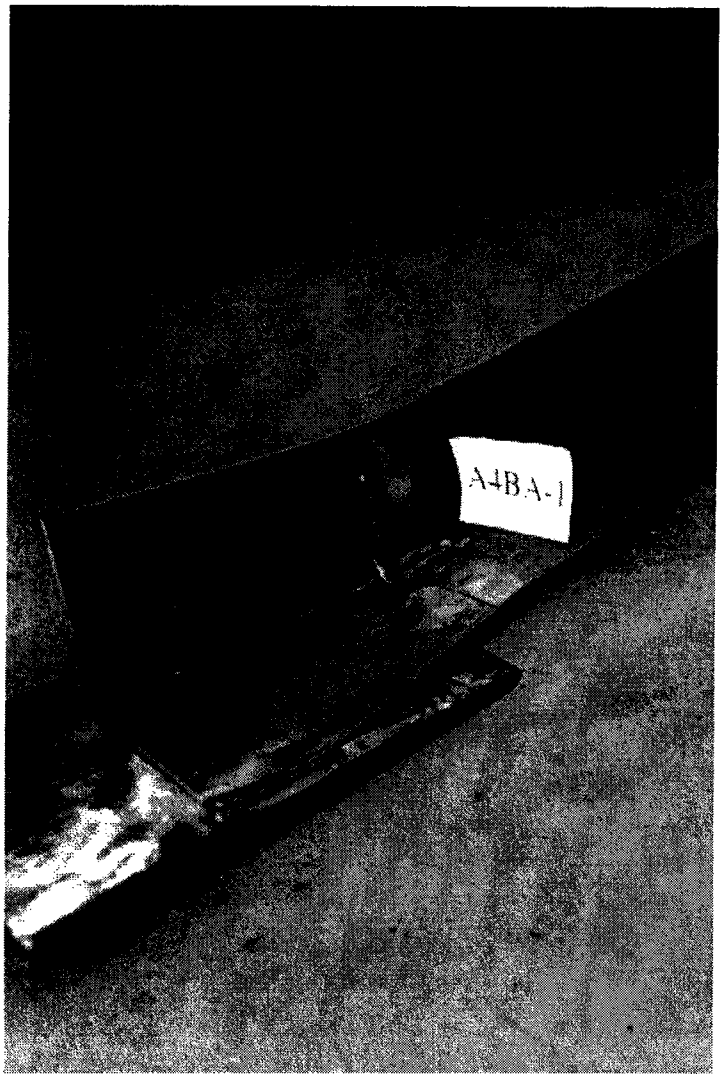

Figure 4.5 Tearing at the Connected Heel

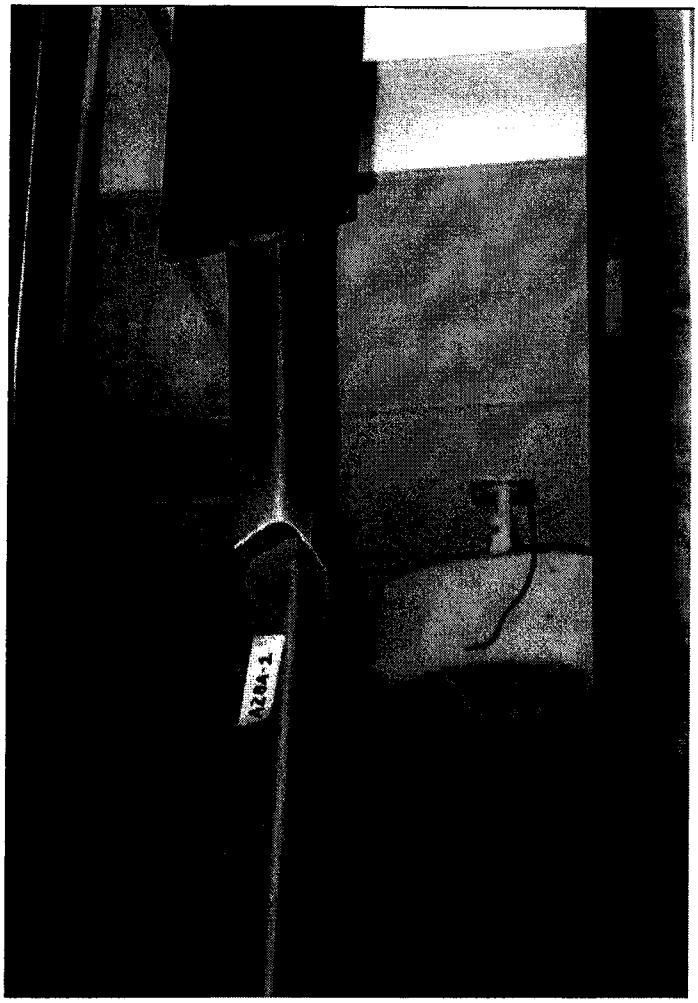

Figure 4.6 Failure at the Gross-Area

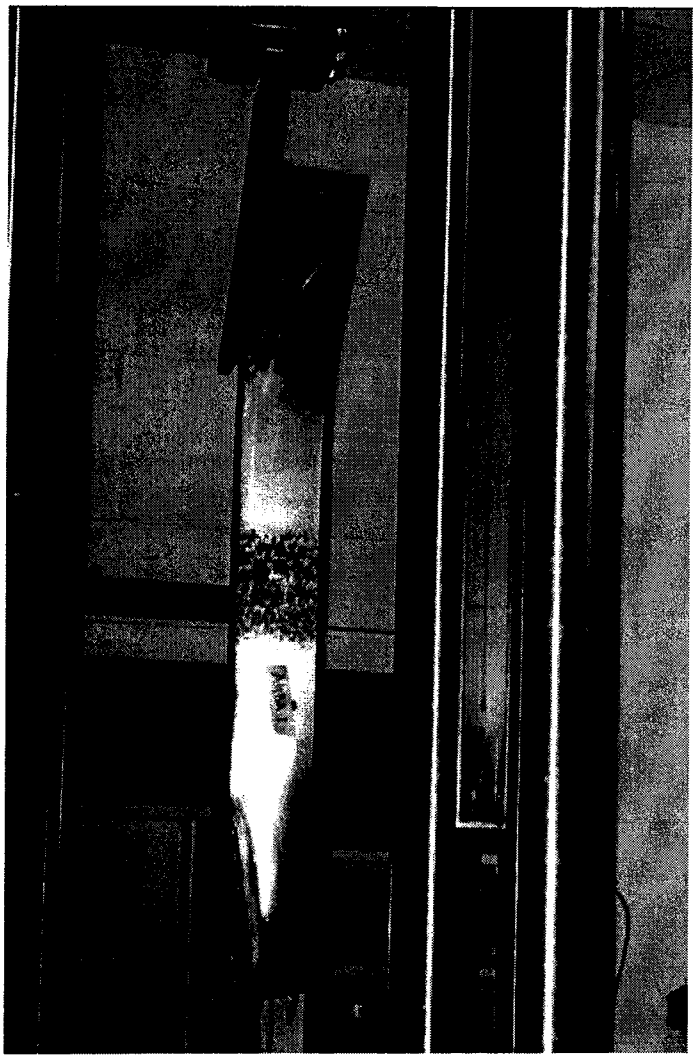

Figure 4.7 Out-of-Plane Bending

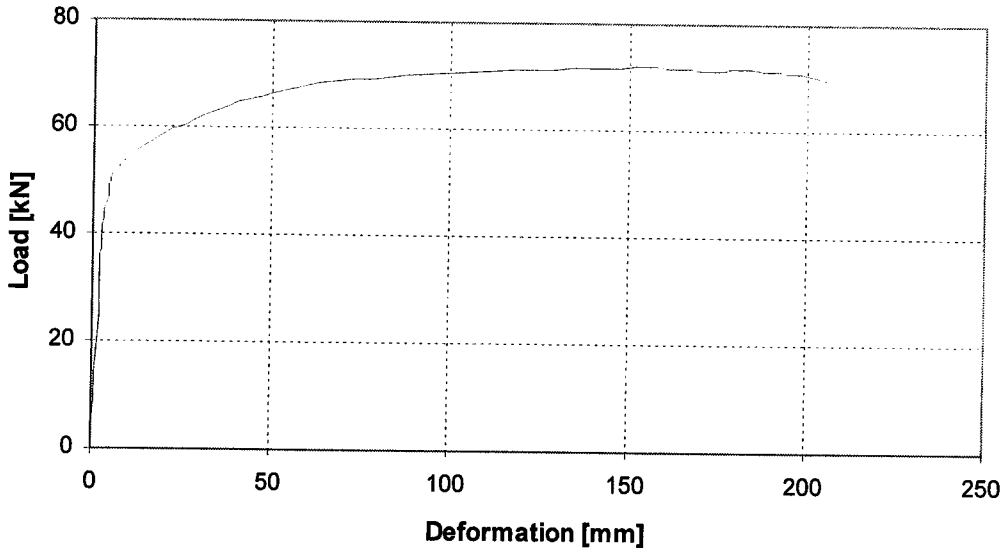

Figure 4.8 Load vs. Deformation for A2ba-1

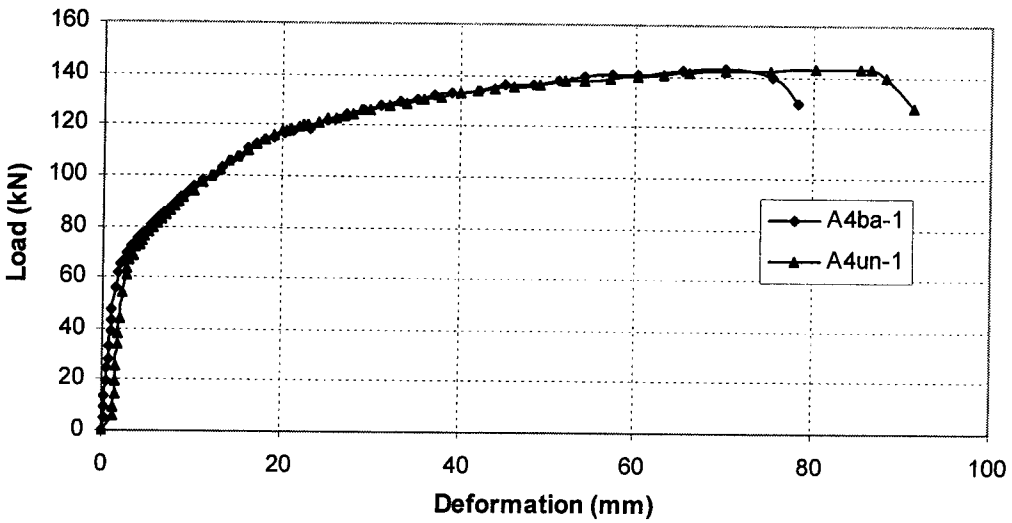

Figure 4.9 Load vs. Deformation for A4ba-1 and A4un-1

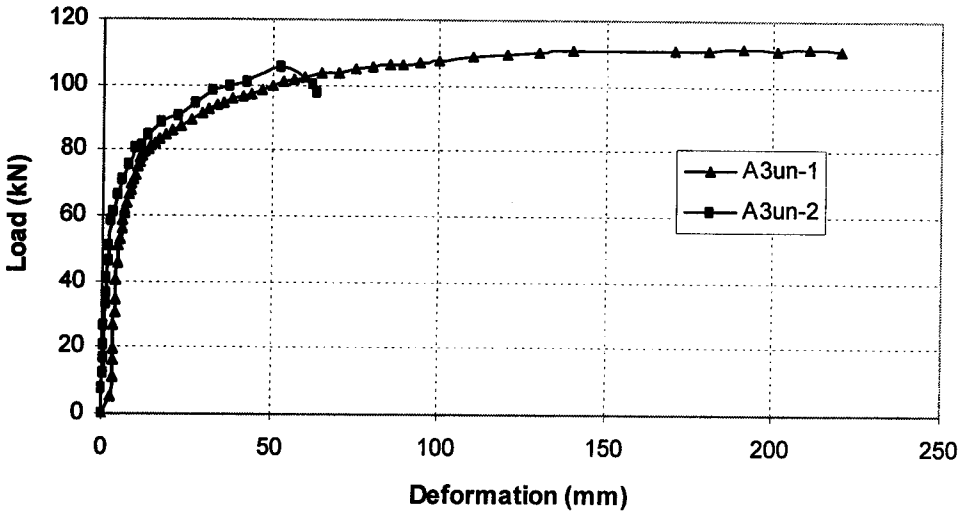

Figure 4.10 Load vs. Deformation for A3un-1 and A3un-2

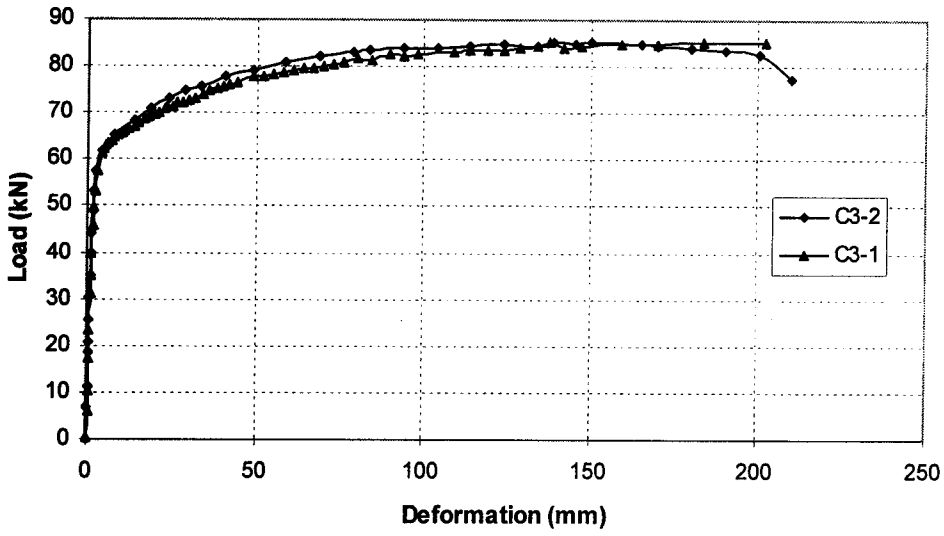

Figure 4.11 Load vs. Deformation for C3-1 and C3-2

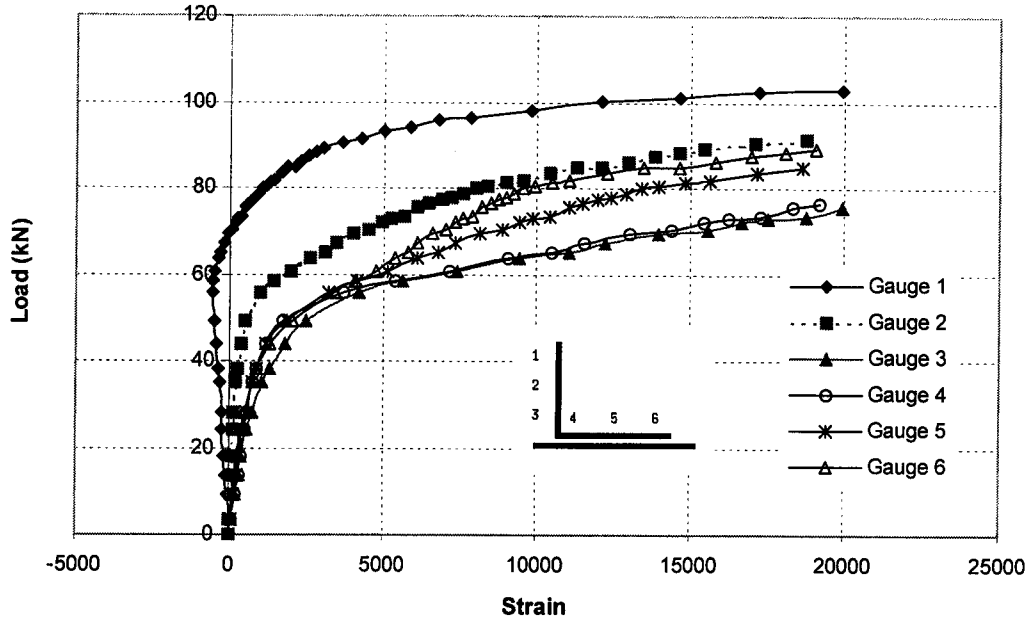

Figure 4.12 Load vs. Strain at the Critical Section for A3ba-1

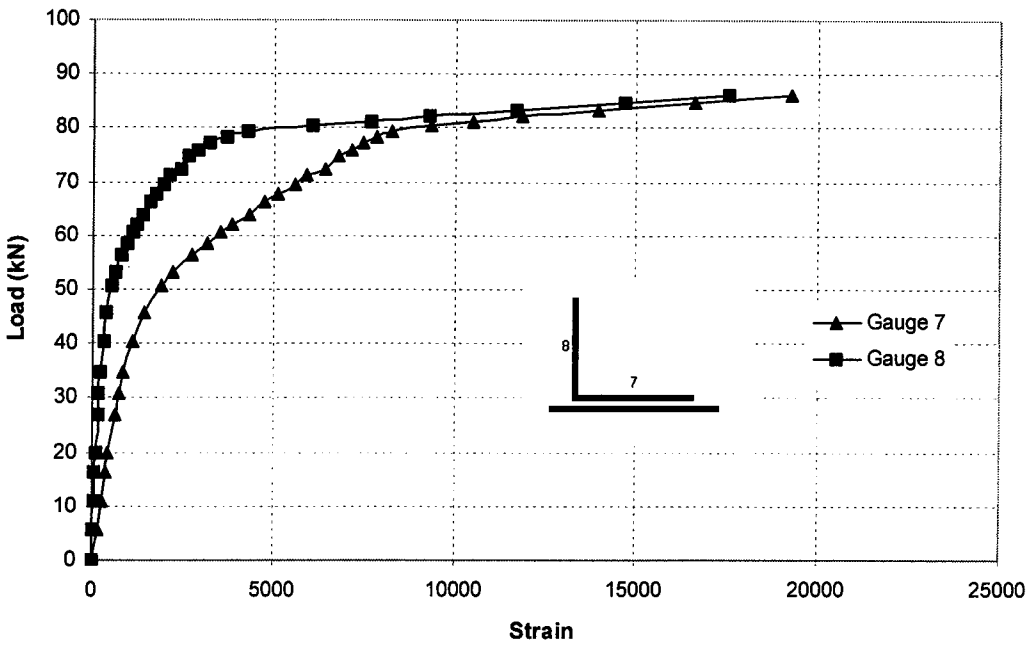

Figure 4.13 Load vs. Strain at the Mid-Length for A3un-1

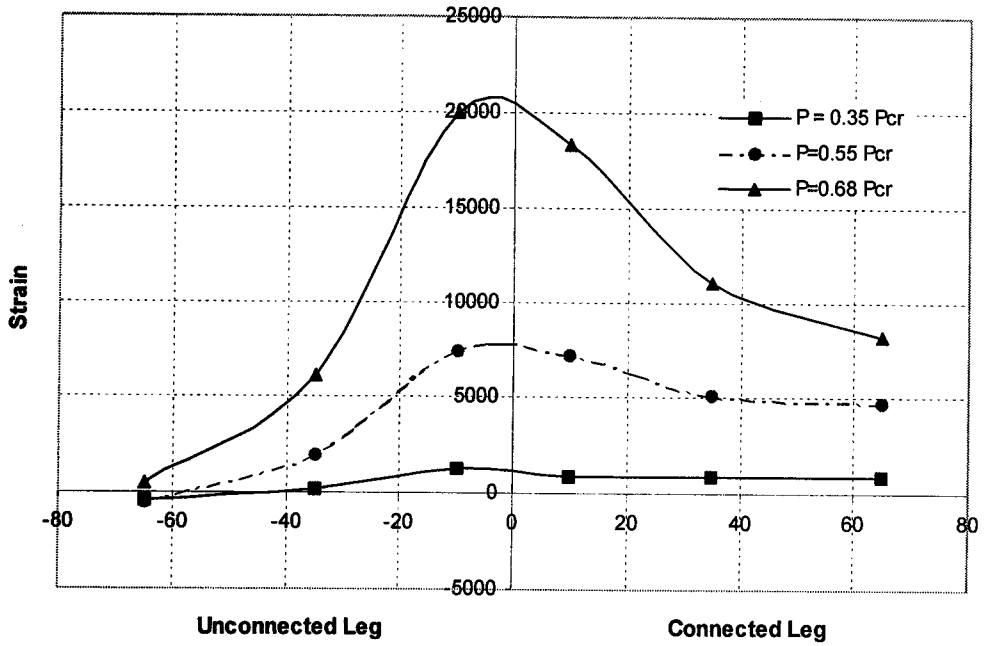

Figure 4.14 Strain Distribution at the Critical Section of A3ba-1

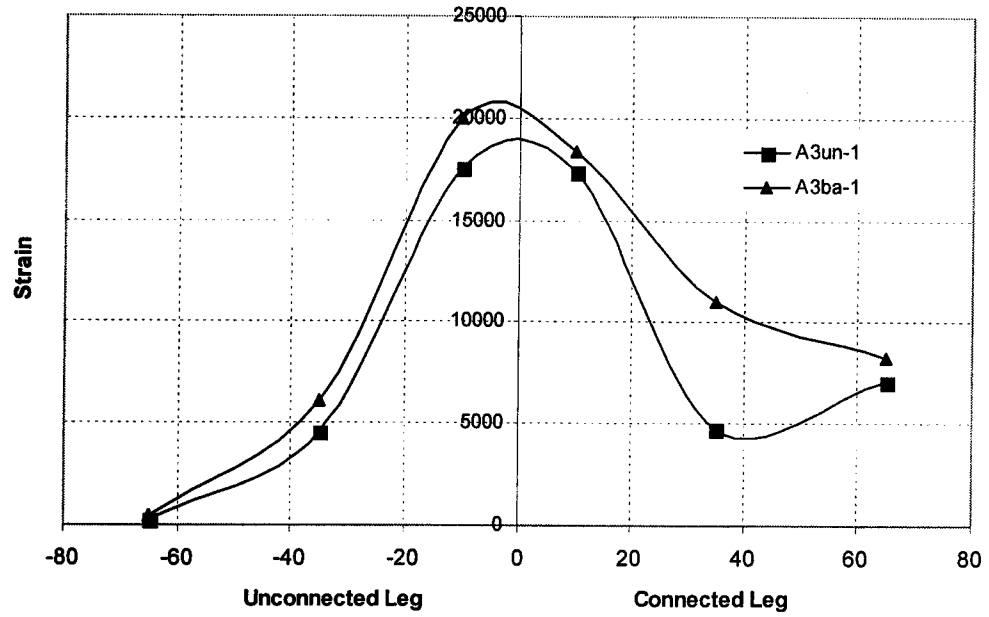

Figure 4.15 Strain Distribution at the Critical Section of A3ba-1 and A3un-1

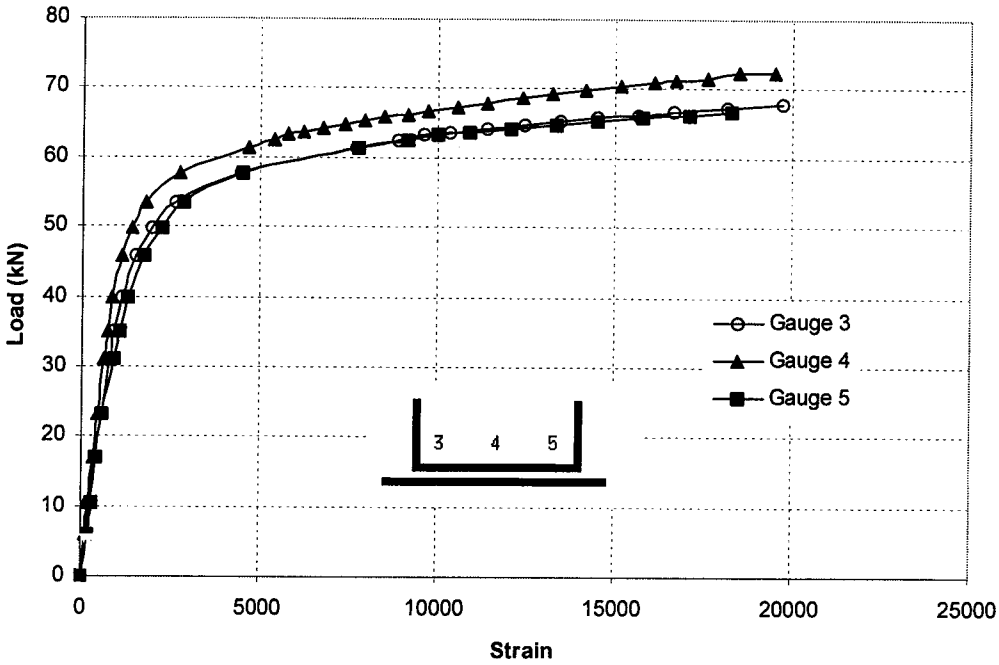

Figure 4.16 Load vs. Strain at the Critical Section at the Web for C3-1

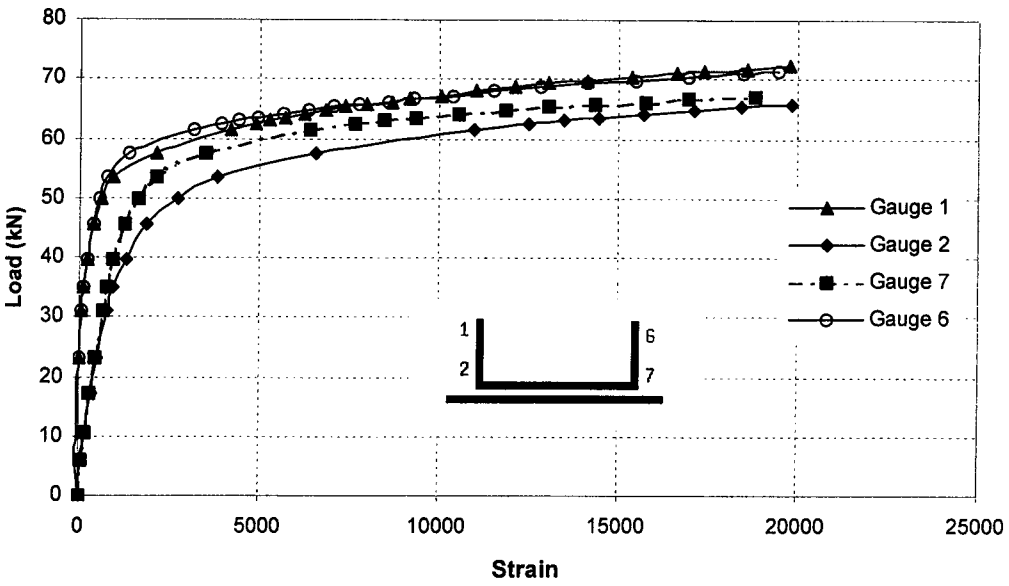

Figure 4.17 Load vs. Strain at the Critical Section at the Flange for C3-1

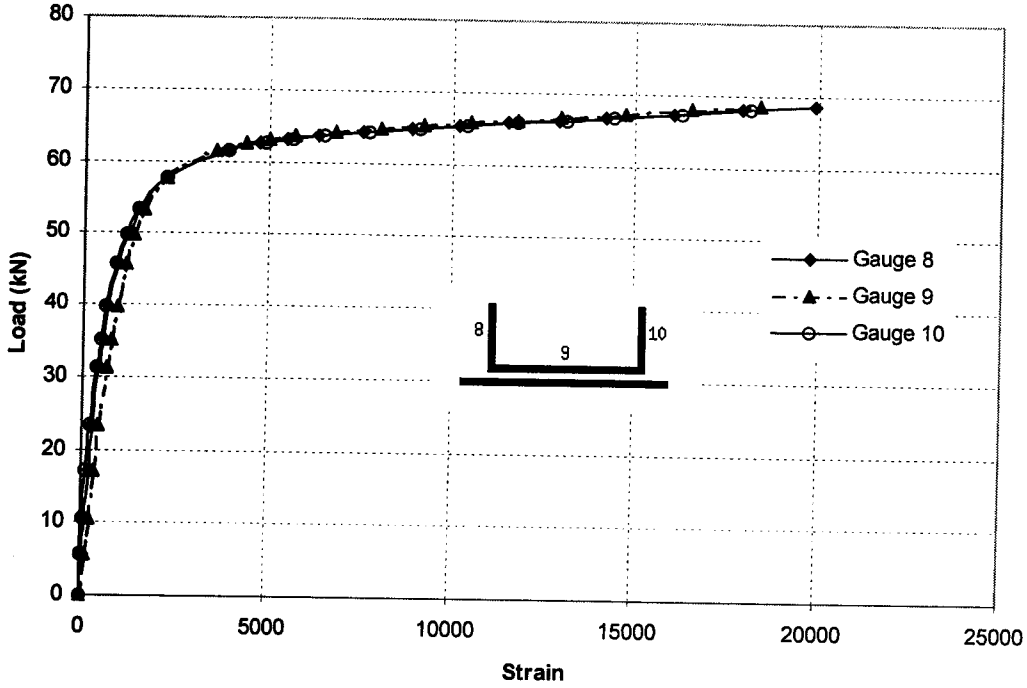

Figure 4.18 Load vs. Strain at the Mid-Length Section for C3-1

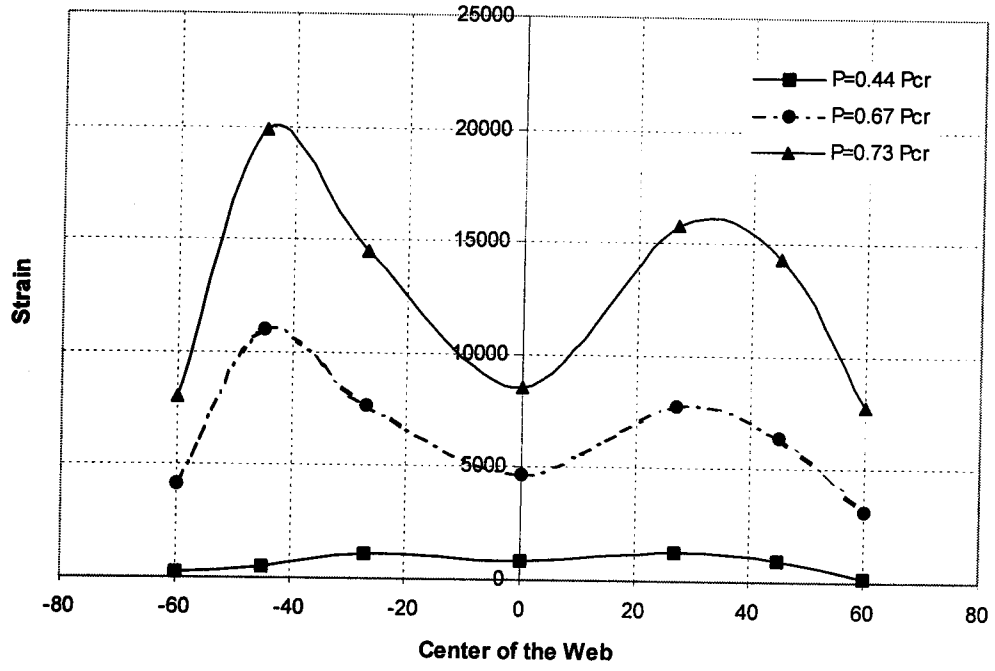

Figure 4.19 Strain Distribution at the Critical Section of C3-1

5. Finite Element Analysis

5.1 General

The purpose of the second part of this research was to determine how the behaviour of welded cold-formed tension members can be reliably predicted using the finite element method. By comparing the results of an analytical model to the results obtained in the experimental study, one may determine the validity of such a model. The finite element analysis was limited to modeling the tests that were performed as described in Chapter 3. The analysis was performed using ABAQUS 5.8 (1998), a commercially available finite element package. The finite-element models gave reasonable prediction in load-deformation curves, strain distribution across the cross-section, failure mode, and deformed shape. Typical input files used to generate C3-1 and A3ba-1 finite element models are presented in Appendix B.

5.2 Finite Element Model

The quadrilateral shell element S4R from the ABAQUS library was used to generate the models. The S4R element is a four-node shell element formulated for large-strain analysis. It accounts for finite membrane strain problems and allows for change in thickness. Each node has six degrees of freedom: three translational and three rotational components. Symmetry of the test specimens about the mid-length allowed modeling only half of the member length, reducing the number of degrees of freedom and, therefore, reducing the computational time required to obtain a numerical solution.

To determine an optimal mesh configuration, three models were constructed using three different meshes: coarse, intermediate, and fine mesh. The meshes are shown in Fig. 5.1 and the number of elements, element sizes and predicted loads are presented in Table 5.1. The maximum predicted load was about the same for all meshes sizes. The intermediate mesh was chosen as the optimal mesh for practical reasons. It leads to a more realistic boundary condition (gusset plate/specimen) when compared to the coarse mesh, and it requires less computational time when compared to the fine mesh. A typical mesh of the models is shown in Fig. 5.2.

To simulate the actual test conditions, the boundary conditions of the finite element model had to be chosen carefully. Since there was little deformation in the weld metal between gusset plate and specimen, rigid beams were used to connect the specimens to the gusset plates.

The load was applied across the cross section at the mid-length of the member. Rotation about "2" (out-of-plane) and "3" (in-plane) axes at the loaded end of member was constrained. In order to account for the out-of-plane bending, rotation of the gusset plate was allowed about the "2" axis. The coordinate system is depicted in Fig. 5.1.

5.3 Material Properties

The material properties used in the analysis were based on the results of the tension coupon tests described in Chapter 4. As seen in Figs. 4.1 and 4.2 different material properties were used for the flat and corner portions of the specimen. This is to account for the effects of cold-forming. Measured engineering stress and stain properties obtained from the coupon tests were transformed into true stress and strain to use in the analytical model.

Figures 5.3 and 5.4 show the material used to model the angle and channel sections. In the analysis, the materials were assumed to behave according to the incremental isotropic hardening material.

Different rupture strains were chosen for the flat and corner portions of the specimen. The mechanical properties of the corners are changed due to welding and cold-forming process. Kenneth W. Karren (1967) showed that the corners ductility drops rapidly with increasing amounts of cold work. The reduction in percentage elongation of the corners as compared to that of the virgin material can be as large as 90%. The rupture strains used for the flat portion of angles and channels were obtained from the coupon tests based on the following equation:

$$\text{Rupture Strain} = Ln\frac{A_0}{A} \qquad [5.1]$$

where A = cross sectional area of the tension coupon at rupture

A_0 = initial cross sectional area of the tension coupon

Since there was no effective way of measuring the cross sectional area of the corners at rupture, the rupture strain was determined by trial and error. A value of 0.90 and 0.65 was used for the flat portion and corner portion of the model, respectively.

5.4 Analytical Results

The following sections present a comparison between the analytical and the experimental results. Those comparisons are based on the load-deformation relationship, strain distribution at the critical cross-section, and mode of failure. Table 5.2 presents the summary of the analytical ultimate strength and shows a comparison with the experimental results. Except for specimens C3-1 and C3-2, the analytical predictions of the ultimate load

are all within 6% of the physical test results values. All 76.2 mm channels are believed to be from another batch having different material properties.

5.4.1 Load-Deformation Relationship

The general shape of the load-deformation response obtained analytically is in good agreement with that observed in the experiment. Fig. 5.5 shows the experimental and analytical load versus deformation curves for specimen A2ba-1. The load-deformations curves for the other specimens are presented in Appendix C. It can be seen that the curves from the analysis agree quite well to the tests results. For some specimens, however, the predicted limit elongation is significantly greater than that of the physical tests. Most of this situation is due to simplified assumption of the rupture strains used in the analysis. For the case of specimens C3-1 and C4-1, it can also be explained by the fact that the actual specimens could not be failed since the stroke capacity of the testing machine was exceeded.

5.4.2 Strain and Stress Distribution

The strain and stress obtained from the finite element analysis were taken as an average of the outer and inner fibers of the shell element. The typical strain distributions at the critical cross section obtained from the analysis for the angle and channel are shown in Fig. 5.6 and Fig. 5.7 for specimens A3ba-1 and C3-1, respectively. Similar to the test results, the analyses show that the strain distribution across the critical section is highly non-uniform, being larger at the corners. It is also noted from the plots that the edge of the outstanding leg of angle is in compression at the early load level, which agrees with the

physical tests. Figure 5.8 presents the experimental and analytical strain distribution at three different load levels for specimen A2un-1. Similar to the test results, at low load level the strain distribution was relatively uniform. As the load increases, the distribution became highly non-uniform, especially at the welds location. It can be seen that the finite element analysis is a good predictor of the physical tests.

The analytical stress contour of specimens A4ba-1 and C2-2 at the last load step is shown in Figs. 5.9 and 5.10. In these plots, darker colors represent higher stresses. As shown in Fig. 5.9 specimen A4ba-1 has a large stress concentration in the heel at the end of the weld, where failure occurred in the actual test. Figure 5.10 shows that specimen C2-2 experiences a greater stress at mid-length as observed in the test.

The stress distribution of each finite element model was examined at the critical cross section and mid-length. A typical stress distribution at the connection is shown in Fig. 5.11 for specimen A2ba-1. It can be seen that there is a large stress concentration at the corner at the end of the weld. Fig. 5.12 compares the stress distribution at the critical cross section of specimens A3un-1 and A3un-2. It is illustrated that a considerable increase in stress concentration occurs when the weld length is reduced. Due to this large stress concentration specimen A3un-2 failed at the connection. Figure 5.13 shows the stress distribution at the critical section and mid-length of specimen C3-2. Although the stress concentration is quite high at the critical section, the member still failed at the mid-length. This is explained by the fact the connected portion of the member can not contract due to the constraint of the weld. This is believed to increase the strength of the member at the connection as compared with that at the mid-length. Therefore, the connected portion of the member can carry more load than the mid-length, which is free to neck (Cheng *et al.* 1998).

5.4.3 Mode of Failure

The mode of failure and deformed shape obtained from the finite element models were compared to the configurations observed during the tests. Figures 5.14 and 5.15 show the mode of failure obtained from both the analytical analysis and the physical test for specimens A2un-1 and A4ba-1, respectively. Similar to the experimental result, specimen A2un-1 failed in the mid-length. Figure 5.14 shows that the unconnected leg of specimen A4ba-1 bent outward as observed in the test. Figure 5.16 presents a side view of specimen A4ba-1. Comparing Fig. 5.16 and Fig. 4.7, it can be seen that the finite element model also predicts the out-of-plane bending of the specimens well. Except for specimen A4un-1, the analytical model was in good agreement with the physical tests. For specimen A4un-1, in the analysis the unconnected leg bent inward instead of outward. This can be attributed to the different arrangement of the welds at the bend of the angle between the experimental and analytical conditions. However, the difference in deformation does not affect the load deformation behaviour of the specimen.

Table 5.1 Meshes Size Study Configuration and Results

Mesh	# of elements	Element Size	Load (kN)
Coarse	350	10.93x15	77.32
Intermediate	1026	6.16x7	77.32
Fine	2550	3.10x5	77.48

Table 5.2 Analytical Results

Specimen	Size (mm)	Ultimate Load (kN) Test	Analysis	Test/ Analysis
C2-1	50.4x28x2.63	60.3	-	-
C2-2	50.4x28x2.63	74.1	77.32	0.96
C3-1	76.6x28x2.63	85	97.23	0.87
C3-2	76.6x28x2.63	85	97.25	0.87
C4-1	101.3x28x2.63	107.7	112.6	0.96
A2ba-1	50.6x50.6x2.63	71.8	71.82	1.00
A2un-1	50.6x50.6x2.63	73.42	73.42	1.00
A3ba-1	75.6x75.6x2.63	109.6	109.4	1.00
A3un-1	75.6x75.6x2.63	111	109.4	1.01
A3un-2	75.6x75.6x2.63	102	108.5	0.94
A4ba-1	101.2x101.2x2.63	142.7	143.5	0.99
A4un-1	101.2x101.2x2.63	142.7	145.1	0.98

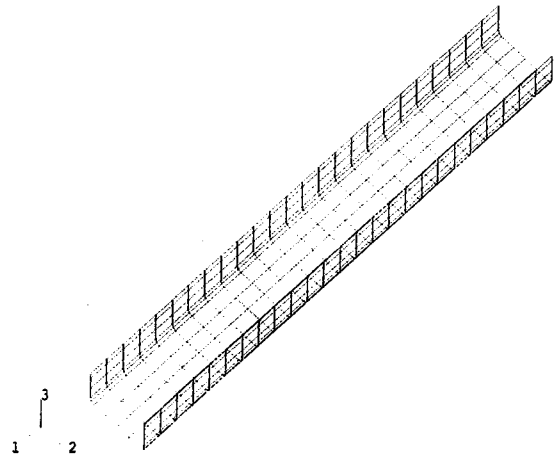

a) Coarse Mesh

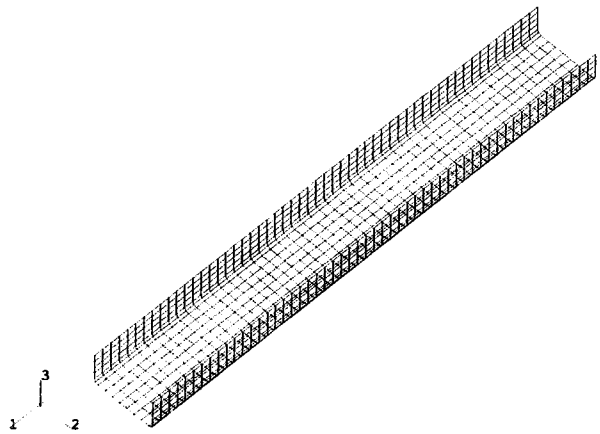

b) Intermediate Mesh

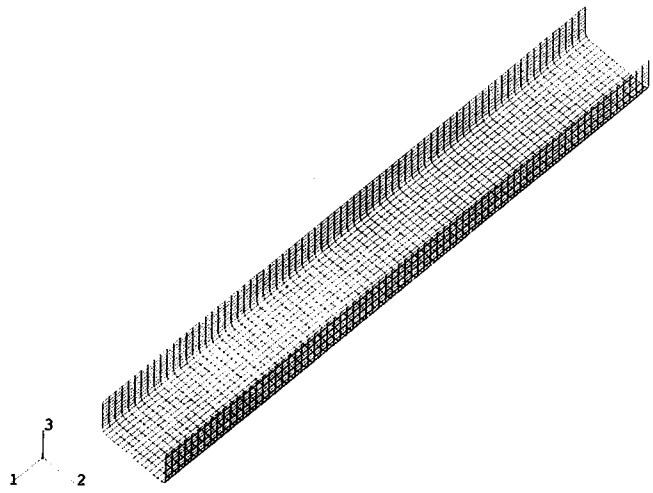

c) Fine Mesh

Figure 5.1 Mesh Size Study for C2-2 Specimen

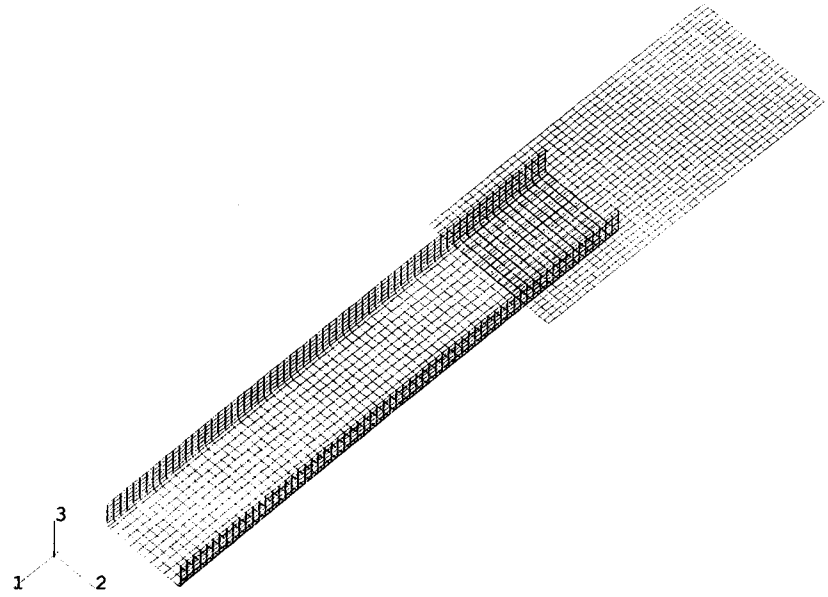

a) Specimen C3-1

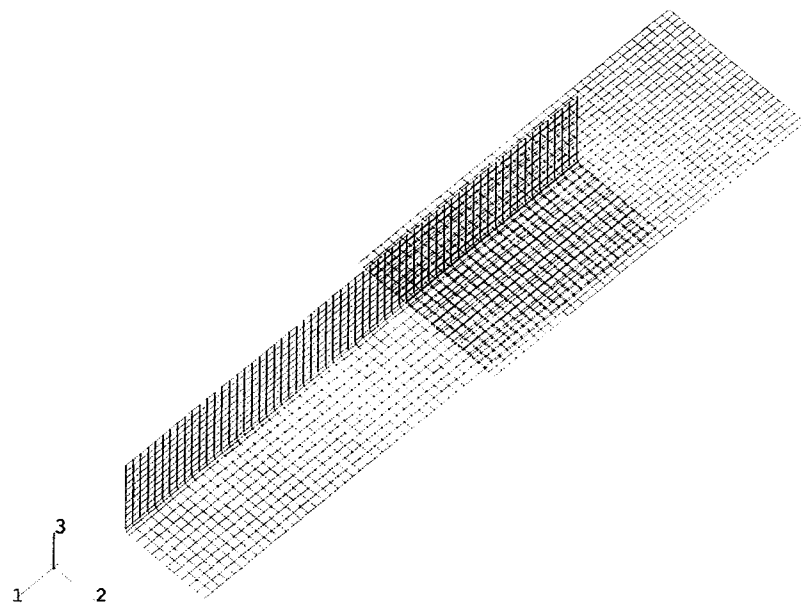

b) Specimen A3ba-1

Fig 5.2 Typical Finite Element Mesh

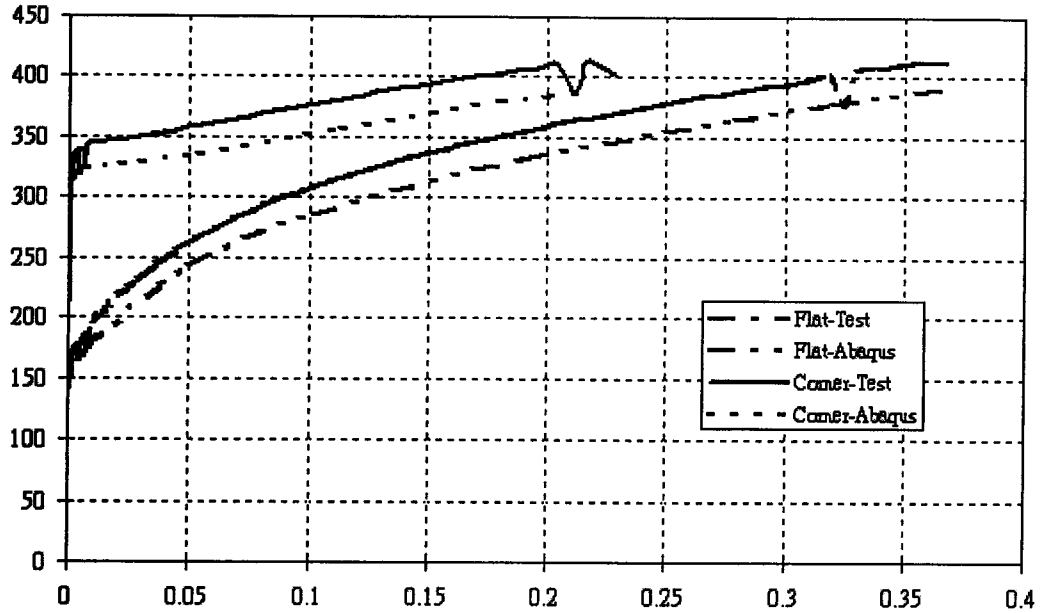

Figure 5.3 Material Model for Angle Sections

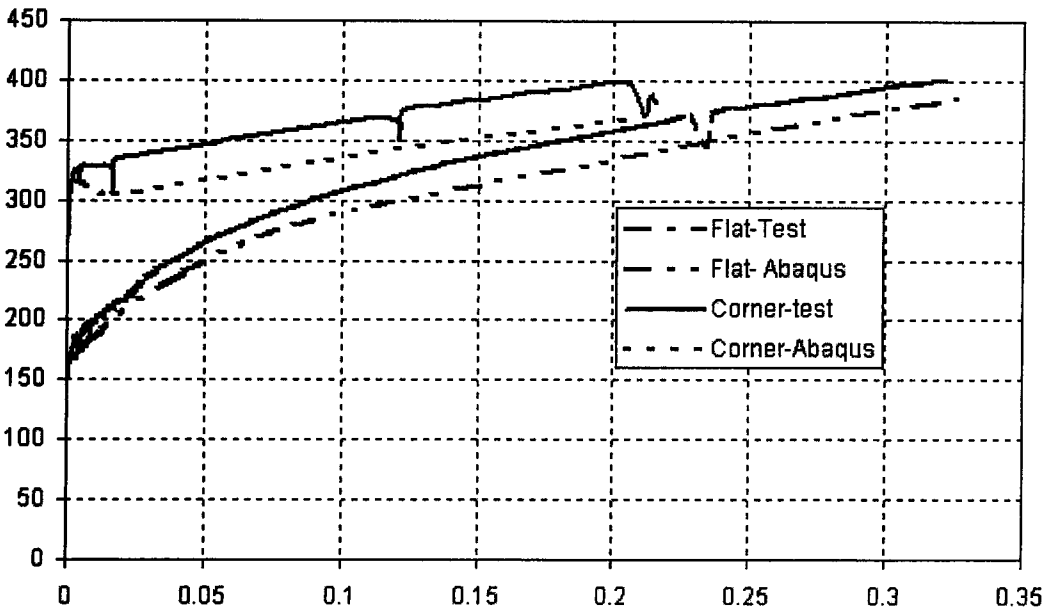

Figure 5.4 Material Model for Channel Sections

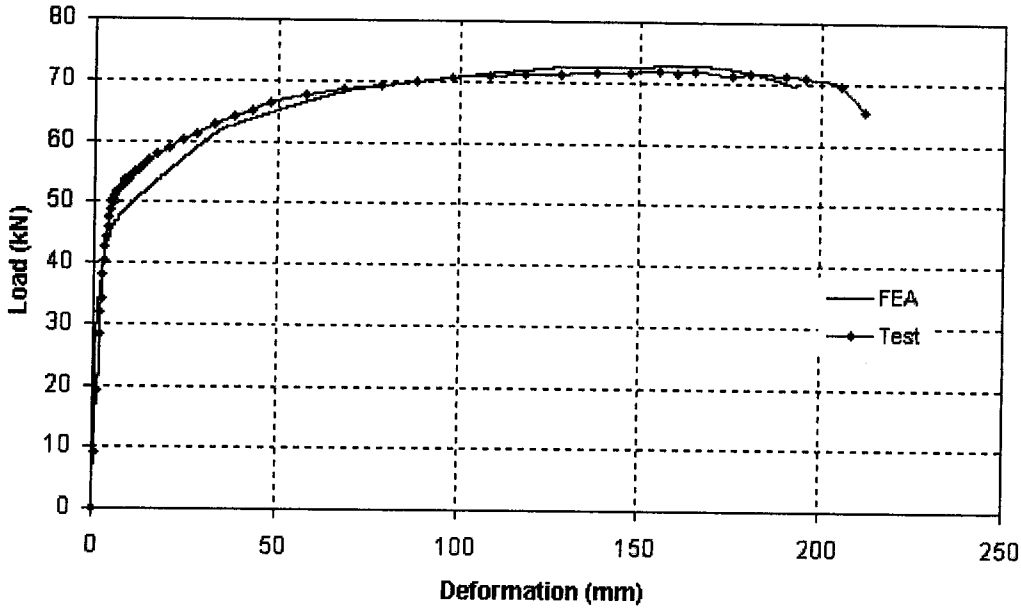

Figure 5.5 Comparison of Load vs. Deformation for A2ba-1

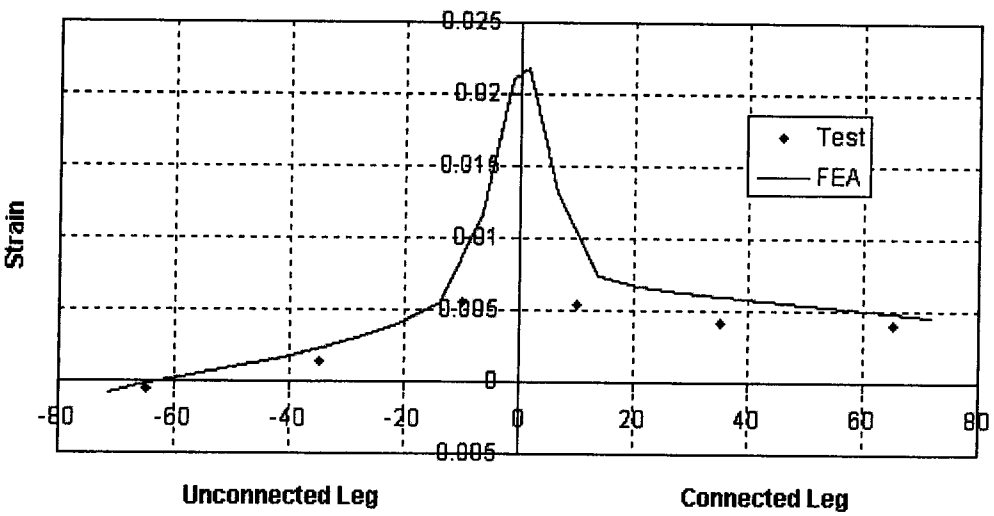

Figure 5.6 Strain Distribution of Specimen A3ba-1at Critical Section (P=0.54Pcr)

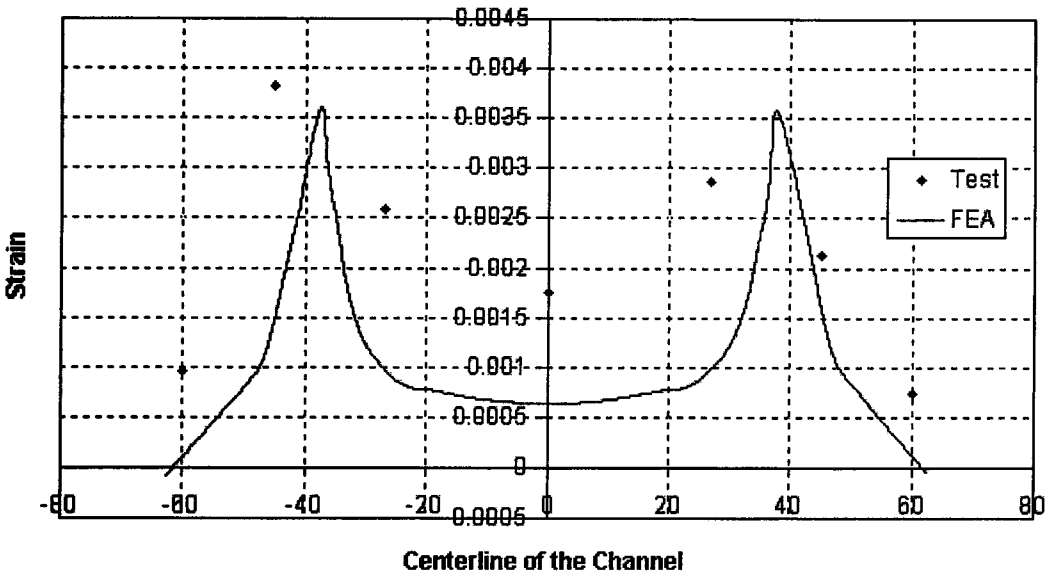

Figure 5.7 Strain Distribution of Specimen C3-1at Critical Section (P=0.55Pcr)

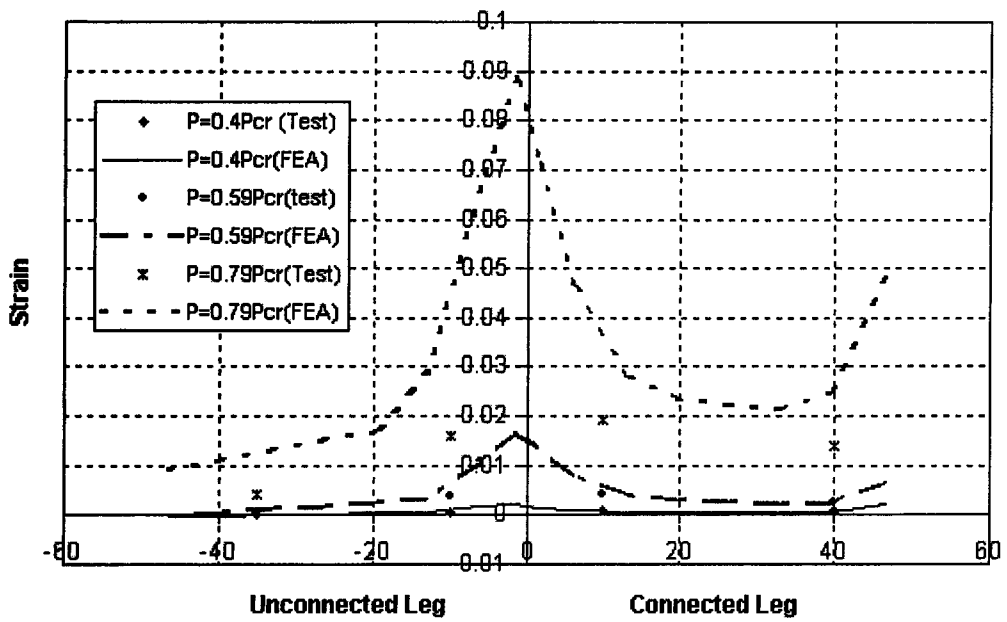

Figure 5.8 Strain Distribution of Specimen A2un-1at Critical Section

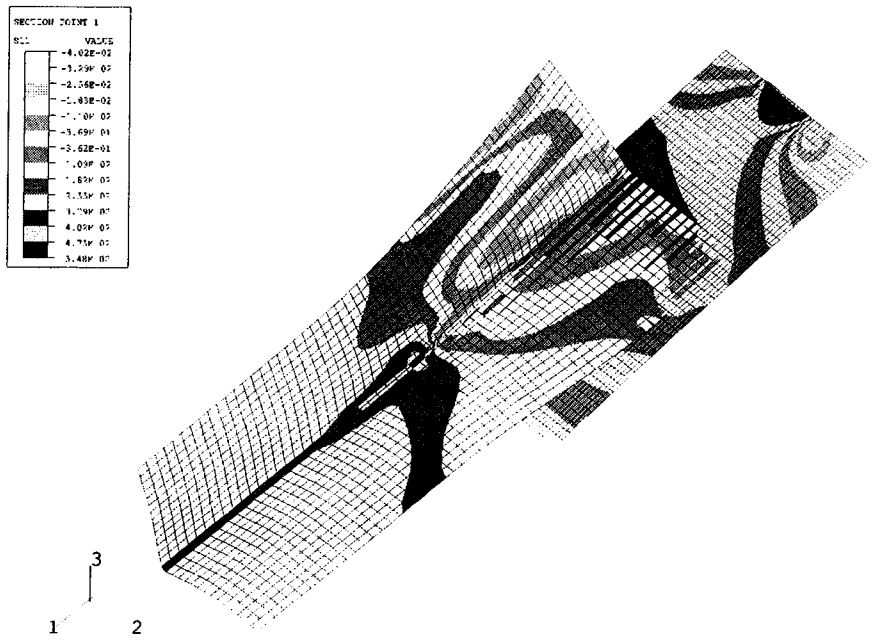

Figure 5.9 Stress (in load Direction) Contour of Specimen A4ba-1 at the Ultimate Load

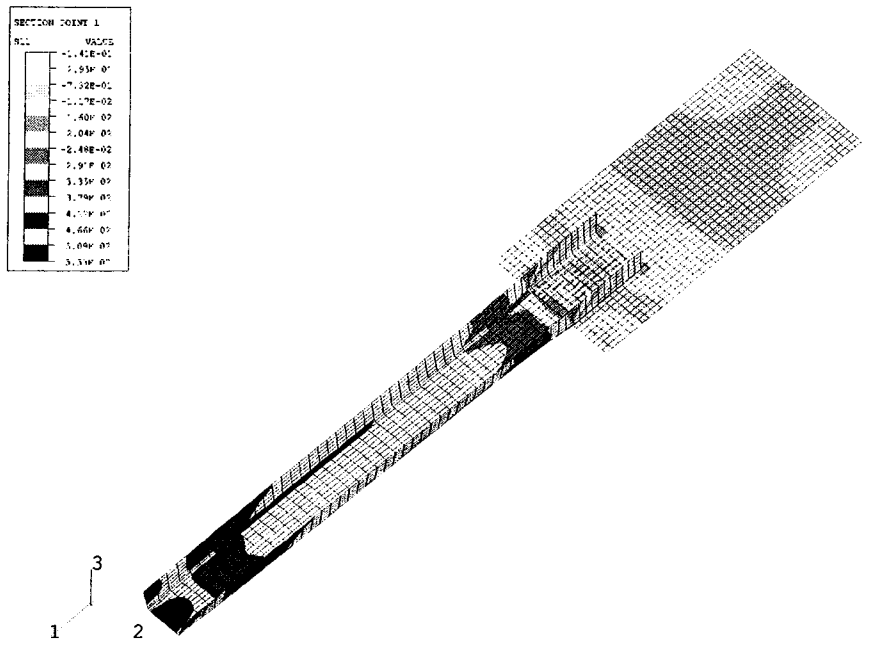

Figure 5.10 Stress (in Load Direction) Contour of Specimen C2-2 at the Ultimate Load

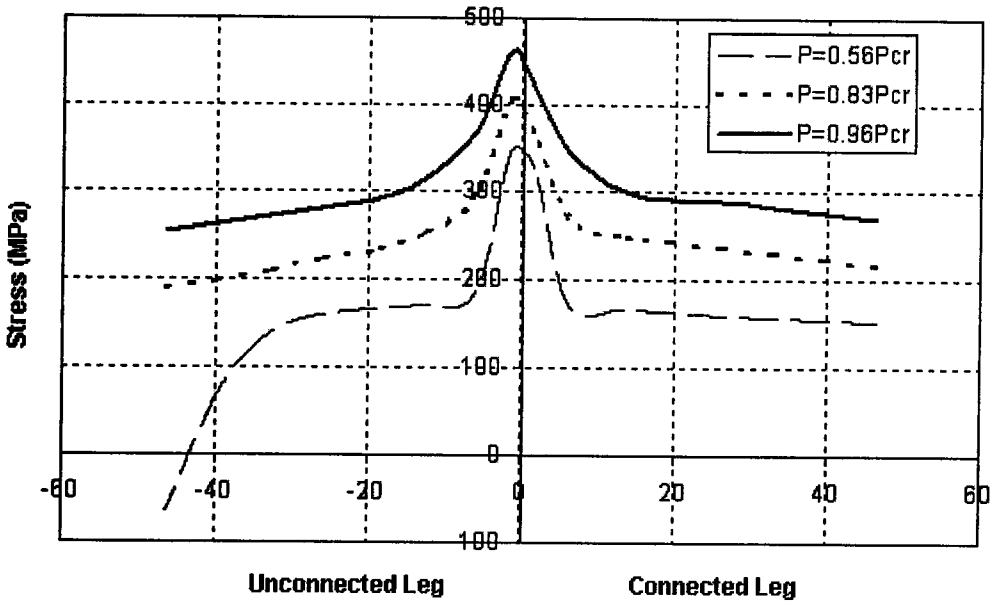

Figure 5.11 Stress Distribution of Specimen A2ba-1at Critical Section

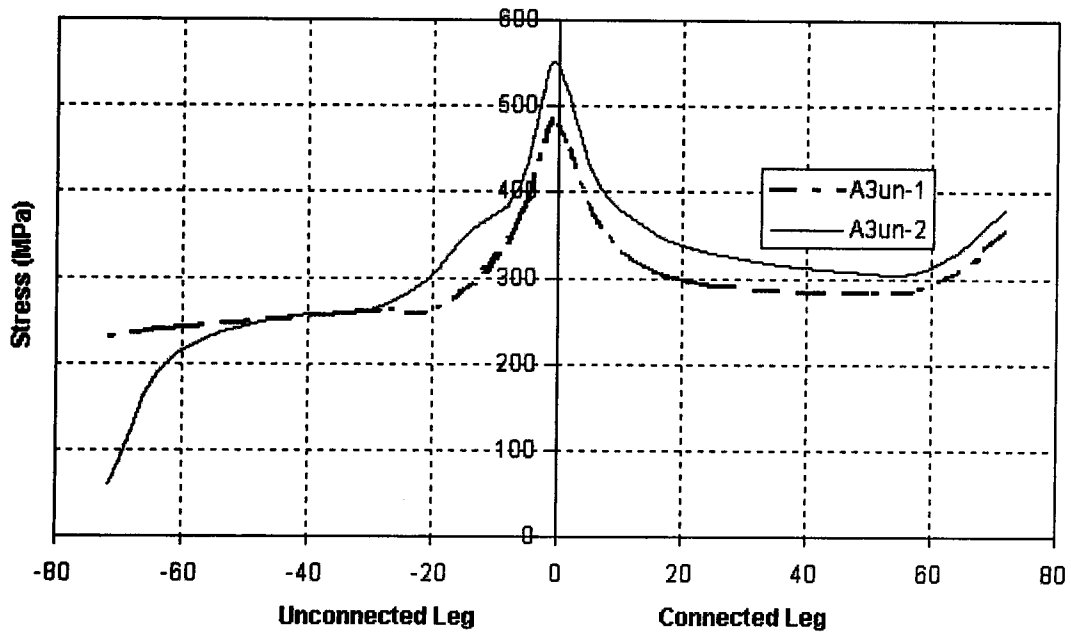

Figure 5.12 Stress Distribution of A3un-1 and A3un-2 at the Critical Section (P=0.96Pcr)

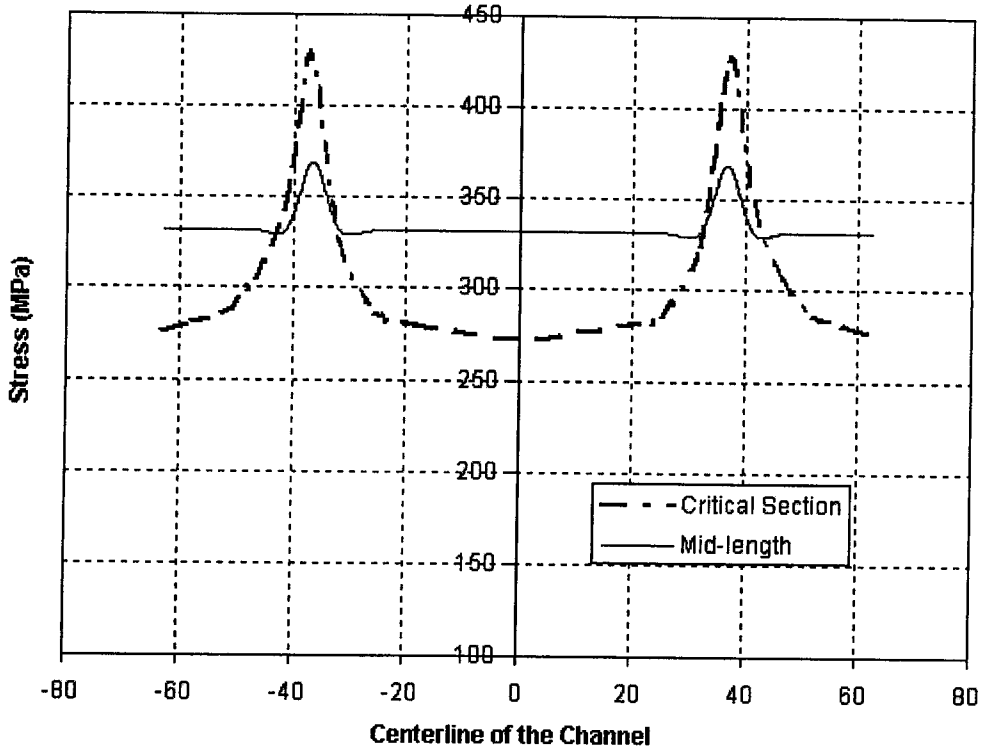

Figure 5.13 Stress Distribution of C3-2 at the Critical Section and Mid-length (P=0.98Pcr)

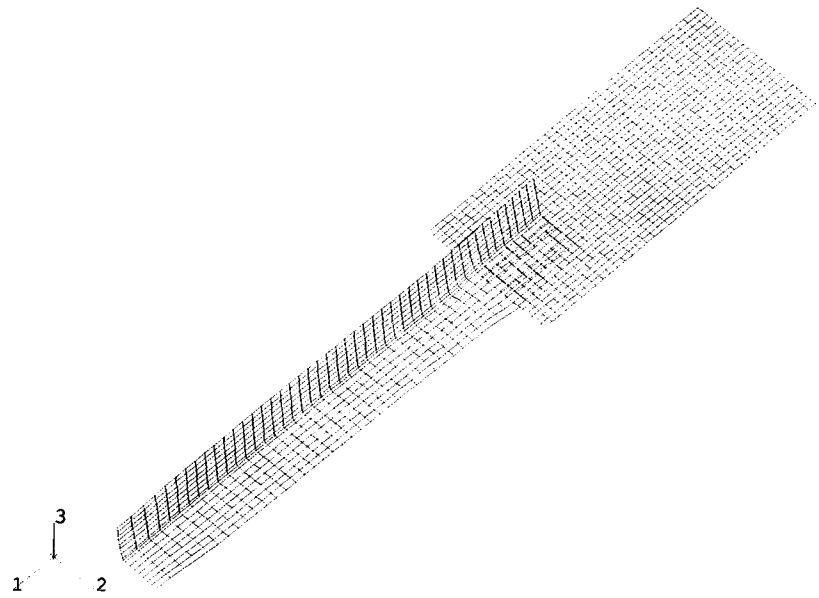

a) Predicted Deformed Shape

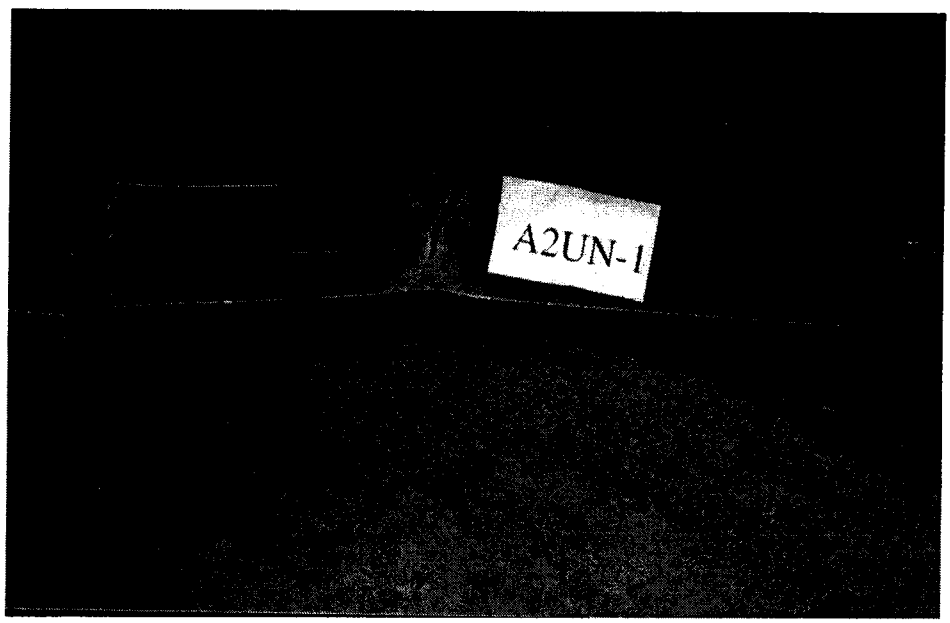

b) Observed Deformed Shape

Figure 5.14 Observed and Predicted Deformed Shape for Specimen A2un-1

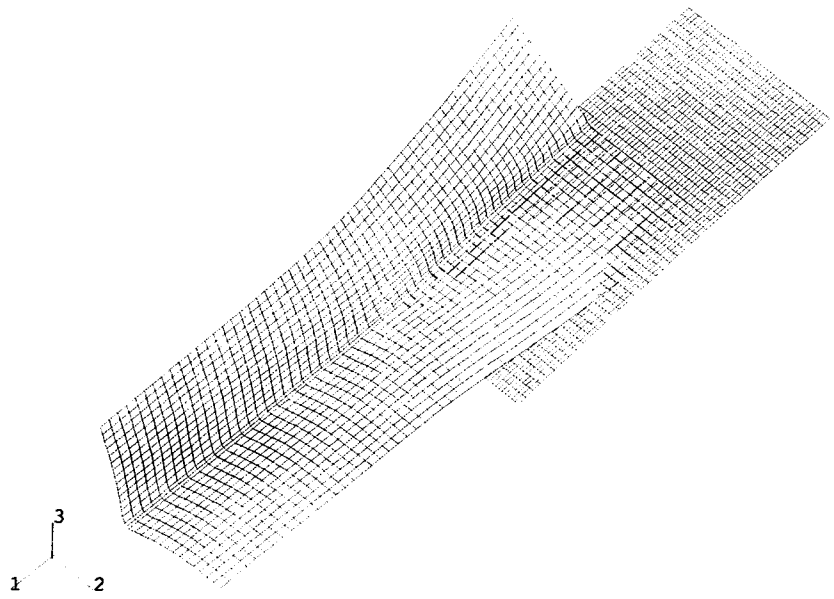

a) Predicted Deformed Shape

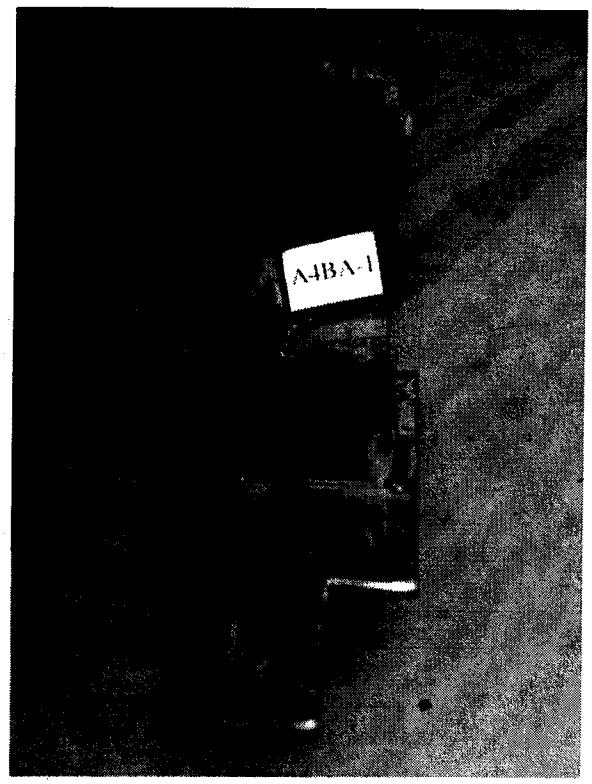

b) Observed Deformed Shape

Figure 5.15 Observed and Predicted Deformed Shape for Specimen A4ba-1

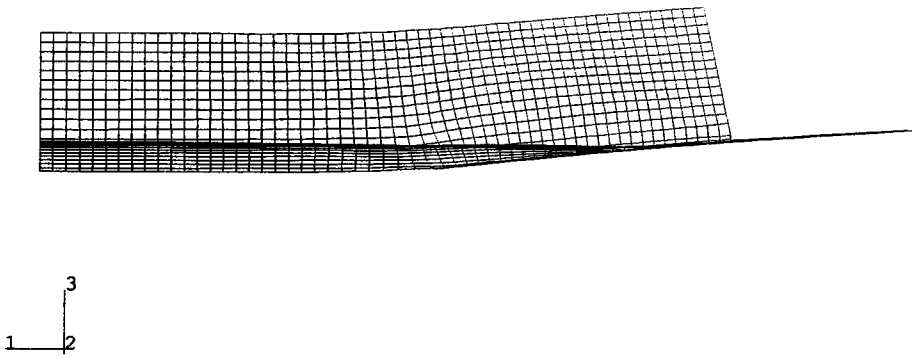

Figure 5.16 Side View of Predicted Deformed Shape of Specimen A4ba-1

6.0 Discussion

6.1 General

The purpose of this chapter is to evaluate the predictions of the net section strength of a steel tension member as given by current design approaches (CSA S16.1-94, AISC-LRFD 2000, and LaBoube and Yu 1995) with previous studies (Davis and Boonsliter 1934, Gibson and Wake 1942, and Esterling and Giroux 1993) and results obtained from this study. Discussion concerning the behavioural differences between the hot-rolled and cold-formed tension members will also be presented.

The test data used in this evaluation are a collection of those reported in this study and those obtained by others. The sources of the test data can be seen in Tables 6.1 and 6.2. Only the specimens that failed in the critical section fracture at the connection and the gross section fracture away from the welds are included, i.e. the specimens failed in the welds are not considered here.

The net section efficiency calculated according to current design specifications (designated as S16.1 and AISC) and the equations (Equations 2.3 and 2.4) proposed by LaBoube and Yu (1995) from the University of Missouri, Rolla (shown as UMR) was presented in Tables 6.1 and 6.2. Table 6.1 shows the net section efficiency of the 18 angle specimens used in this evaluation, where both single angle specimens and double angle specimens welded back-to-back to gusset plates are included. Test specimens welded with a combination of longitudinal and transverse welds are also included. Table 6.2 includes a total of 11 channel specimens from this study and others. Again, both single and double

channel specimens and both longitudinal welds only and combination of longitudinal and transverse welds are included in this comparison.

6.2 Discussion of Tests Results

6.2.1 Angle Sections

It can be seen from Table 6.1 that for those data collected from previous studies, where all specimens tested were hot-rolled steel sections, the equations developed by LaBoube and Yu (1995) and those outlined in AISC-LRFD (2000) and CSA-S16.1-94 (1994), in the great majority of the cases, give net section efficiencies that fall within 10% of the net section efficiencies obtained experimentally. The test to predicted ratios range from 0.93 to 1.24 with a mean value of 1.024 and a coefficient of variation of 7.66 %. The experimental net section efficiency factors range from 0.75 to 087.

On the other hand, all approaches are quite conservative when compared to the test results obtained in the study reported herein. Except specimen A3un-2, all other specimens yielded a net section efficiency factor close to 1.0. Even with specimen A3un-2, which has weld lengths as short as angle leg, an efficiency factor of 0.96 was obtained.

Besides the large differences in the net section efficiency between the specimens collected in previous studies (hot-rolled steel sections) and the specimens tested in this study (cold-formed steel sections), the mode of failure of the hot-rolled and cold-formed sections was also different. The hot-rolled angle steel sections, as described by Easterling and Girox (1993) and Gibson and Wake (1942), exhibited a tearing failure initiating at the welded toe. For the cold-formed angle specimens failed at the critical section, specimens A3un-2, A4ba-1, and A4un-1, the tearing failure initiated at the corner of the specimen as

shown in Fig. 6.1. This phenomenon can be mainly attributed to two reasons. Regarding to hot-rolled steel members, tearing failure initiated at the welded toe because the corner of the hot-rolled steel member is a lot thicker than the toe and the weld sizes at the corner and the toe are normally the same. For the cold-formed steel members, the cross section thickness is uniform and the weld size at the corner is normally larger than the one at the toe. Thus, as discussed in section 5.3, there is loss of ductility at the corner due to the welding and the cold-forming process, resulting in a premature tearing failure at the corner.

Although the stress concentration was quite high at the critical section, as discussed in Chapter 5, specimens A2ba-1, A2un-1, A3ba-1, and A3un-1 still failed at the gross section fracture away from the connection. As load was applied, the first yield lines started at the critical section of the member around the corners. As the load increased, the yielded region extended out from the critical sections to the mid-length of the specimen. By the time the load reached its ultimate value, the member started to neck at the mid-length and failure occurred. This can be explained by the fact the connected portion of the member cannot contract due to the constraint of the weld. This biaxial stress in the connected leg is believed to increase the strength of the member at the connection as compared with that at the mid-length (Cheng *et al.* 1998). This can also be used to explain the high efficiency factors for specimens A3un-2, A4ba-1, and A4un-1.

6.2.2 Channel Sections

It is seen from Table 6.2 that only one channel specimen from Easterling and Girox (1993) failed at the critical section. All other sections failed at the gross section away from the connection. The design equation proposed by LaBoube and Yu (1995) and those given

by current design approaches (CSA S16.1-94, AISC-LRFD 2000) give a good prediction of the net section efficiency. CSA S16.1-94 and AISC-LRFD 2000 lead to about the same net section efficiency. The specimen that failed at the connection (C-B-3) was welded both transversally and longitudinally. It was found (Easterling and Giroux 1993) that the net section efficiency is not increased by the addition of transverse welds.

As seen in Table 6.2, all cross-sections reported herein are fully effective ($U \geq 1.0$); except for both 76 mm (3 in) specimens that have a net section efficiency of 0.947. As pointed out by Gibson and Wake (1942) and Easterling and Giroux (1993) the load eccentricity can have a major effect on the strength of the members. Easterling and Giroux (1993) showed that although the great majority of the channels specimens failed at the gross cross section, as shown in Table 6.2, the experimental net section efficiency ranged from 0.88 to 0.92. Due to this load eccentricity, the member tends to behave as a beam-column and the secondary moment can cause a significant reduction on the member strength. It is believed that for the C2-2 specimen (50 mm) the P-δ effect was not significant because this specimen is more flexible than the 76 mm specimen; therefore being able to align itself with the tensile force reducing the eccentricity effect. For the case of the 100 mm specimen (C4-1), its eccentricity is smaller than that of the 76 mm specimens, hence reduces considerably the second order effect. On the other hand, the eccentricity effect on the strength of cold-formed steel sections can be questionable since specimens C3-1 and C3-2 failed exactly at the same load although specimen C3-1 is 34 % longer than specimen C3-2, and therefore more flexible. Since all coupon specimens were taken from the 100 mm (4 in) specimen there is also a possibility that the 76 mm (3 in) channel specimens have different material properties from others. The test to predicted

ratios of the ultimate loads for both angle and channel specimens are excellent, close to 1.0, as shown in Table 5.2, except for the 76 mm channel specimens, which yielded a ratio of 0.87 for both specimens. This supports the possibility of different material was used to manufacture the 76 mm channel sections. Unfortunately, there is no way to verify this postulation. There are many questions concerning the loss of efficiency of the 76 mm channel specimens and more investigation is required in order to explain this discrepancy.

Although specimen C3-2 experienced high stress concentration at the end of the connection it still failed at the mid-length. As mentioned in Chapter 4, the weld length for specimen C3-1 and C3-2 were 95 and 80 mm long respectively and both specimens failed at the mid-length and reached the same ultimate strength. Easterling and Giroux (1993) pointed out that increasing the weld length would not affect the shear lag coefficient. Probably, the shortest weld length tested was already long enough to develop the capacity required to transfer the load from the gusset plate to the specimen since different resistance factors were used in designing members and connections. Therefore, increasing this weld length would not affect the shear lag coefficient. However, Cheng *et al.* (1998) showed that reducing the weld length would cause an increase of stress concentration that can result in a fracture of the member at connection. Specimen A3un-2, which was tested with a weld length 80% shorter than that of A3un-1, did present a very high stress concentration and result in a failure at the connection.

6.2.3 Evaluation of Current Design Methods

All three design provisions (S16.1, AISC, and UMR) adequately predict the net section efficiency factors for welded hot-rolled channel and angle sections. However, the

design provisions, which are mainly based on the Munse and Chesson's net section efficiency equation (Equation 2.2), do not apply to welded cold-formed channels and angles. Most of the cold-formed specimens failed at the gross cross section fracture away from the connection. Even with the specimens that failed at the connection, the efficiency factors are much higher than the equations predicted. Based on Tables 6.1 and 6.2, it would be more appropriate to use a lower bound net section efficiency factor of 0.95 for both welded cold-formed channel and angle sections. The use of 0.95 is to consider both the shear lag effect and the load eccentricity. However, more test data are needed to verify this value. Additional research is also needed to provide a rational design method for the transition from cold-formed sections to hot-rolled members.

Table 6.1 Evaluation of the Net Area Efficiency of Angle Sections

Data Source	Test Designation	Specimen Configuration	Member (mm)	L/w	U_{AISC}	$U_{S16.1}$	U_{UMR}	$U_{Experim.}$	$U_{Experim.}/U_{AISC}$	$U_{Experim.}/U_{S16.1}$	$U_{Experim.}/U_{UMR}$
Easterling & Giroux	L-L-1	Double angle	51x51x4.8	2.24	0.87	0.82	0.85	0.81	0.93	0.99	0.96
	L-L-2	Double angle	51x51x4.8	2.24	0.87	0.82	0.85	0.82	0.94	1.00	0.97
	L-L-3	Double angle	51x51x4.8	2.24	0.87	0.82	0.85	0.82	0.94	1.00	0.97
	L-B-1a[1]	Double angle	102x76x6.4	0.88	0.79	0.81	0.75	0.82	1.04	1.01	1.09
	L-B-1c[1]	Double angle	51x51x4.8	1.50	0.81	0.78	0.77	0.80	0.99	1.03	1.04
	L-B-2[1]	Double angle	51x51x4.8	1.50	0.81	0.78	0.77	0.75	0.93	0.96	0.97
	L-B-3[1]	Double angle	51x51x4.8	1.50	0.81	0.78	0.77	0.80	0.99	1.03	1.04
Gibson & Wake		Single angle	64x64x7.9	1.50	0.78	0.79	0.74	0.78	1.00	0.99	1.05
		Double angle	64x64x7.9	1.50	0.78	0.79	0.74	0.86	1.10	1.09	1.16
		Double angle	64x64x7.9	1.27	0.75	0.73	0.70	0.87	1.16	1.19	1.24
Davis & Boomsliter	W3		76x76x7.9	2.13	0.86	0.90	0.84	0.87	1.01	0.97	1.04
Study Reported Herein	A2ba-1[2]	Single angle	50.6x50.6x2.63	1.48	0.82	0.72	0.78	1.02	1.24	1.42	1.31
	A2un-1[2]	Single angle	50.6x50.6x2.63	1.48	0.82	0.72	0.78	1.05	1.28	1.46	1.35
	A3ba-1[2]	Single angle	75.6x75.6x2.63	1.65	0.83	0.78	0.79	1.03	1.24	1.32	1.30
	A3un-1[2]	Single angle	75.6x75.6x2.63	1.65	0.84	0.79	0.81	1.04	1.24	1.32	1.28
	A3un-2	Single angle	75.6x75.6x2.63	1.06	0.77	0.65	0.71	0.96	1.25	1.50	1.35
	A4ba-1	Single angle	101.2x101.2x2.63	1.51	0.83	0.78	0.8	0.99	1.19	1.39	1.24
	A4un-1	Single angle	101.2x101.2x2.63	1.51	0.83	0.78	0.8	0.99	1.19	1.39	1.24

[1] Specimens with longitudinal and transverse welds.

[2] Members failed at the gross section away from the welds.

Table 6.2 Evaluation of the Net Area Efficiency of Channel Sections

Data Source	Test Designation	Specimen Configuration	Member	L/w	U_{AISC}	$U_{S16.1}$	U_{UMR}	$U_{Experim.}$	$U_{Experim.}/U_{AISC}$	$U_{Experim.}/U_{S16.1}$	$U_{Experim.}/U_{UMR}$
Easterling & Giroux	C-L-1	Double Channel	C75x6*[1]	1.67	0.90	0.85	0.90	0.89	0.99	1.05	0.99
	C-L-2	Double Channel	C75x6*[1]	1.67	0.90	0.85	0.90	0.90	1.00	1.06	1.00
	C-L-3	Double Channel	C75x6*[1]	1.67	0.90	0.85	0.90	0.91	1.01	1.07	1.01
	C-B-1[3]	Double Channel	C75x6*[1]	1.67	0.90	0.93	0.90	0.92	1.02	1.00	1.02
	C-B-2[3]	Double Channel	C75x6*[1]	1.67	0.90	0.93	0.90	0.92	1.02	1.00	1.02
	C-B-3[3]	Double Channel	C75x6*	1.67	0.90	0.93	0.90	0.88	0.98	0.96	0.98
Study Reported Herein	C2-1	Single Channel	50.4x28x2.63**[2]	1.50	0.89	0.87	0.90	-	-	-	-
	C2-2	Single Channel	50.4x28x2.63**[1]	1.50	0.89	0.87	0.90	1.046	1.18	1.20	1.16
	C3-1	Single Channel	76.6x28x2.63**[1]	1.24	0.90	0.81	0.90	0.947	1.06	1.17	1.06
	C3-2	Single Channel	76.6x28x2.63**[1]	1.04	0.90	0.80	0.90	0.947	1.06	1.18	1.06
	C4-1	Single Channel	101.3x28x2.63**[1]	1.13	0.90	0.81	0.90	1.00	1.11	1.23	1.11

* Member designated by the nominal depth in millimeters followed by the nominal mass in kilograms per meter.

** Cross sections dimensions in millimeters.

[1] Members failed at the gross section away from the welds.

[2] Weld failure.

[3] Members welded both longitudinally and transversally.

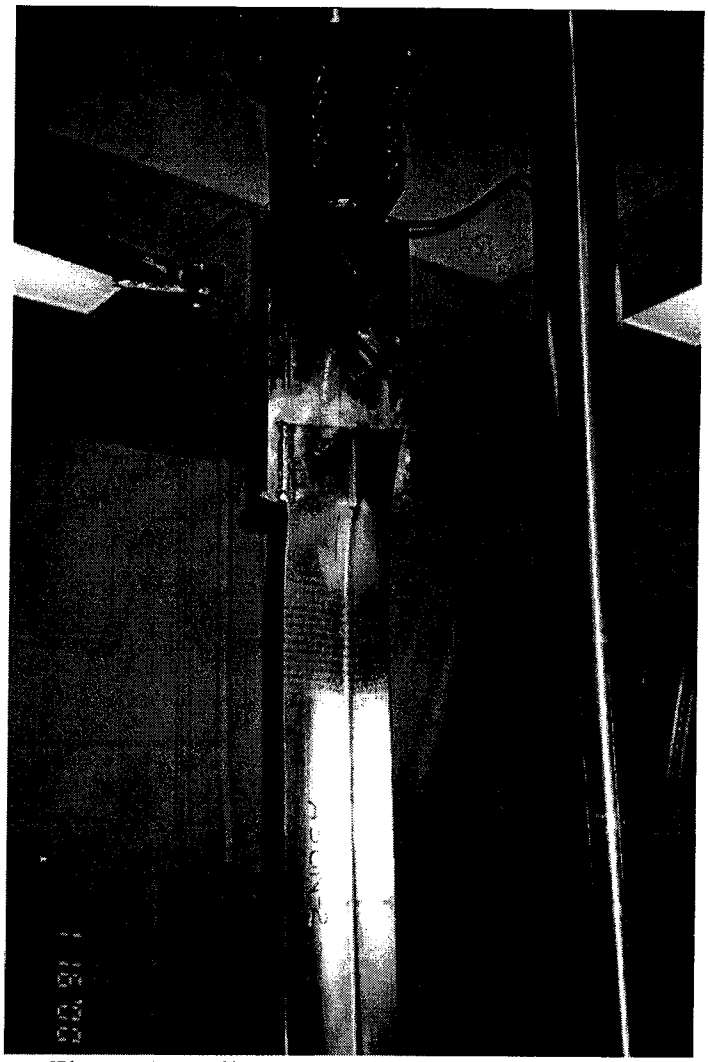

Figure 6.1 Failure Mode of Specimen A3un-2

7.0 Summary and Conclusions

7.1 Summary

The purpose of this study was to investigate the shear lag effect on welded cold-formed steel angles and channels under tension. A total of 12 specimens, seven angle sections and five channel sections, were fabricated and tested. Finite element analysis was performed to predict the strength and behaviour of the specimens. Stress-strain distribution at the critical section and the failure mode of the specimen were also evaluated. The experimental and analytical investigations were compared to validate the finite element models. The finite element models were found to be a good predictor of the physical tests. A comparison of test and analytical results obtained from this study with current design methods and existing test results was also made. Due to the limited number of tests conducted, few conclusions are drawn below to be confirmed by further research in the future.

7.2 Conclusions

Based on the experimental investigations and numerical analyses reported herein, it was concluded that:

1. The strength capacity of welded cold-formed angles may be affected by the connection length and cross-sectional geometry, although the effects on welded cold-formed angles are much less than the ones on welded hot-rolled angles.
2. Both balanced and unbalanced welding design used for angle specimens lead to the same ultimate strength.

3. Shear lag effects at the connection will not control the capacity of welded cold-formed channels under tension. All the channel sections, except for one that failed in the welds, failed at the gross section fracture away from the welds.
4. The finite element analysis results correlated fairly well with the physical tests in both behavour and strength predictions.
5. Current design methods, which are mainly based on the expression given by Chesson and Munse (Equation 2.2), as stated on AISC-LRFD (2000), were not able to provide a good prediction of the net section efficiency for the welded cold-formed angle steel sections. Before more research results are available, a conservative section efficiency factor of 0.95 can be used for cold-formed angle sections in tension.
6. For the design of welded cold-formed channel sections in tension, to account for a possible load eccentricity effect, a section efficiency factor of 0.95 is recommended based on a limited test data. Further tests and analyses are required in order to confirm this value.

7.3 Recommendations

1. Further tests and analyses are desirable in order to develop a design equation that predicts the net section efficiency of welded cold-formed angles and channels more accurately.
2. Research is needed to study the shear lag effects on other types of cold-formed sections, such as thin sheet steel plates.

3. It is also necessary to further investigate the transitional behaviour of welded tension members from cold-formed sections to hot-rolled sections to provide a more rational design method
4. Research into the weld failure in a welded tension member is needed in order to develop such requirements as the minimum weld length and minimum weld size for a welded tension member to avoid the premature weld failure.

References

ABAQUS Version 5.8 (1998). ABAQUS/Standard User's Manual. Hibbitt, Karlsson, & Sorenson Inc., Pawtucket, Rhode Island.

American Institute of Steel Construction (2000). Load and Resistance Factor Design Specification for Structural Steel Building. Chicago, Illinois.

American Iron and Steel Institute (1996). Specification for the Design of Cold-Formed Steel Structural Members. Washington, D.C..

American Society for Testing Materials (1997). A370 Standard Test Methods and Definitions for Mechanical Testing of Steel Products. ASTM, Philadelphia, PA.

Canadian Standards Association (1994). CAN/CSA-S16.1-94 Limit States Design of Steel Structures. Canadian Standards Association, Rexdale, Ontario

Canadian Standards Association (1994). CAN/CSA-S136-94. Cold-Formed Steel Structural Members. Canadian Standards Association, Rexdale, Ontario.

Cheng, J. J. R, Kulak, G. L and Khoo, H. A. (1998). " Strength of Slotted Tubular Tension Members". Canadian Journal of Civil Engineering. Vol. 25, No. 6, pp 982-991.

Chesson, E. and Munse, W. H. (1963). "Riveted and Bolted Joints: Truss-Type Tensile Connections". Journal of Structural Division. Vol. 89. No. ST1. pp 67-106.

Chesson, E. and Munse, W. H. (1963). "Riveted and Bolted Joints: Net Section Design". Journal of Structural Division. Vol. 89. No. ST1. pp 107-126.

Davis, R. P., and Boomsliter, G. P. (1934). "Tensile Tests of Welded and Riveted Structural Members". Journal of the American Welding Society, April, pp. 21-27.

Easterling, W. S., Gonzalez Giroux L. (1993). "Shear lag Effects in Steel Tension Members". Engineering Journal of the American Institute of Steel Construction, Vol.30, pp. 77-89.

Gibson, G. J. and Wake, B. T. (1942). "An investigation of Welded Connections for Angle Tension Members". The Journal of the American Welding Society, Welding Research Supplement, Vol.21 No.1 pp. 44s-49s.

Karren K. W. and Winter G. (1967). "Effects of Cold-Forming on Light-Gage Steel Members". Journal of the Structural Division, ASCE, Vol. 93, No. ST1. pp. 433-469.

LaBoube, R. A. and Yu. W. W. (1995). "Tensile and Bearing Capacities of Bolted Connections." Final Summary Report, University of Missouri-Rolla, Rolla, Missouri.

McKibben, F. P. (1906). "Tension Tests of Steel Angles." Proceedings of the ASTM, Vol. 6, pp. 267-274.

Winter, G. (1959). "Cold-Formed, Light-Gage Steel Construction" Journal of the Structural Division, ASCE, Vol. 85, No. ST9. pp. 151-173.

Wu, Y. and Kulak, G. L. (1993). Shear Lag in Bolted Single and Double Angle Tension Members. Structural Engineering Report No. 187, Department of Civil Engineering, University of Alberta, Edmonton, Alberta.

Yip, A. S-M and Cheng, J .J. R (2000). Shear Lag in Bolted Cold-Formed Steel Angles and Channels in Tension. Structural Engineering Report No. 223, Department of Civil Engineering, University of Alberta, Edmonton, Alberta.

APPENDIX A

Load vs. Deformation Curves for the Test Specimens

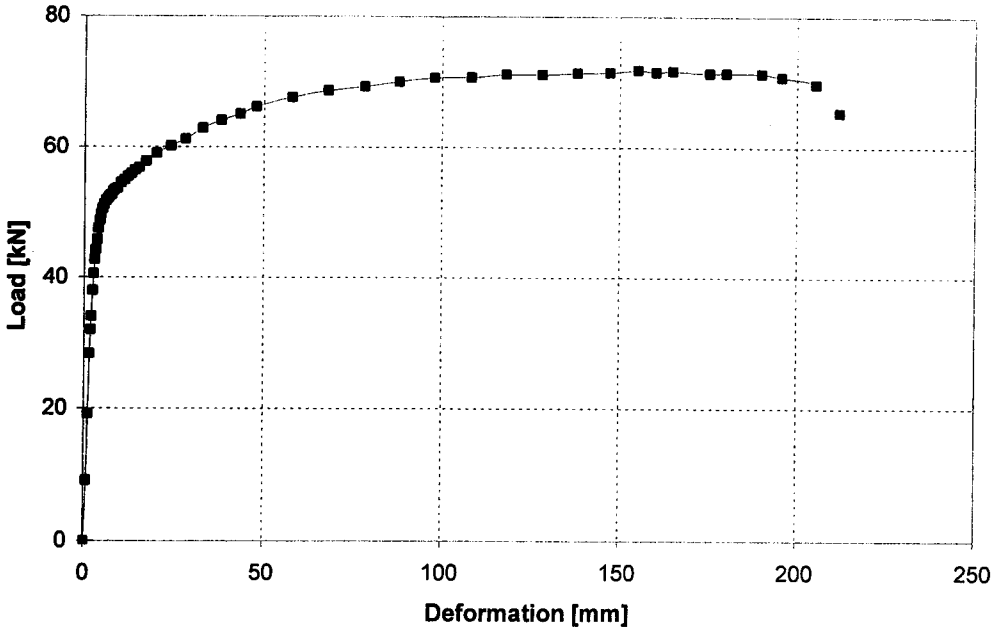

Figure A.1 Load vs. Deformation Curve for Specimen A2ba-1

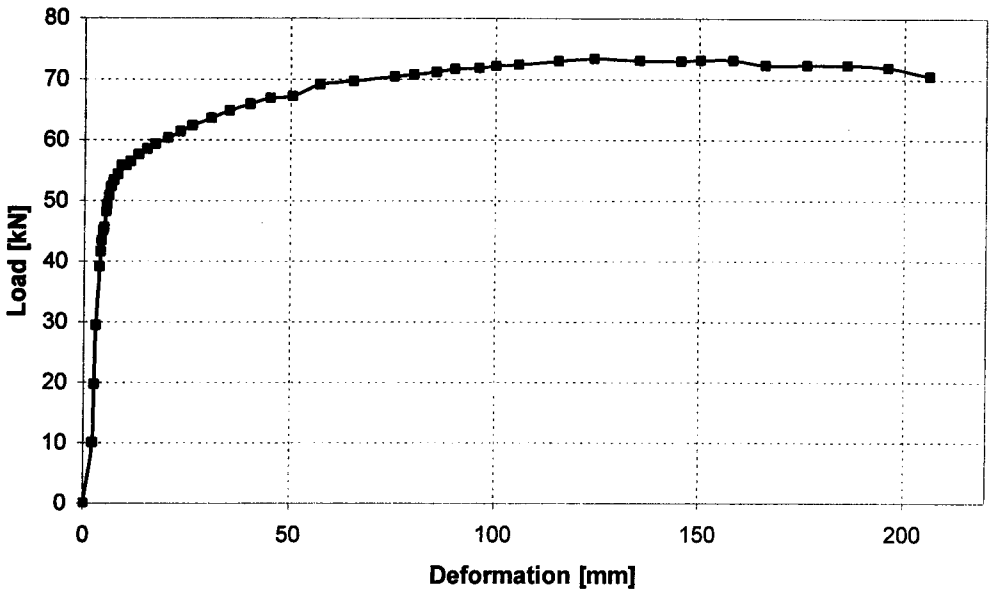

Figure A.2 Load vs. Deformation Curve for Specimen A2un-1

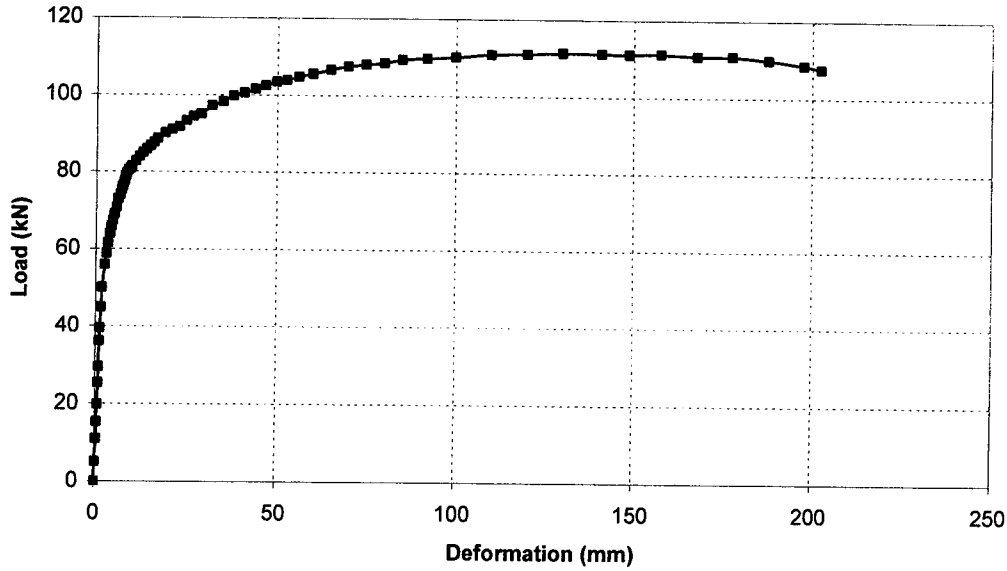

Figure A.3 Load vs. Deformation Curve for Specimen A3ba-1

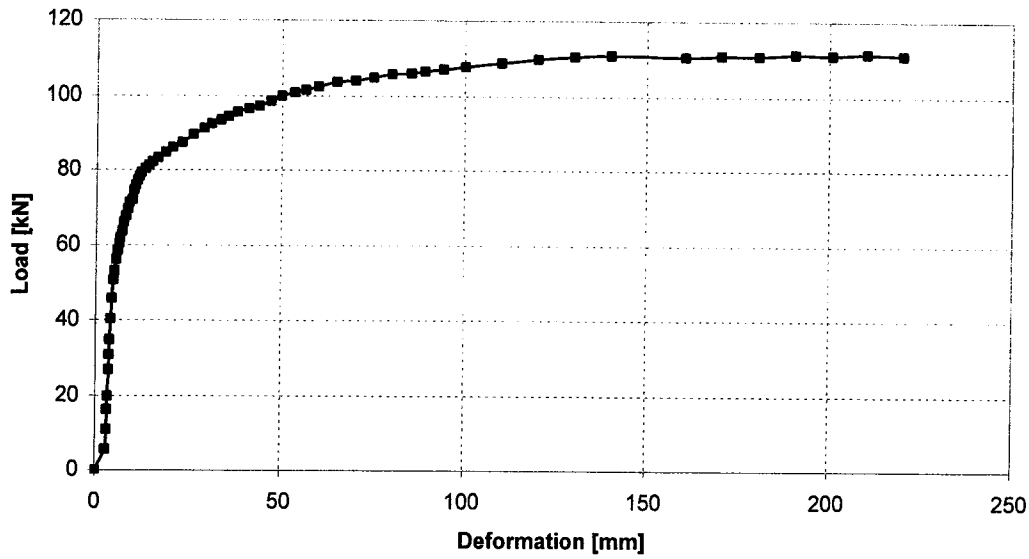

Figure A.4 Load vs. Deformation Curve for Specimen A3un-1

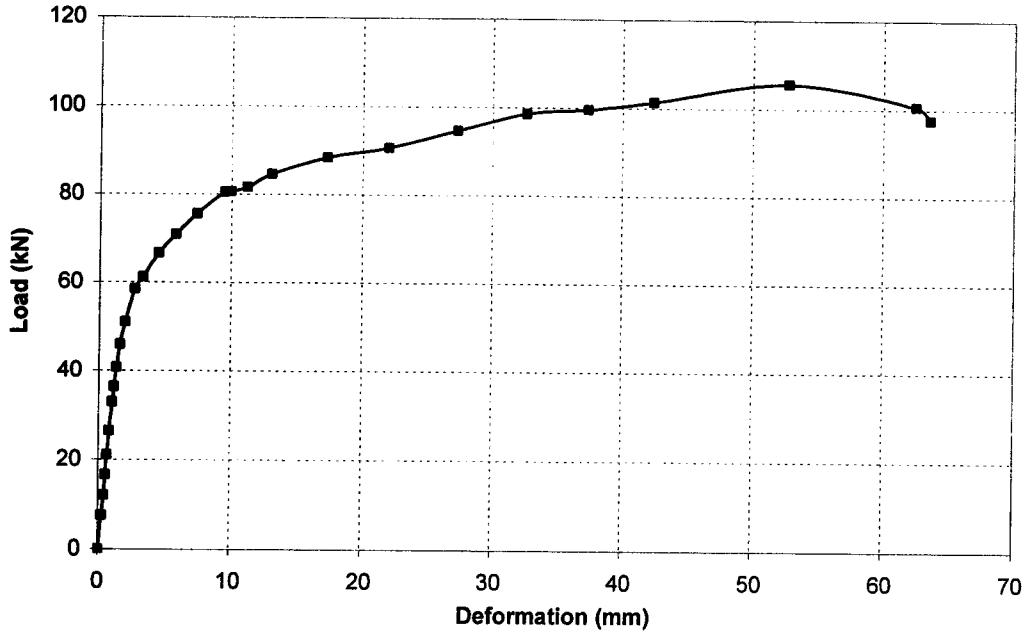

Figure A.5 Load vs. Deformation Curve for Specimen A3un-2

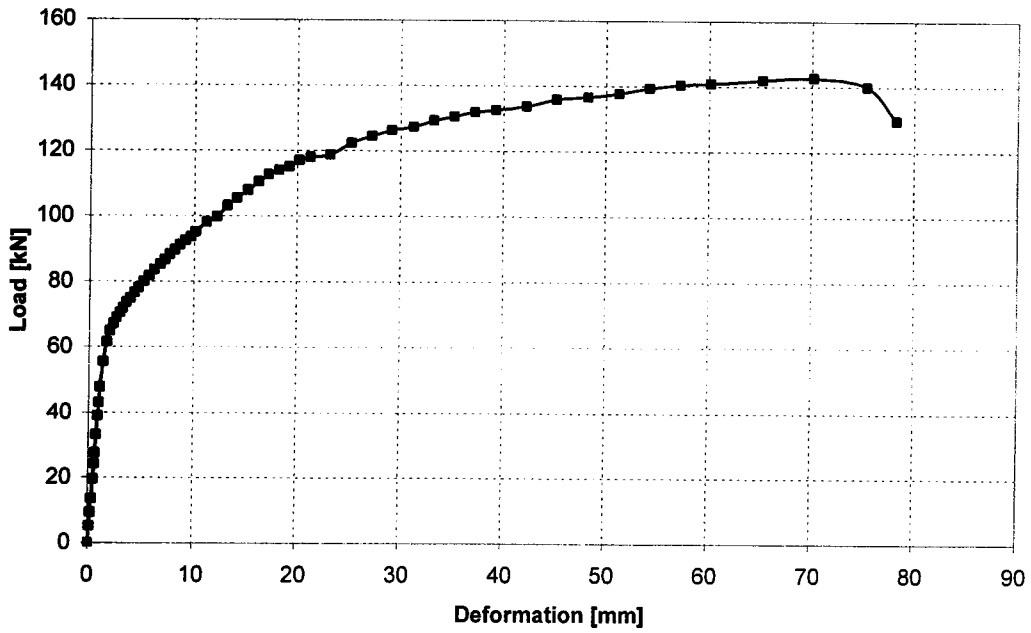

Figure A.6 Load vs. Deformation Curve for Specimen A4ba-1

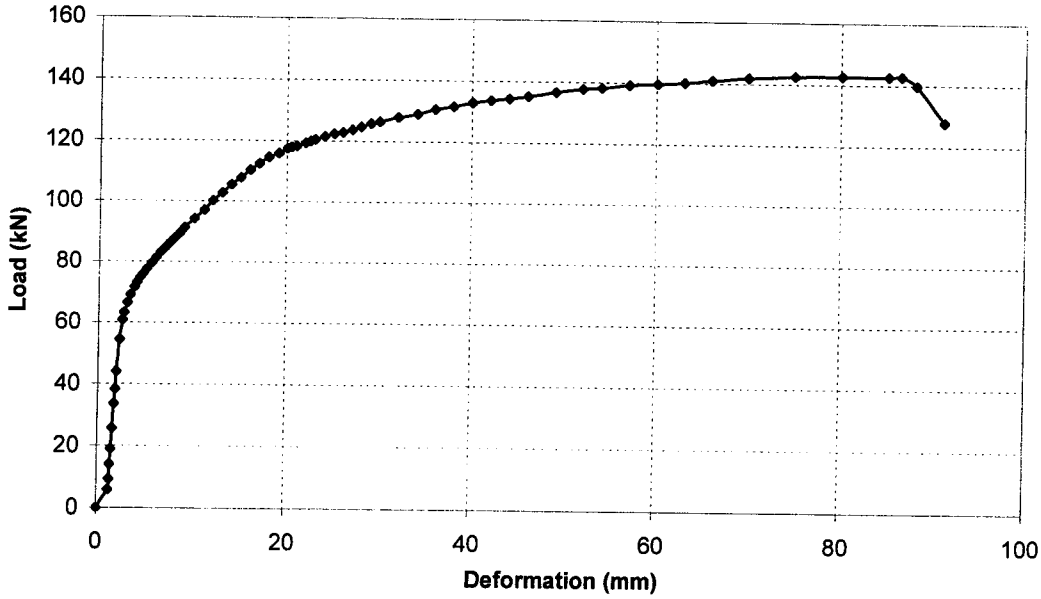

Figure A.7 Load vs. Deformation Curve for Specimen A4un-1

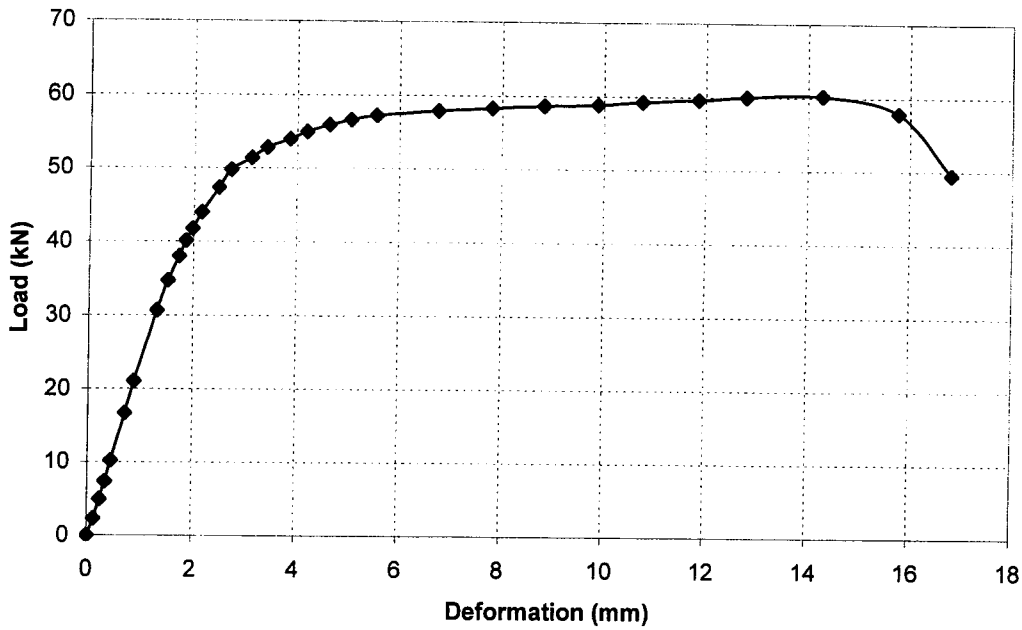

Figure A.8 Load vs. Deformation Curve for Specimen C2-1

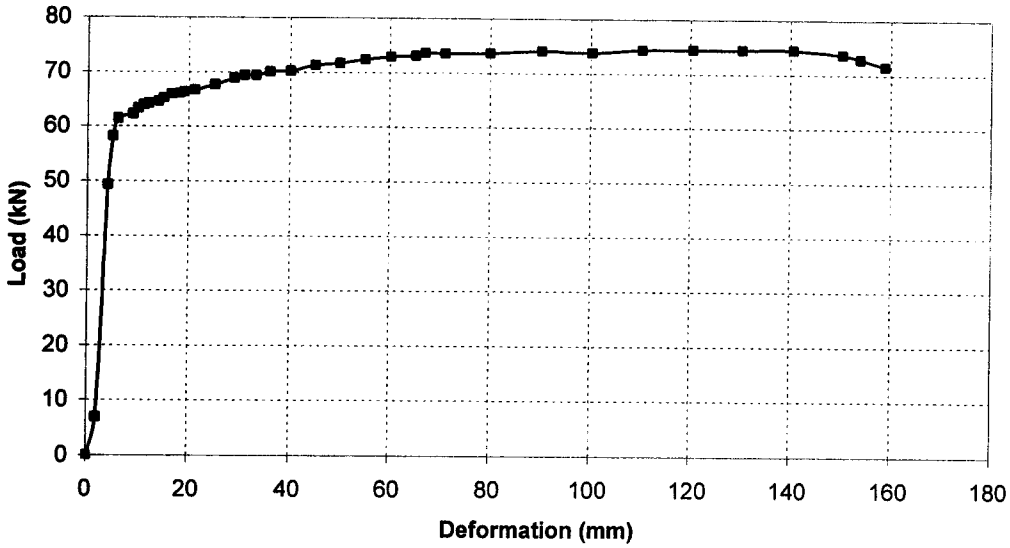

Figure A.9 Load vs. Deformation Curve for Specimen C2-2

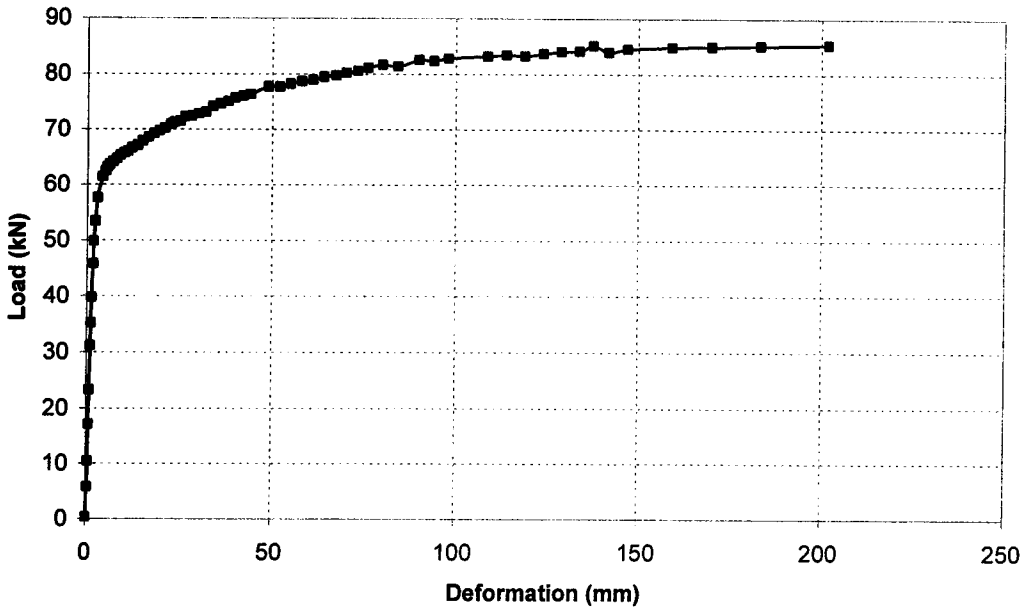

Figure A.10 Load vs. Deformation Curve for Specimen C3-1

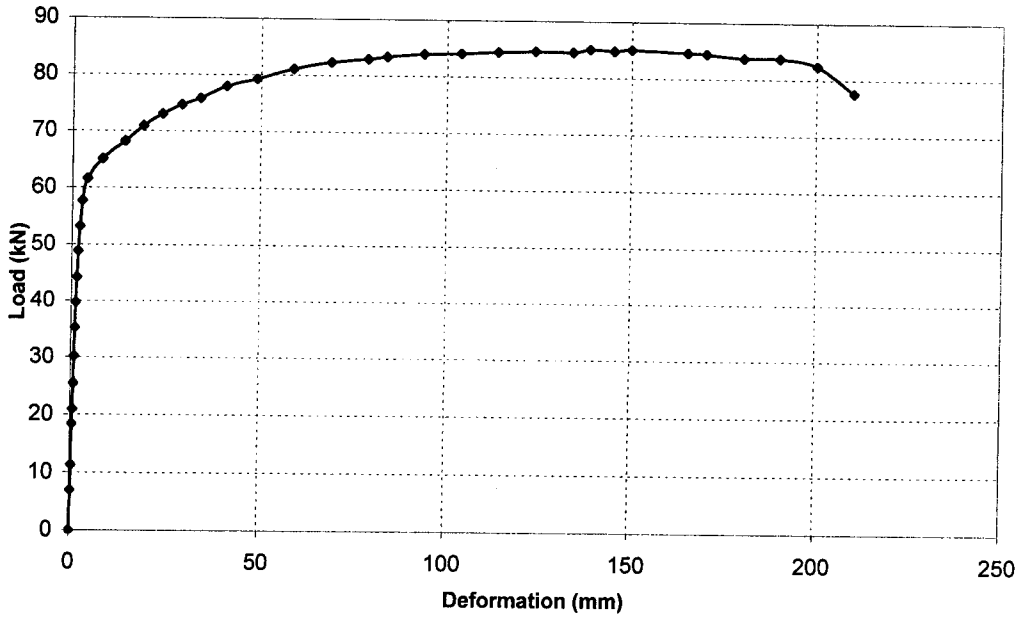

Figure A.11 Load vs. Deformation Curve for Specimen C3-2

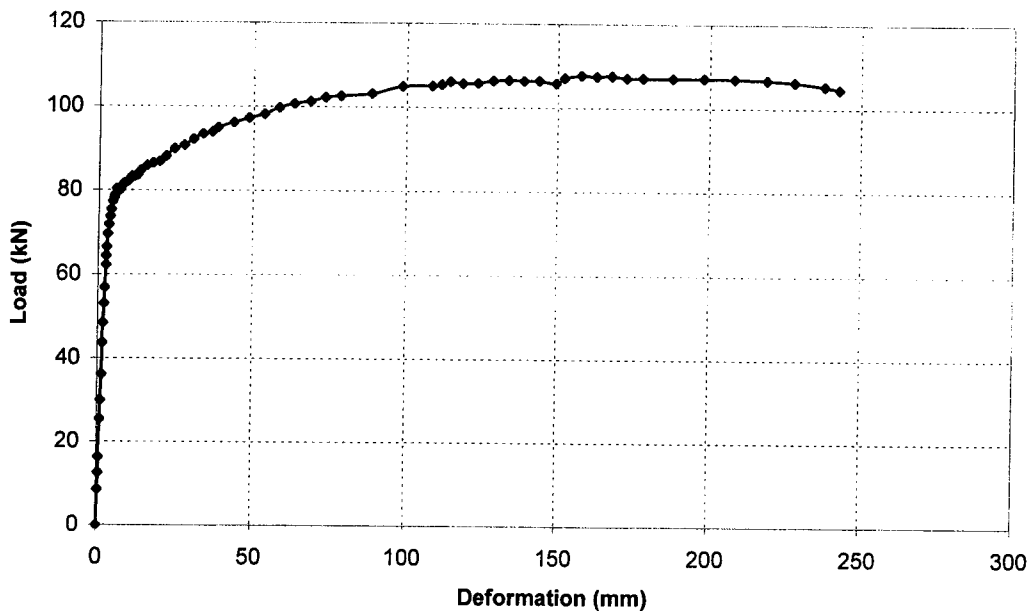

Figure A.12 Load vs. Deformation Curve for Specimen C4-1

APPENDIX B

Typical Input File For The Finite Element Analysis

C3-1 Input File

```
*HEADING
3 INCH CHANNEL THICKNESS 2.63
*USER SUBROUTINES, INPUT=alem.for
**
**define nodes in "SET1
**
*NODE, NSET=S1
100, 0, 79.8, 28.0
101, 0, 79.8, 23.584
102, 0, 79.8, 18.588
103, 0, 79.8, 13.592
104, 0, 79.8, 8.596
105, 0, 79.8, 3.6
106, 0, 78.75, 1.05
107, 0, 76.2, 0
108, 0, 68.94, 0
109, 0, 61.68, 0
110, 0, 54.42, 0
111, 0, 47.16, 0
112, 0, 39.9, 0
113, 0, 32.64, 0
114, 0, 25.38, 0
115, 0, 18.12, 0
116, 0, 10.86, 0
117, 0, 3.6, 0
118, 0, 1.05, 1.05
119, 0, 0, 3.6
120, 0, 0, 8.596
121, 0, 0, 13.592
122, 0, 0, 18.588
123, 0, 0, 23.584
124, 0, 0, 28.00
**
*NCOPY, SHIFT, CHANGENUMBER=420, OLDSET=S1, NEWSET=S2
98
0, 0, 1, 0, 0, -1, 0
**
*NFILL, NSET=SET1
S1, S2, 14, 30
**
**define nodes in "SET2
**
*NCOPY, SHIFT, CHANGENUMBER=30, OLDSET=S2, NEWSET=S3
7
0, 0, 1, 0, 0, -1, 0
**
*NCOPY, SHIFT, CHANGENUMBER=1560, OLDSET=S3, NEWSET=S4
364
0, 0, 1, 0, 0, -1, 0
**
*NFILL, NSET=SET2
S3, S4, 52, 30
```

```
**
**
**define node sets for boundary conditions
**
*NSET, NSET=BC1
119, 149, 179, 209, 239, 269, 299, 329
359, 389, 419, 449, 479, 509, 539
118, 148, 178, 208, 238, 268, 298, 328
358, 388, 418, 448, 478, 508, 538
*NSET, NSET=BC2
106, 136, 166, 196, 226, 256, 286, 316
346, 376, 406, 436, 466, 496, 526
105, 135, 165, 195, 225, 255, 285, 315
345, 375, 405, 435, 465, 495, 525
**
**define node sets for loading
**
*NSET, NSET=PLNODES
2110, 2111, 2112, 2113, 2114, 2115, 2116, 2117, 2118, 2119, 2120, 2121
2122, 2123, 2124, 2125, 2126, 2127, 2128, 2129, 2130, 2131, 2132, 2133,
2134
**
**
**define gusset plate nodes
**
*NODE
3000, -196, -27, -0.001
3026, -196, 103, -0.001
**
*NGEN, NSET=EDGE1
3000, 3026, 1
**
*NCOPY, SHIFT, CHANGENUMBER=1134, OLDSET=EDGE1, NEWSET=EDGE2
294
0, 0, 1, 0, 0, -1, 0
**
*NFILL, NSET=PLATE
EDGE1, EDGE2, 42, 27
**
**
*NSET, NSET=WELD1
3760, 3787, 3814, 3841, 3868, 3895, 3922, 3949
3976, 4003, 4030, 4057, 4084, 4111, 4138
3761, 3788, 3815, 3842, 3869, 3896, 3923, 3950
3977, 4004, 4031, 4058, 4085, 4112, 4139
**
*NSET, NSET=WELD2
3777, 3804, 3831, 3858, 3885, 3912, 3939, 3966
3993, 4020, 4047, 4074, 4101, 4128, 4155
3778, 3805, 3832, 3859, 3886, 3913, 3940, 3967
3994, 4021, 4048, 4075, 4102, 4129, 4156
**
**define node sets for support
**
*NSET, NSET=SUPPORT
3008, 3009, 3010, 3011, 3012, 3013, 3014, 3015, 3016, 3017, 3018
**
```

```
**define gusset plate elements
**
*ELEMENT, TYPE=S4R, ELSET=PLATE1
2000, 3000, 3001, 3028, 3027
2001, 3001, 3002, 3029, 3028
2002, 3002, 3003, 3030, 3029
2003, 3003, 3004, 3031, 3030
2004, 3004, 3005, 3032, 3031
2005, 3005, 3006, 3033, 3032
2006, 3006, 3007, 3034, 3033
2007, 3007, 3008, 3035, 3034
2008, 3008, 3009, 3036, 3035
2009, 3009, 3010, 3037, 3036
2010, 3010, 3011, 3038, 3037
2011, 3011, 3012, 3039, 3038
2012, 3012, 3013, 3040, 3039
2013, 3013, 3014, 3041, 3040
2014, 3014, 3015, 3042, 3041
2015, 3015, 3016, 3043, 3042
2016, 3016, 3017, 3044, 3043
2017, 3017, 3018, 3045, 3044
2018, 3018, 3019, 3046, 3045
2019, 3019, 3020, 3047, 3046
2020, 3020, 3021, 3048, 3047
2021, 3021, 3022, 3049, 3048
2022, 3022, 3023, 3050, 3049
2023, 3023, 3024, 3051, 3050
2024, 3024, 3025, 3052, 3051
2025, 3025, 3026, 3053, 3052
**
**
*ELGEN, ELSET=GUSSETPLATE
2000, 42, 27, 26
2001, 42, 27, 26
2002, 42, 27, 26
2003, 42, 27, 26
2004, 42, 27, 26
2005, 42, 27, 26
2006, 42, 27, 26
2007, 42, 27, 26
2008, 42, 27, 26
2009, 42, 27, 26
2010, 42, 27, 26
2011, 42, 27, 26
2012, 42, 27, 26
2013, 42, 27, 26
2014, 42, 27, 26
2015, 42, 27, 26
2016, 42, 27, 26
2017, 42, 27, 26
2018, 42, 27, 26
2019, 42, 27, 26
2020, 42, 27, 26
2021, 42, 27, 26
2022, 42, 27, 26
2023, 42, 27, 26
2024, 42, 27, 26
```

```
2025, 42, 27, 26
**
**
**define elements for the specimen
**
**first-row
**
*ELEMENT, TYPE=S4R, ELSET=R1
1, 100, 101, 131, 130
2, 101, 102, 132, 131
3, 102, 103, 133, 132
4, 103, 104, 134, 133
5, 104, 105, 135, 134
**
*ELEMENT, TYPE=S4R, ELSET=R2
6, 105, 106, 136, 135
7, 106, 107, 137, 136
**
*ELEMENT, TYPE=S4R, ELSET=R3
8, 107, 108, 138, 137
9, 108, 109, 139, 138
10, 109, 110, 140, 139
11, 110, 111, 141, 140
12, 111, 112, 142, 141
13, 112, 113, 143, 142
14, 113, 114, 144, 143
15, 114, 115, 145, 144
16, 115, 116, 146, 145
17, 116, 117, 147, 146
**
*ELEMENT, TYPE=S4R, ELSET=R4
18, 117, 118, 148, 147
19, 118, 119, 149, 148
**
*ELEMENT, TYPE=S4R, ELSET=R5
20, 119, 120, 150, 149
21, 120, 121, 151, 150
22, 121, 122, 152, 151
23, 122, 123, 153, 152
24, 123, 124, 154, 153
**
*ELGEN, ELSET=FLANGE1
1, 67, 30, 24
2, 67, 30, 24
3, 67, 30, 24
4, 67, 30, 24
5, 67, 30, 24
**
*ELGEN, ELSET=CORNER1
6, 67, 30, 24
7, 67, 30, 24
**
*ELGEN, ELSET=WEB
8, 67, 30, 24
9, 67, 30, 24
10, 67, 30, 24
11, 67, 30, 24
```

```
12, 67, 30, 24
13, 67, 30, 24
14, 67, 30, 24
15, 67, 30, 24
16, 67, 30, 24
17, 67, 30, 24
**
*ELGEN, ELSET=CORNER2
18, 67, 30, 24
19, 67, 30, 24
**
*ELGEN, ELSET=FLANGE2
20, 67, 30, 24
21, 67, 30, 24
22, 67, 30, 24
23, 67, 30, 24
24, 67, 30, 24
**
**
**define groups for output
**
*ELSET, ELSET=CRITICAL
337, 338, 339, 340, 341, 342, 343, 344, 345, 346, 347, 348
349, 350, 351, 352, 353, 354, 355, 356, 357, 358, 359, 360
**
**
*ELSET,ELSET=MID
1585, 1586, 1587, 1588, 1589, 1590, 1591, 1592, 1593, 1594, 1595, 1596
1597, 1598, 1599, 1600, 1601, 1602, 1603, 1604, 1605, 1606, 1607, 1608
**
**define group for properties
**
*ELSET, ELSET=FLAT
FLANGE1, FLANGE2, WEB
**
*ELSET, ELSET=CORNER
CORNER1, CORNER2
**
*ELSET, ELSET=CHANNEL
FLAT, CORNER
**
**
**define element properties
**
**gusset plate
**
*SHELLSECTION , ELSET=GUSSETPLATE, MATERIAL=STEEL3
12.7
**
**
**specimen
**
*INITIAL CONDITION, TYPE=SOLUTION, USER
*SHELLSECTION, ELSET=FLAT, MATERIAL=STEEL1
2.63

*TRANSVERSE SHEAR STIFFNESS
```

```
170950, 170950
*SHELLSECTION, ELSET=CORNER, MATERIAL=STEEL2
2.63
*TRANSVERSE SHEAR STIFFNESS
170950, 170950
**
**
**define material properties for specimen
**
**material1
*MATERIAL, NAME=STEEL1
*DEPVAR
18
*USER MATERIAL, CONSTANTS=42, UNSYMM
199000, 0.3, 1, 0, 0.00001, 0, 0.90, 1
0.001, 3.5, 2.48E+09, 2, -7.0704D-1, 0, -2.170786D2, 2.4
3.008677D2, 2.45, -8.585641D1, 2.55, 0, 0, 0, 0
163, 0, 175, 0.0048, 184.4, 0.0086, 230, 0.035
279.24, 0.083, 346, 0.229, 379, 0.312, 385, 0.329
1970.5, 4
**
**material2
*MATERIAL, NAME=STEEL2
*DEPVAR
18
*USER MATERIAL, CONSTANTS=38, UNSYMM
199000, 0.3, 1, 0, 0.00001, 0, 0.65, 1
0.001, 3.5, 2.48E+09, 2, -7.0704D-1, 0, -2.170786D2, 2.4
3.008677D2, 2.45, -8.585641D1, 2.55, 0, 0, 0, 0
292.16, 0, 305.3, 0.001, 316.07, 0.0046, 305, 0.0166
343, 0.12, 370.6, 0.211, 1650.5, 4
**
**gusset plate
**
*MATERIAL, NAME=STEEL3
*ELASTIC
200000, 0.3
*PLASTIC, HARDENING=ISOTROPIC
350, 0
351, 0.1
**
**
**define boundary conditions
**
*MPC
BEAM, BC1, WELD1
BEAM, BC2, WELD2
**
**
*BOUNDARY
SUPPORT, 1, 4
SUPPORT, 6
PLNODES, 5, 6
**
**
```

```
**apply loads
**
*STEP, NLGEOM
*STATIC, DIRECT
0.1, 1
**
*BOUNDARY
PLNODES, 1, , 1
**
**output
**
**
*NODEFILE, FREQUENCY=1, NSET=PLNODES
U
*NODEFILE, FREQUENCY=1, NSET=BC1
U
*NODEFILE, FREQUENCY=1, NSET=PLNODES
RF
*NODEFILE, FREQUENCY=1, NSET=BC1
RF
**
*NODEPRINT, FREQUENCY=0
*ELFILE, FREQUENCY=1, ELSET=CRITICAL
SDV
E
S
**
*ELFILE, FREQUENCY=1, ELSET=MID
SDV
E
S
*ELPRINT, FREQUENCY=0
**
*RESTART, WRITE, OVERLAY
*ENDSTEP
**
*STEP, NLGEOM, INC=10200
*STATIC
0.01, 1, 0, 0.0001
**
*BOUNDARY
PLNODES, 1, 1, 150
**
**output
**
**
*NODEFILE, FREQUENCY=10, NSET=PLNODES
U
*NODEFILE, FREQUENCY=10, NSET=BC1
U
*NODEFILE, FREQUENCY=10, NSET=PLNODES
RF
*NODEFILE, FREQUENCY=10, NSET=BC1
RF
**
```

```
*NODEPRINT, FREQUENCY=0
*ELFILE, FREQUENCY=10, ELSET=CRITICAL
SDV
E
S
**
*ELFILE, FREQUENCY=10, ELSET=MID
SDV
E
S
*ELPRINT, FREQUENCY=0
**
*RESTART, WRITE, OVERLAY
*ENDSTEP
**
**
*STEP, NLGEOM, INC=10200
*STATIC
0.01, 1, 0, 0.0001
**
*BOUNDARY
PLNODES, 1, 1, 200
**
**output
**
**
*NODEFILE, FREQUENCY=10, NSET=PLNODES
U
*NODEFILE, FREQUENCY=10, NSET=BC1
U
*NODEFILE, FREQUENCY=10, NSET=PLNODES
RF
*NODEFILE, FREQUENCY=10, NSET=BC1
RF
**
*NODEPRINT, FREQUENCY=0
*ELFILE, FREQUENCY=10, ELSET=CRITICAL
SDV
E
S
**
*ELFILE, FREQUENCY=10, ELSET=MID
SDV
E
S
*ELPRINT, FREQUENCY=0
**
*RESTART, WRITE, OVERLAY
*ENDSTEP
**
```

A3ba-1 Input File

```
*HEADING
3 INCH ANGLE-BA THICKNESS 2.63
*USER SUBROUTINES, INPUT=alem.for
**
**define nodes in "SET1
**
*NODE, NSET=S1
100, 0, 76.2, 0
101, 0, 68.94, 0
102, 0, 61.68, 0
103, 0, 54.42, 0
104, 0, 47.16, 0
105, 0, 39.9, 0
106, 0, 32.64, 0
107, 0, 25.38, 0
108, 0, 18.12, 0
109, 0, 10.86, 0
110, 0, 3.6, 0
111, 0, 1.0544, 1.0544
112, 0, 0, 3.6
113, 0, 0, 10.86
114, 0, 0, 18.12
115, 0, 0, 25.38
116, 0, 0, 32.64
117, 0, 0, 39.9
118, 0, 0, 47.16
119, 0, 0, 54.42
120, 0, 0, 61.68
121, 0, 0, 68.94
122, 0, 0, 76.2
**
*NCOPY, SHIFT, CHANGENUMBER=207, OLDSET=S1, NEWSET=S2
63
0, 0, 1, 0, 0, -1, 0
**
*NFILL, NSET=SET1
S1, S2, 9, 23
**
**define nodes in "SET2
**
*NCOPY, SHIFT, CHANGENUMBER=23, OLDSET=S2, NEWSET=S3
7
0, 0, 1, 0, 0, -1, 0
**
*NCOPY, SHIFT, CHANGENUMBER=322, OLDSET=S3, NEWSET=S4
98
0, 0, 1, 0, 0, -1, 0
**
*NFILL, NSET=SET2
S3, S4, 14, 23
**
```

```
**define nodes in "SET3
**
*NCOPY, SHIFT, CHANGENUMBER=23, OLDSET=S4, NEWSET=S5
7
0, 0, 1, 0, 0, -1, 0
**
*NCOPY, SHIFT, CHANGENUMBER=828, OLDSET=S5, NEWSET=S6
252
0, 0, 1, 0, 0, -1, 0
**
*NFILL, NSET=SET3
S5, S6, 36, 23
**
**define node sets for boundary conditions
**
*NSET, NSET=BC2
100, 123, 146, 169, 192, 215, 238, 261, 284, 307
**
*NSET, NSET=BC1
111, 134, 157, 180, 203, 226, 249, 272, 295, 318, 341, 364, 387
410, 433, 456, 479, 502, 525, 548, 571, 594, 617, 640, 663
**
**define node sets for loading
**
*NSET, NSET=PLNODES
1503, 1504, 1505, 1506, 1507, 1508, 1509, 1510, 1511, 1512, 1513, 1514
1515, 1516, 1517, 1518, 1519, 1520, 1521, 1522, 1523, 1524, 1525
**
**
**define gusset plate nodes
**
*NODE
2000, -132, -45, -0.001
2026, -132, 85, -0.001
**
*NGEN, NSET=EDGE1
2000, 2026, 1
**
*NCOPY, SHIFT, CHANGENUMBER=1134, OLDSET=EDGE1, NEWSET=EDGE2
294
0, 0, 1, 0, 0, -1, 0
**
*NFILL, NSET=PLATE
EDGE1, EDGE2, 42, 27
**
**
*NSET, NSET=WELD1
2494, 2521, 2548, 2575, 2602, 2629, 2656, 2683, 2710, 2737, 2764, 2791
2818, 2845, 2872, 2899, 2926, 2953, 2980, 3007, 3034, 3061, 3088, 3115,
3142
**
*NSET, NSET=WELD2
2510, 2537, 2564, 2591, 2618, 2645, 2672, 2699, 2726, 2753
**
**define node sets for support
**
```

```
*NSET, NSET=SUPPORT
2008, 2009, 2010, 2011, 2012, 2013, 2014, 2015, 2016, 2017, 2018
**
**define gusset plate elements
**
*ELEMENT, TYPE=S4R, ELSET=PLATE1
1500, 2000, 2001, 2028, 2027
1501, 2001, 2002, 2029, 2028
1502, 2002, 2003, 2030, 2029
1503, 2003, 2004, 2031, 2030
1504, 2004, 2005, 2032, 2031
1505, 2005, 2006, 2033, 2032
1506, 2006, 2007, 2034, 2033
1507, 2007, 2008, 2035, 2034
1508, 2008, 2009, 2036, 2035
1509, 2009, 2010, 2037, 2036
1510, 2010, 2011, 2038, 2037
1511, 2011, 2012, 2039, 2038
1512, 2012, 2013, 2040, 2039
1513, 2013, 2014, 2041, 2040
1514, 2014, 2015, 2042, 2041
1515, 2015, 2016, 2043, 2042
1516, 2016, 2017, 2044, 2043
1517, 2017, 2018, 2045, 2044
1518, 2018, 2019, 2046, 2045
1519, 2019, 2020, 2047, 2046
1520, 2020, 2021, 2048, 2047
1521, 2021, 2022, 2049, 2048
1522, 2022, 2023, 2050, 2049
1523, 2023, 2024, 2051, 2050
1524, 2024, 2025, 2052, 2051
1525, 2025, 2026, 2053, 2052
**
**
*ELGEN, ELSET=GUSSETPLATE
1500, 42, 27, 26
1501, 42, 27, 26
1502, 42, 27, 26
1503, 42, 27, 26
1504, 42, 27, 26
1505, 42, 27, 26
1506, 42, 27, 26
1507, 42, 27, 26
1508, 42, 27, 26
1509, 42, 27, 26
1510, 42, 27, 26
1511, 42, 27, 26
1512, 42, 27, 26
1513, 42, 27, 26
1514, 42, 27, 26
1515, 42, 27, 26
1516, 42, 27, 26
1517, 42, 27, 26
1518, 42, 27, 26
1519, 42, 27, 26
1520, 42, 27, 26
1521, 42, 27, 26
```

```
1522, 42, 27, 26
1523, 42, 27, 26
1524, 42, 27, 26
1525, 42, 27, 26
**
**
**
**define elements for the specimen
**
**first-row
**
*ELEMENT, TYPE=S4R, ELSET=R1
1, 100, 101, 124, 123
2, 101, 102, 125, 124
3, 102, 103, 126, 125
4, 103, 104, 127, 126
5, 104, 105, 128, 127
6, 105, 106, 129, 128
7, 106, 107, 130, 129
8, 107, 108, 131, 130
9, 108, 109, 132, 131
10, 109, 110, 133, 132
**
*ELEMENT, TYPE=S4R, ELSET=R3
11, 110, 111, 134, 133
12, 111, 112, 135, 134
**
*ELEMENT, TYPE=S4R, ELSET=R2
13, 112, 113, 136, 135
14, 113, 114, 137, 136
15, 114, 115, 138, 137
16, 115, 116, 139, 138
17, 116, 117, 140, 139
18, 117, 118, 141, 140
19, 118, 119, 142, 141
20, 119, 120, 143, 142
21, 120, 121, 144, 143
22, 121, 122, 145, 144
**
*ELGEN, ELSET=LEG1
1, 61, 23, 22
2, 61, 23, 22
3, 61, 23, 22
4, 61, 23, 22
5, 61, 23, 22
6, 61, 23, 22
7, 61, 23, 22
8, 61, 23, 22
9, 61, 23, 22
10, 61, 23, 22
**
*ELGEN, ELSET=CORNER
11, 61, 23, 22
12, 61, 23, 22
**
```

```
*ELGEN, ELSET=LEG2
13, 61, 23, 22
14, 61, 23, 22
15, 61, 23, 22
16, 61, 23, 22
17, 61, 23, 22
18, 61, 23, 22
19, 61, 23, 22
20, 61, 23, 22
21, 61, 23, 22
22, 61, 23, 22
**
**
**define group for output
**
*ELSET, ELSET=CRITICAL
529, 530, 531, 532, 533, 534, 535, 536, 537, 538, 539
540, 541, 542, 543, 544, 545, 546, 547, 548, 549, 550
*ELSET, ELSET=MID
1321, 1322, 1323, 1324, 1325, 1326, 1327, 1328, 1329, 1330, 1331
1332, 1333, 1334, 1335, 1336, 1337, 1338, 1339, 1340, 1341, 1342
**
**
**define group for properties
**
*ELSET, ELSET=LEGS
LEG1, LEG2
**
*ELSET, ELSET=ANGLE
LEGS, CORNER
**
**
**define element properties
**
**gusset plate
**
*SHELLSECTION , ELSET=GUSSETPLATE, MATERIAL=STEEL3
12.7
**
**
**specimen
**
*INITIAL CONDITION, TYPE=SOLUTION, USER
*SHELLSECTION, ELSET=LEGS, MATERIAL=STEEL1
2.63
*TRANSVERSE SHEAR STIFFNESS
170950, 170950
*SHELLSECTION, ELSET=CORNER, MATERIAL=STEEL2
2.63
*TRANSVERSE SHEAR STIFFNESS
170950, 170950
**
**
**define material properties for specimen
**
```

```
**material1
*MATERIAL, NAME=STEEL1
*DEPVAR
18
*USER MATERIAL, CONSTANTS=44, UNSYMM
202000, 0.3, 1, 0, 0.00001, 0, 0.90, 1
0.001, 3.5, 2.48E+09, 2, -7.0704D-1, 0, -2.170786D2, 2.4
3.008677D2, 2.45, -8.585641D1, 2.55, 0, 0, 0, 0
142, 0, 166, 0.0044, 175, 0.008, 243, 0.05
285, 0.102, 332, 0.19, 364, 0.28, 377, 0.32
391, 0.368, 1600, 4
**
**material2
*MATERIAL, NAME=STEEL2
*DEPVAR
18
*USER MATERIAL, CONSTANTS=42, UNSYMM
202000, 0.3, 1, 0, 0.00001, 0, 0.65, 1
0.001, 3.5, 2.48E+09, 2, -7.0704D-1, 0, -2.170786D2, 2.4
3.008677D2, 2.45, -8.585641D1, 2.55, 0, 0, 0, 0
267, 0, 313, 0.001, 321, 0.004, 324, 0.0065
335, 0.054, 357, 0.114, 386, 0.211, 1621, 4.0
**
**gusset plate
**
*MATERIAL, NAME=STEEL3
*ELASTIC
200000, 0.3
*PLASTIC, HARDENING=ISOTROPIC
350, 0
351, 0.1
**
**
**define boundary conditions
**
*MPC
BEAM, BC1, WELD1
BEAM, BC2, WELD2
**
**
*BOUNDARY
SUPPORT, 1, 4
SUPPORT, 6
PLNODES, 5, 6
**
**
**apply loads
**
*STEP, NLGEOM
*STATIC, DIRECT
0.1, 1
**
*BOUNDARY
PLNODES, 1, , 0.5
**
**
```

```
**output
**
**
*NODEFILE, FREQUENCY=1, NSET=PLNODES
U
*NODEFILE, FREQUENCY=1, NSET=BC1
U
*NODEFILE, FREQUENCY=1, NSET=PLNODES
RF
*NODEFILE, FREQUENCY=1, NSET=BC1
RF
**
*NODEPRINT, FREQUENCY=0
*ELFILE, FREQUENCY=1, ELSET=CRITICAL
SDV
E
S
*ELFILE, FREQUENCY=1, ELSET=MID
SDV
E
S
*ELPRINT, FREQUENCY=0
**
*RESTART, WRITE, OVERLAY
*ENDSTEP
**
**
*STEP, NLGEOM, INC=10000
*STATIC
0.01, 1, 0, 0.00015
**
*BOUNDARY
PLNODES, 1, 1, 200
**
**output
**
**
*NODEFILE, FREQUENCY=10, NSET=PLNODES
U
*NODEFILE, FREQUENCY=10, NSET=BC1
U
*NODEFILE, FREQUENCY=10, NSET=PLNODES
RF
*NODEFILE, FREQUENCY=10, NSET=BC1
RF
**
*NODEPRINT, FREQUENCY=0
*ELFILE, FREQUENCY=4, ELSET=CRITICAL
SDV
E
S
*ELFILE, FREQUENCY=4, ELSET=MID
SDV
E
S
*ELPRINT, FREQUENCY=0
**
```

```
*RESTART, WRITE, OVERLAY
*ENDSTEP
**
```

APPENDIX C

Comparison of Load vs. Deformation Curves Obtained from the Physical Tests and Finite Element Analysis

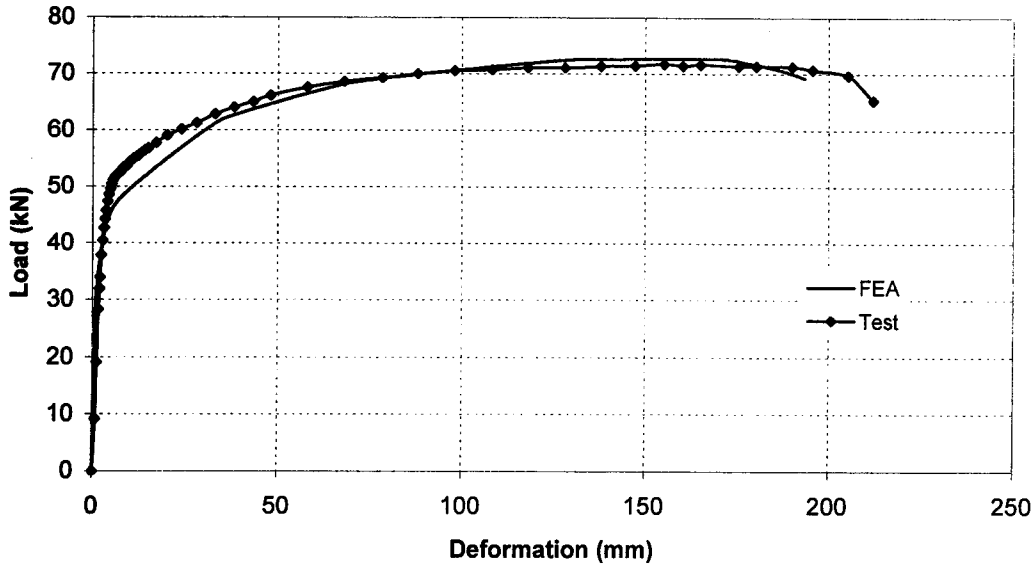

Figure C.1 Comparison of Load vs. Deformation Curves for A2ba-1

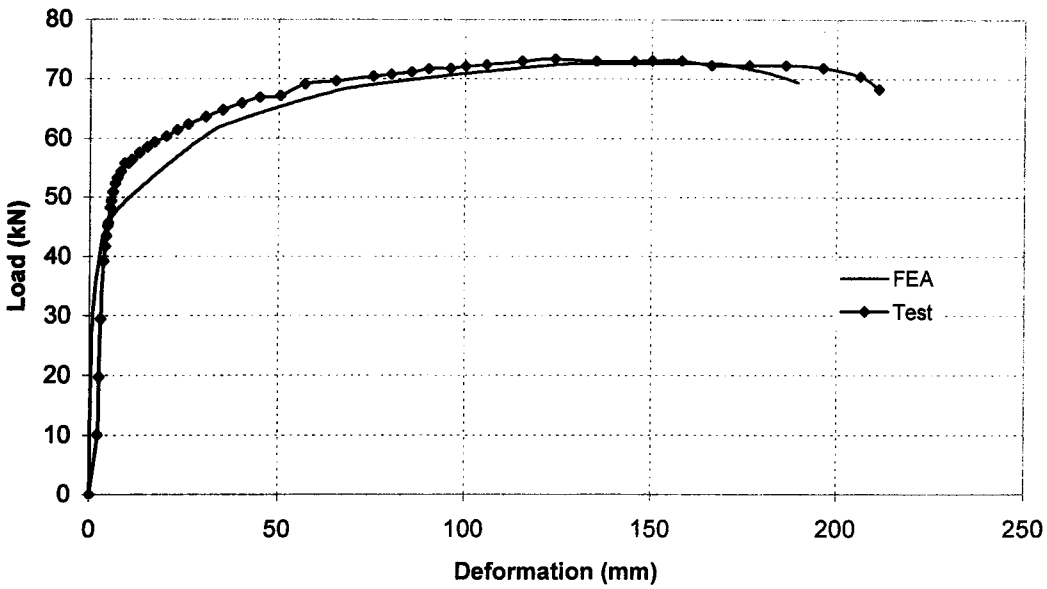

Figure C.2 Comparison of Load vs. Deformation Curves for A2un-1

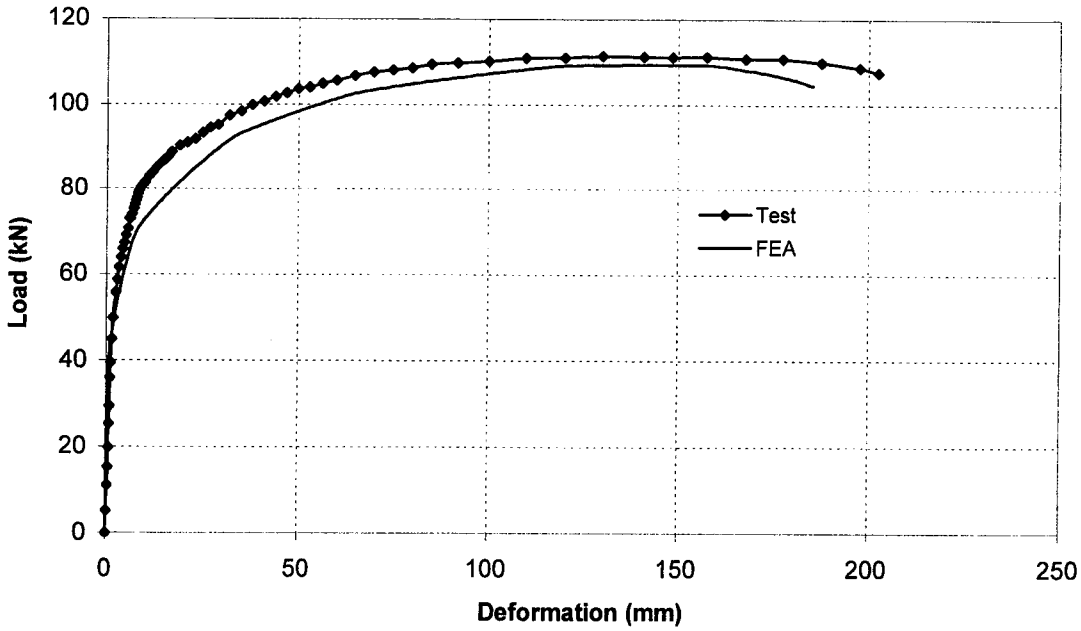

Figure C.3 Comparison of Load vs. Deformation Curves for A3ba-1

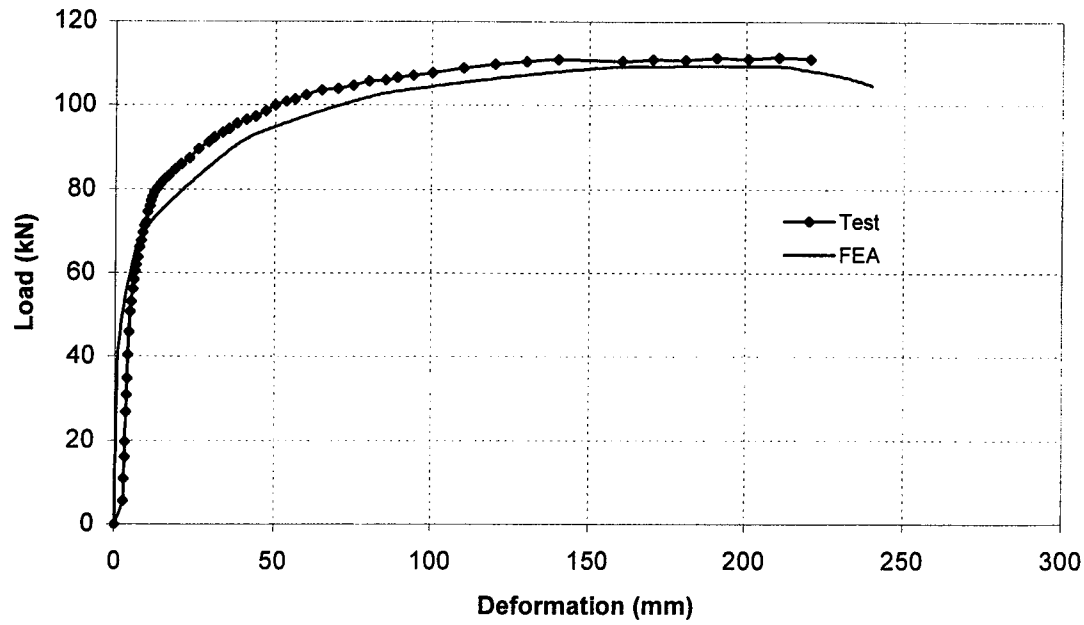

Figure C.4 Comparison of Load vs. Deformation Curves for A3un-1

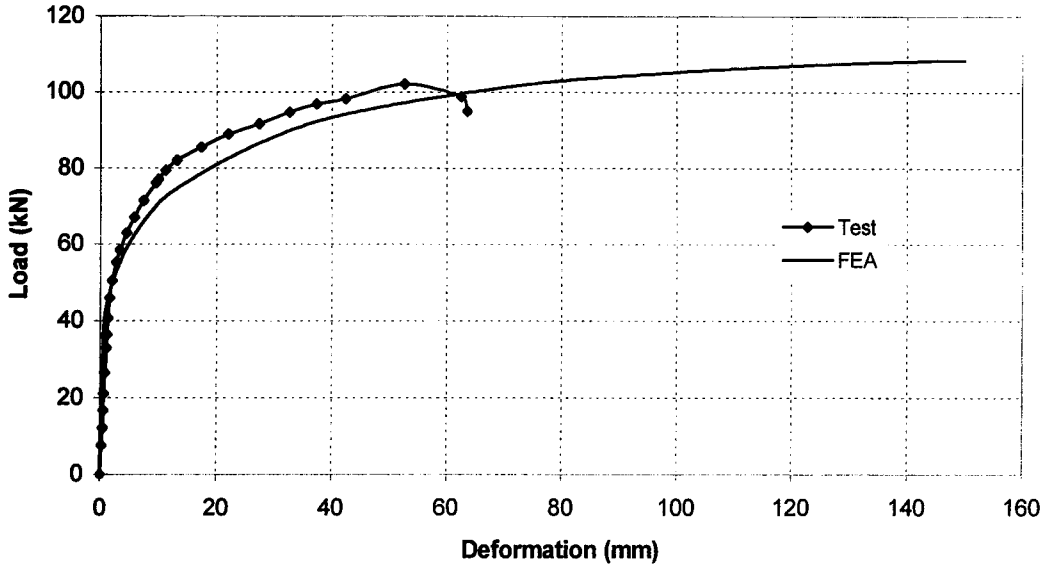

Figure C.5 Comparison of Load vs. Deformation Curves for A3un-2

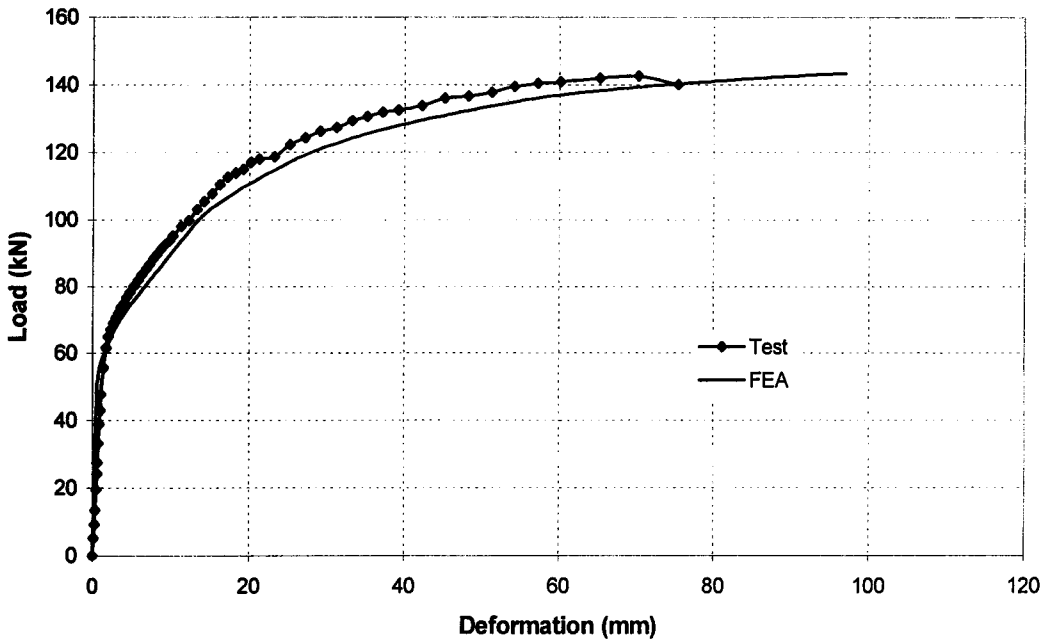

Figure C.6 Comparison of Load vs. Deformation Curves for A4ba-1

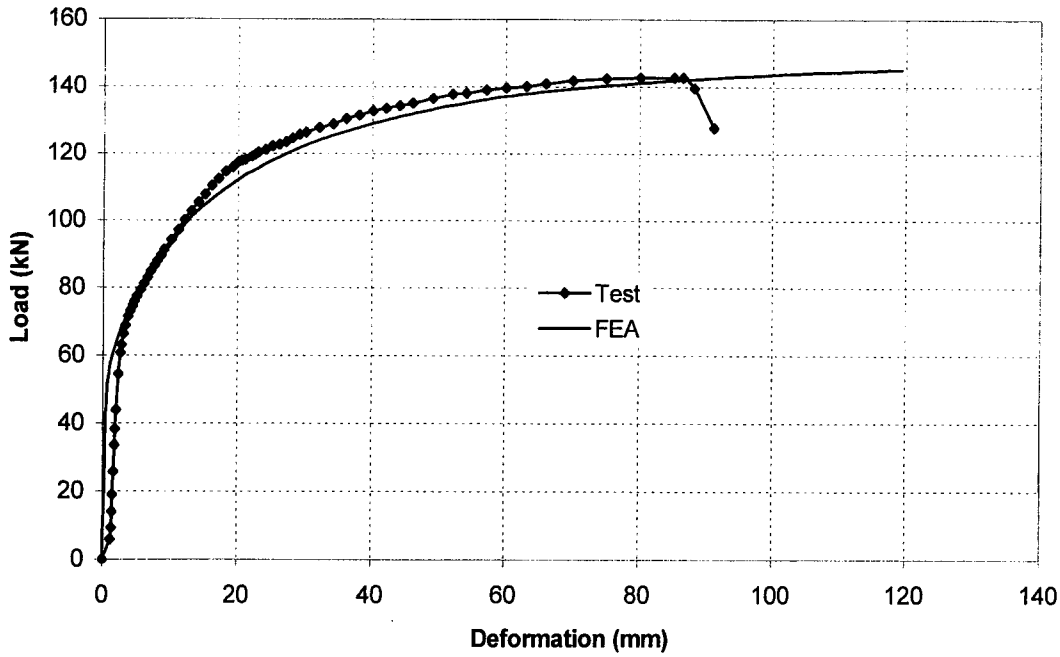

Figure C.7 Comparison of Load vs. Deformation Curves for A4un-1

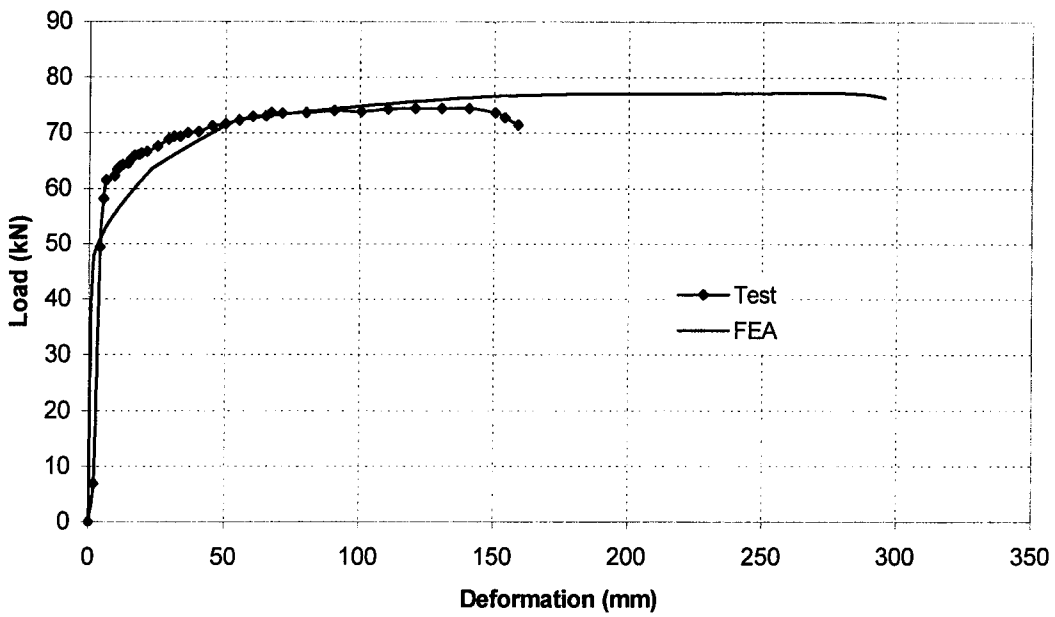

Figure C.8 Comparison of Load vs. Deformation Curves for C2-2

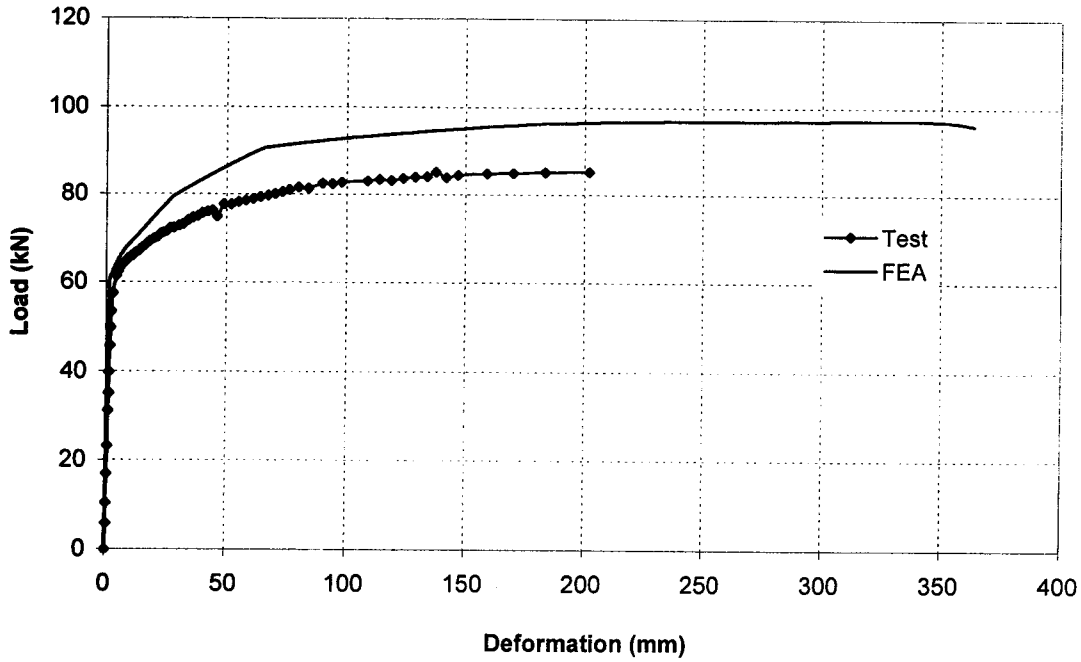

Figure C.9 Comparison of Load vs. Deformation Curves for C3-1

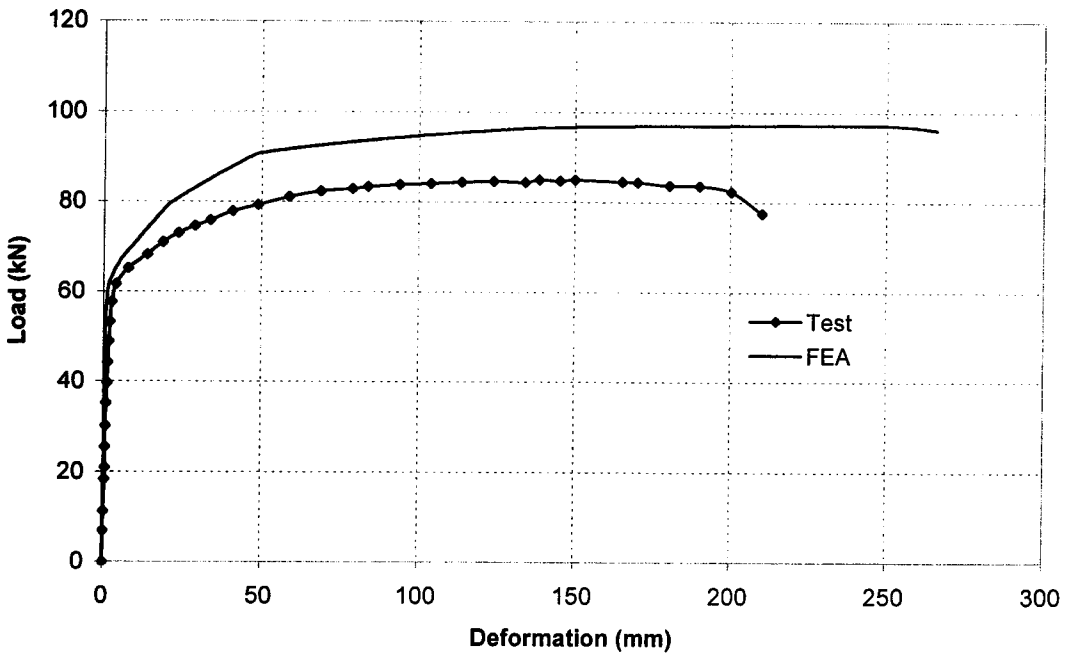

Figure C.10 Comparison of Load vs. Deformation Curves for C3-2

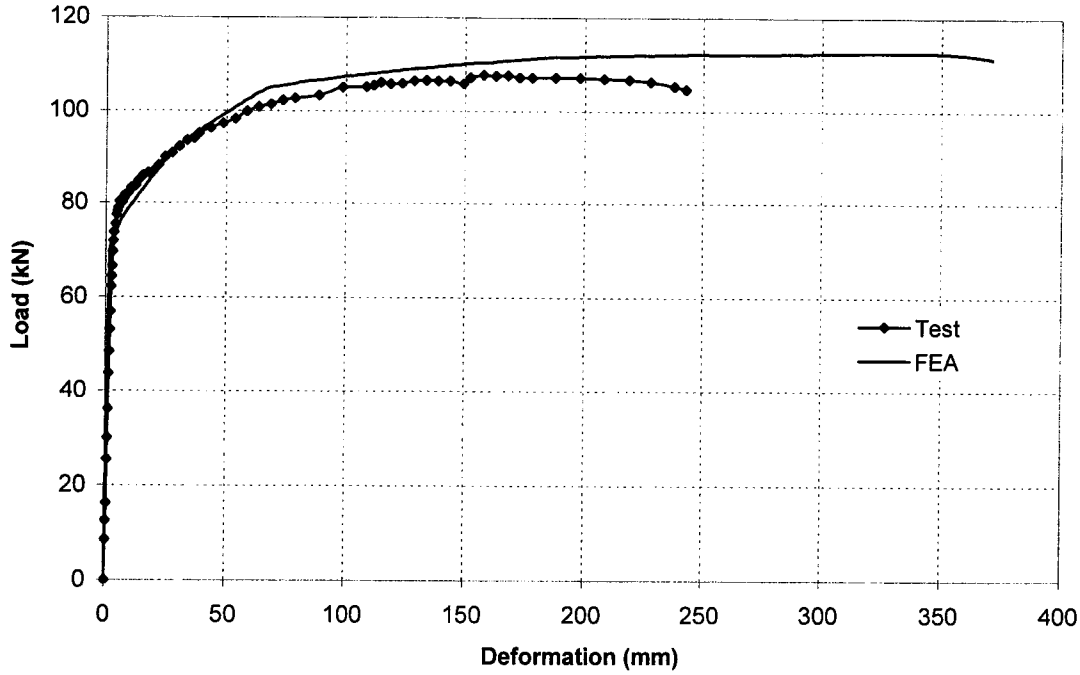

Figure C.11 Comparison of Load vs. Deformation Curves for C4-1

Recent Published Structural Engineering Reports
Department of Civil and Environmental Engineering
University of Alberta

211. *Fatigue of Riveted Tension Members* by Jeffrey DiBattista and Geoffrey L. Kulak, November 1995.

212. *Behaviour of Masonry Cavity Walls Subjected to Vertical Eccentric Loads* by Ru Wang, Alaa E. Elwi, Michael A. Hatzinikolas and Joseph Warwaruk, February 1996.

213. *Thermal Ice Loads on Structures* by Azita Azarnejad and Terry M. Hrudey, November 1996.

214. *Transmission of High Strength Concrete Column Loads Through Concrete Slabs* by Carlos E. Ospina and Scott D.B. Alexander, January 1997.

215. *Seismic Behaviour of Steel Plate Shear Walls* by Robert G. Driver, Geoffrey L. Kulak, D.J.Laurie Kennedy and Alaa E. Elwi, February 1997.

216. *Extended End Plate Moment Connections under Cyclic Loading* by Bryan T. Adey, Gilbert Y. Grondin and J.J. Roger Cheng, June 1997.

217. *Connection of Infill Panels in Steel Plate Shear Walls* by Ann S. Schumacher, Gilbert Y. Grondin and Geoffrey L. Kulak, August 1997.

218. *Shear Rehabilitation of G-Girder Bridges using CFRP Sheets* by John G.S. Alexander and J.J. Roger Cheng, October 1997.

219. *Seismic Evaluation of Steel Buildings with Concentrically Braced Frames* by Manoj S. Medhekar and D.J. Laurie Kennedy, October 1997.

220. *Rational Design of Prestressed and Reinforced Concrete Tanks* by Abdelaziz A. Rashed, David M. Rogowsky and Alaa E. Elwi, December 1997.

221. *Repair of Cracked Steel Elements using Composite Fibre Patching* by Gaylene D. Kennedy and J.J. Roger Cheng, May 1998.

222. *Strength of Joints that Combine Bolts and Welds* by Thomas J. Manuel and Geoffrey L. Kulak, July *1998*.

223. *Strip Model for Capacity of Slab-Column Connections* by Shahab Afhami, Scott D.B. Alexander, and Sidney H. Simmonds, August 1998.

224. *Behaviour of Large Diameter Line Pipe under Combined Loading* by Patrick R. DelCol, Gilbert Y. Grondin, J.J. Roger Cheng and David W. Murray, September 1998.

225. *An Analysis of the Cyclic Behaviour of Steel Gusset Plate Connections* by Scott S. Walbridge, Gilbert Y. Grondin, and J.J. Roger Cheng, September 1998.

226. *Rehabilitation of Unreinforced Masonry Walls with Externally Applied Fiber Reinforced Polymers* by Michael L. Albert, J.J. Roger Cheng, and A.E. Elwi, October, 1998.

227. *Fatigue of Bearing-Type Shear Splices* by Georg Josi, G.Y. Grondin, and G.L. Kulak, April, 1999.

228. *Out-of-Plane Cyclic Behavior of Masonry Walls Reinforced Externally with GFRP* by Marc D. Kuzik, A.E. Elwi, and J.J. Roger Cheng, August 1999.

229. *Cyclic Behavior of Stiffened Gusset Plate–Brace Member Assemblies* by Trina Nast, G.Y. Grondin, and J.J.R. Cheng, November 1999.

230. *Behaviour of Sleeper-supported Line Pipe* by Jeffrey D. DiBattista, J.J.R. Cheng, and D.W. Murray, April 2000.

231. *Field Assessment of Crowchild Trail Bridge* by Kong K. Taing, J.J.R. Cheng, and S. Afhami, January 2000.

232. *Ductile Fracture of Steel* by Heng Aik Khoo, J.J. Roger Cheng, and T.M. Hrudey, August 2000.

233. *Shear Lag in Bolted Cold-Formed Steel Angles and Channels in Tension* by Amy Sin-Man Yip and J.J. Roger Cheng, September 2000.

234. *Behaviour of Reinforced Concrete Beams Strengthened in Shear with FRP Sheets* by Christophe Deniaud and J.J. Roger Cheng, October 2000.

235. *Behaviour of Distortion-Induced Fatigue Cracks in Bridge Girders* by R. Fraser, G.Y. Grondin, and G.L. Kulak, December 2000.

236. *Stiffener Tripping in Stiffened Steel Plates* by I.A. Sheikh, A.E. Elwi and G.Y. Grondin, January 2001.

237. *Critical Buckling Strains for Energy Pipelines* by A.B. Dorey, J.J.R. Cheng and D.W. Murray, May 2001.

238. *Local buckling and Fracture Behaviour of Line Pipe under Cyclic Loading* by Brian Myrholm, J.J.R. Cheng and D.W. Murray, May 2001.

239. *Behaviour of Welded Cold-Formed Steel Tension* Members by Alvaro Lemenhe and J.J.R. Cheng, July 2001.